A kinetic model of glucose catabolism in *Plasmodium falciparum*

by

Gerald Patrick Penkler

Dissertation approved for the degree of Doctor of Philosophy in the Faculty of Science (Biochemistry) at Stellenbosch University and the Faculty of Earth and Life Sciences at Vrije Universiteit Amsterdam

Department of Biochemistry
University of Stellenbosch
Private Bag X1, Matieland, 7602, South Africa
&
Department of Molecular Cell Physiology
Vrije Universiteit Amsterdam
De Boelelaan 1085, NL-1081 HV, The Netherlands

Promoters:

Prof J.L. Snoep

Department of Biochemistry
University of Stellenbosch

Prof H.V. Westerhoff

Department of Molecular Cell Physiology
Vrije Universiteit Amsterdam

Co-promoter:

Prof M. Rautenbach

Department of Biochemistry
University of Stellenbosch

March 2013

Declaration

By submitting this dissertation electronically, I declare that the entirety of the work contained therein is my own, original work, that I am the sole author thereof (save to the extent explicitly otherwise stated), that reproduction and publication thereof by Stellenbosch University and Vrije Universiteit Amsterdam will not infringe any third party rights and that I have not previously in its entirety or in part submitted it for obtaining any qualification.

Date: .....

Summary

A kinetic model of glucose catabolism in *Plasmodium falciparum*

G. P. Penkler

Department of Biochemistry
University of Stellenbosch
Private Bag X1, Matieland, 7602, South Africa
&
Department of Molecular Cell Physiology
Vrije Universiteit Amsterdam
De Boelelaan 1085, NL-1081 HV, The Netherlands

Dissertation: Ph.D (Biochemistry)

March 2013

Malaria infects over 200 million individuals and leads to the death of over 600 000 people annually. Currently artemisinin combination therapy treatments are effective in treating the disease, but resistance has started to emerge in Cambodia and it is suspected in parts of Vietnam. To maintain the drive to eradicate malaria globally, a great deal of research is aimed at identifying novel prevention strategies, vaccines and antimalarial compounds.

Plasmodium falciparum, the most deadly of the malaria parasites, is entirely dependent on glycolysis for ATP. Several of the enzymes within this pathway have been proposed as drug targets and studied in isolation, but the pathway as a whole has not been considered. In this study we employ a bottom up approach for drug target identification in *P. falciparum* glycolysis.

In this thesis we present the biochemical characterisation each of the glycolytic enzymes in *P. falciparum* trophozoites. The kinetic rate equations, which described the kinetic behaviour of the individual enzymes, were incorporated into a kinetic model. The unfitted model was validated in its ability to predict experimentally measured steady state metabolite concentrations and fluxes as well as the experimental inhibition of the glucose transporter.

The validated model provided a tool for drug target identification in *P. falciparum* glycolysis. Metabolic control analysis and differential control analysis identified the glucose transporter, PfHT1, as a drug target based on its high control of glycolytic flux in the parasite, but low control of flux in the host erythrocyte. This differential control makes the transporter an attractive drug target, as even if both the erythrocyte and parasite glucose *transporters* are inhibited to the same degree, it is expected that the parasite *glycolytic flux* would be inhibited to a much greater degree.

To demonstrate the differential control of the glucose transporter on the flux and provide further evidence that PfHT1 is an attractive drug target, we investigated the inhibition of the glucose transporter in isolated trophozoites by cytochalasin B. We also measured the inhibition of lactate production flux by cytochalasin B in both isolated *P. falciparum* trophozoites as well as in erythrocytes. Our findings demonstrated that differential control analysis can be used as a tool for drug target identification and that PfHT1 is an attractive drug target.

In this study the fields of biochemistry and systems biology were merged to create a detailed kinetic model of asexual *P. falciparum* glycolysis and identify several drug targets in the pathway. The model prediction and experimental evidence of differential flux control of the glucose transporter in the host and parasite, has highlighted PfHT1 as a drug target and also demonstrates the strength of differential control analysis in identifying drug targets within a system. The kinetic model is a valuable tool for furthering our understanding of *P. falciparum* glycolysis and it provides a good foundation for expansion to identify drug targets in the entire central carbon metabolism of *P. falciparum*

Opsomming

'N KINETIESE MODEL VAN GLUKOSE KATABOLISME IN *Plasmodium falciparum*

G. P. Penkler

Departement Biochemie
Universiteit van Stellenbosch
Privaatsak X1, Matieland 7602, Suid Afrika
&
Departement Molekulêre Selfisiologie
Vrije Universiteit Amsterdam
De Boelelaan 1085, NL-1081 HV, Nederland

Proefskrif: Ph.D (Biochemie)

Maart 2013

Malaria infekteer meer as 200 miljoen mense en veroorsaak jaarliks tot 600 000 sterftes. Tans is die artemisinien-kombinasieterapie effektief in die bestryding van die siekte, maar weerstandbiedendheid van die parasiet teen die middel blyk reeds 'n merkbare effek in Kambodja en vermoedelik ook in dele van Viëtnam te hê. Om 'n wêreldwye bestryding van malaria moontlik te maak, is 'n groot deel van die huidige navorsing gemik op die identifisering van nuwe voorkomingsstrategieë, entstowwe en malariateenmiddels.

Plasmodium falciparum, die dodelikste van die malaria-parasiete, is geheel en al afhanklik van glikolise vir ATP vorming. Verskeie van die ensieme in hierdie metaboliese pad is as teenmiddelteikens voorgestel, en in isolasie bestudeer, maar die pad as 'n geheel is nie bestudeer nie. In hierdie studie het

ons 'n 'bottom-up' benadering vir teenmiddel teikenidentifisering in *P. falciparum* glikolise gebruik.

In hierdie tesis bied ons die biochemiese karakterisering van elk van die glikolitiese ensieme in *P. falciparum* trofozoïete aan. Die kinetiese vergelykings wat die kinetiese gedrag van die individuele ensieme beskryf, is geintegreer in 'n enkele kinetiese model. Die model waarop geen datapassing toegepas is nie, is gevalideer om eksperimenteel bepaalde bestendige-toestand metabolietkonsentrasies en fluksiewaardes, asook die eksperimentele inhibisie van die glukose transporter, te voorspel.

Die gevalideerde model verskaf 'n bykomende hulpmiddel om teenmiddelteikens te identifiseer in *P. falciparum* glikolise. Metaboliese kontrole-analise en differensiële kontrole-analise het die glukose transporter, PfHT1, as 'n teenmiddelteiken geïdentifiseer, gebaseer op sy hoë kontrole van glikolitiese fluksie in die parasiet, tesame met 'n lae beheer van die glukose transporter op die fluksie in die gasheer eritrosiet. Dié differensiële kontrole maak die glukose transporter 'n aantreklike teenmiddelteiken, want selfs as beide die eritrosiet en die parasiet glukose transporters tot dieselfde mate geïnhibeer word, sal dit steeds 'n hoër glikolietiese fluksieinhibisie van die parasiet tot gevolg hê.

Om die differensiële kontrole van die glukose transporter op die fluks te demonstreer en verdere bewyse te lewer dat PfHT1 'n teenmiddelteiken kan wees, het ons die inhibisie van die glukosetransporter in geïsoleerde trofozoïete deur sitokalasien B ondersoek. Ons het ook die inhibisie van die laktaatproduksiefluksie deur sitokalasien B in beide geïsoleerde *P. falciparum* trofozoïete sowel as in eritrosiete ondersoek. Ons bevindings bewys dat differensiële kontroleanalise as 'n hulpmiddel vir teenmiddelteikenidentifikasie gebruik kan word en dat PfHT1 'n aantreklike teenmiddelteiken is.

In hierdie studie is die velde van biochemie en sisteembiologie gekombineer om 'n gedetaileerde kinetiese model van ongeslagtelike *P. falciparum* glikolise te konstueer en verskeie teenmiddelteikens in die metaboliese pad te identifiseer. Die modelvoorspelling sowel as eksperimentele bewyse van die differensiële flukskontrole van die glukose transporter in die gasheer en parasiet het PfHT1

uitgelig as 'n teenmiddelteiken en demonstreer ook die krag van differensiële kontrole analise in die identifisering van teenmiddelteikens binne 'n biologiese stelsel. Die kinetiese model is 'n waardevolle hulpmiddel vir die bevordering van ons begrip van *P. falciparum* glikolise en dit bied 'n goeie basis vir uitbreiding om teenmiddelteikens in die hele sentrale koolstofmetabolisme van *P. falciparum* te identifiseer.

Acknowledgements

I would like to thank numerous individuals and organisations who made the research presented in this thesis possible:

I would like to express my sincere gratitude to *Prof. Jacky Snoep,* my supervisor, for providing excellent guidance, scientific discussion, insight and enthusiasm throughout these past few years.

I would like to thank *Prof. Marina Rautenbach* for the important part she played and for the many ideas and discussions, especially whilst troubleshooting HPLC and UPLC-MS detection methods and during the compilation of this dissertation.

I would like to say thank you to *Prof. Hans Westerhoff* for the insightful and stimulating discussions.

The research presented in this dissertation required a great deal of funding. I would like to thank the *National Research Foundation* (NRF) for funding this research, as well as for providing me with a bursary.

I am grateful towards *Prof. Pete Smith* from University of Cape Town for facilitating the orders of Albumax II™ from New Zealand as well as for supplying different strains of malaria.

For me, my malaria cultures were happiest when I attended to them with daily metronomic frequency. These parasites do not understand the meaning of a weekend, a public holiday or heaven forbid - a long weekend! I would therefore like to thank my colleagues, *Waldo Adams, Francois du Toit, Francois Brand, Hazel Makowa,* and *Adrienne Leussa* for occasionally sharing the culturing duty on weekends.

Initially we used our own blood for culturing malaria. This worked well, but it is quite unpleasant and was simply not sustainable. I would like to express my sincere gratitude to the *Western Province Blood Bank* (Medi Clinic, Somerset West) for agreeing to supply our research with fresh blood whenever required. I would also like to thank my co-supervisor, *Prof. Marina Rautenbach* who facilitating this arrangement.

Family and friends are important. Not only does one receive moral support and much needed comic relief, but in my case, family also provided two engineers. I would like to thank my family and friends for the many happy times, encouragement and support during the time this research was integrated. I am extremely grateful to my dad, *Anton Penkler* and brother, *William Penkler* for discussion, ideas and assistance in the design and programming of my quench-flow device. I would also like to thank them for the great deal of time and effort they contributed towards the design and construction of a small continuous centrifuge.

Our laboratory is a busy place, and smooth operation requires a number of 'cogs' to be aligned and well lubricated. I am extremely grateful to our lab manager, *Mr Arrie Arends*, who performed this function in a most efficient and cheerful manner.

Our malaria team is still small, but each colleague has a distinct role and our projects have a common goal - modelling the entire central carbon metabolism and discovering how the parasite metabolism can be best disrupted for therapeutic purposes. Working as a team is terrific and I would like to thank *Franco du Preez, Waldo Adams, Francois du Toit, Francois Brand, Dawie van Niekerk, Hazel Makowa, Adrienne Leussa* and *Lauren Palmer* for each of their contributions to my work, sharing enthusiasm and providing fun discussions, not necessarily work related.

Dedications

I dedicate this thesis to:
My Mom & Dad
and thank them for their love, support and 10 years of tertiary education
&
My fantastic sisters and brother,
Michelle, Frances, Rachel and William
for fulfilling the sibling role with distinction
&
My dear Suzanne
for the much appreciated support, encouragement,
and continued wonderful times together

Contents

Declaration i

Summary ii

Opsomming iv

Acknowledgements vii

Dedications ix

Contents x

List of Figures xii

List of Tables xiv

Abbreviations xvi

1 General Introduction 1

2 Introduction: Modelling the Central carbon metabolism 5
2.1 Introduction 5
2.2 Glycolysis 11
2.3 Summary 28

3 Enzyme Kinetics and Model construction 31
3.1 Introduction 31
3.2 Methods 34
3.3 Results and Discussion 39
3.4 General Discussion 83
3.5 Conclusion 85

4 Model Validation and Analysis 86
4.1 Introduction 86
4.2 Methods 89
4.3 Results 93

4.4 Discussion 104
4.5 Conclusion 108

5 Differential control analysis **110**
5.1 Introduction 110
5.2 Methods 113
5.3 Results 115
5.4 Discussion 129

6 General Discussion **134**
6.1 Conclusion 137

Appendices **138**

A Model Validation & Analysis **139**
A.1 Metabolic Control Analysis 139
A.2 Parameter Sensitivity Analysis 142
A.3 Response Coefficients 146

B Quench Flow Device **149**
B.1 Introduction 149
B.2 Materials 149
B.3 Machine Design 150
B.4 Calibration 153
B.5 Discussion 155

List of References **156**

List of Figures

2.1 Overview of asexual *P. falciparum* central carbon metabolism. . . 12
2.2 Overview of asexual *P. falciparum* tricarboxylic acid cycle. 22

3.1 Overview of asexual *P. falciparum* glycolysis 33
3.2 Biochemical characterisation of *P. falciparum* hexokinase 40
3.3 Biochemical characterisation of *P. falciparum* phosphoglucoisomerase 42
3.4 Biochemical characterisation of *P. falciparum* phosphofructokinase 45
3.5 Kinetic characterisation of *P. falciparum* aldolase 47
3.6 Kinetic characterisation of *P. falciparum* triosephosphate isomerase 49
3.7 Biochemical characterisation of *P. falciparum* glyceraldehyde 3-phosphate dehydrogenase 51
3.8 Biochemical characterisation of *P. falciparum* phosphoglycerate kinase 54
3.9 Biochemical characterisation of *P. falciparum* phosphoglycerate mutase 56
3.10 Biochemical characterisation of *P. falciparum* enolase 57
3.11 Kinetic characterisation of *P. falciparum* pyruvate kinase 59
3.12 Kinetic characterisation of *P. falciparum* lactate dehydrogenase . 62
3.13 The specific activity of the glucose transporter PfHT1 as a function of quench time 67
3.14 Kinetic characterisation of *P. falciparum* PfHT1 68
3.15 Comparison of the V_{max} values of the *P. falciparum* glycolytic enzymes 73

4.1 HPLC chromatograms of ^{14}C labelled external metabolites produced by isolated *P. falciparum* trophozoites 95
4.2 Model predictions of external fluxes compared to experimental results 96

5.1 Inhibition of ^{14}C labelled glucose transport into isolated trophozoites by cytochalasin B 120
5.2 Inhibition of glycolytic flux in *P. falciparum* and uninfected erythrocytes by cytochalasin B compared to model prediction of flux inhibition. 122
5.3 Specific activities for the glycolytic enzymes of *P. falciparum* in the presence or absence of cytochalasin B 125

5.4 Determination of the control coefficient for *P. falciparum* PFHT1 127

A.1 Model predictions of steady state flux for glucose uptake and lactate, pyruvate and glycerol production as a function of the ATP:ADP ratio 142
A.2 Model predictions of steady state metabolite concentrations in upper glycolysis 143
A.3 Model predictions of steady state metabolite concentrations in lower glycolysis 144
A.4 Broad range parameter sensitivity analysis of the monocarboxylate transporter 145
A.5 Effect of the glyceraldehyde 3-phosphate dehydrogenase on model prediction. 146

B.1 Schematic description of the quench-flow device 151
B.2 Determination of the quench-flow device dead time 154

List of Tables

2.1 Summary of kinetic parameters present in scientific literature for the glycolytic enzymes of *Plasmodium spp.*. 20

3.1 Summary of the kinetic parameters for *P. falciparum* hexokinase . 41
3.2 Summary of the average kinetic parameters for the three *P. falciparum* PGI isozymes 43
3.3 Summary of kinetic parameter values for *P. falciparum* phosphofructokinase 46
3.4 Summary of kinetic parameters for *P. falciparum* aldolase 48
3.5 Summary of Kinetic parameters for *P. falciparum* triosephosphate isomerase 50
3.6 Summary of kinetic parameters for *P. falciparum* glyceraldehyde 3-phosphate dehydrogenase 52
3.7 A summary of kinetic parameters for *P. falciparum* phosphoglycerate kinase 55
3.8 Summary of kinetic parameters for *P. falciparum* phosphoglycerate mutase 56
3.9 Summary of the kinetic parameters for *P. falciparum* enolase . . . 58
3.10 Summary of kinetic parameters for *P. falciparum* pyruvate kinase 61
3.11 Summary of kinetic parameters for *P. falciparum* lactate dehydrogenase 62
3.12 Summary of the kinetic parameters obtained for the glycerol producing enzyme 64
3.13 Summary of the kinetic parameters for *P. falciparum* hexose transport 68
3.14 Summary of kinetic parameters for *P. falciparum* lactate and pyruvate transport obtained from scientific literature 71
3.15 Maximal specific activity for each of the glycolytic enzymes in *P. falciparum* as measured in this study 74
3.16 Summary of the kinetic parameters used for model construction . 76
3.17 External metabolite concentrations and moiety concentrations . . 81
3.18 Kinetic model initial conditions and steady state predictions . . . 82

4.1 Experimentally determined glycolytic fluxes in *P. falciparum* trophozoites 97

4.2 Summary of metabolite concentrations as predicted by the model and determined experimentally in this work and in scientific literature 99
4.3 Selected flux control coefficients 101
4.4 Summary of selected concentration control coefficients 102

5.1 Summary of glucose flux control coefficients in *P. falciparum* and human erythrocytes 118
5.2 Flux control coefficients for the *P. falciparum* glucose transporter. 128

A.1 Complete set of flux control coefficients for the model of *P. falciparum* glycolysis during the asexual trophozoite phase 140
A.2 Complete set of concentration control coefficients for the model of *P. falciparum* glycolysis during the asexual trophozoite phase. . . 141
A.3 Summary of selected flux response coefficients: Part 1 147
A.4 Summary of selected flux response coefficients: Part 2 148

Abbreviations

Acetyl-CoA	Acetyl-coenzyme A
ADP	Adenosine diphosphate
ALD	Fructose bisphosphate Aldolase (E.C. 4.1.2.13)
αKG	α-ketoglutarate
APADH	3-acetylpyridine adenine dinucleotide
AspTA	Aspartate transaminase (E.C. 2.6.1.1)
ATP	Adenosine triphosphate
AQP	Aquaglyceroporin
CytB	Cytochalasin B
DHAP	Dihydroxyacetone Phosphate
2DOG	2-Deoxy-D-glucose
B1,3PG	1,3-bisphosphoglycerate
B2,3PG	2,3-bisphosphoglycerate
ENO	Enolase (E.C. 4.2.1.11)
ETC	Electron Transport Chain
F1,6BP	Fructose 1,6-Bisphosphate
F1P	Fructose -1-Phosphate
F6P	Fructose 6-Phosphate
$FADH_2$	Reduced flavin adenine dinucleotide
G3PDH	Glyceraldehyde-3-phosphate dehydrogenase (E.C. 1.2.1.12)
G6P	Glucose 6-Phosphate
G6PD(H)	Glucose-6-phosphate- 1-dehydrogenase (E.C. 1.1.1.49)
GAP	Glyceraldehyde-3-Phosphate
GFATM	Global Fund to Fight AIDS, Tuberculosis and Malaria.
GlycerolPDH	α-Glycerol phosphate dehydrogenase (E.C. 1.1.1.8)
GlrDH	α-Glycerol phosphate dehydrogenase (E.C. 1.1.1.8)
GluPho	Glucose-6-phosphate dehydrogenase-6-phosphogluconolactonase (G6PD-6PGL)
Glc	D-Glucose
GlcTr	Glucose Transporter
Glu	Glutamate
GLUT1	Glucose Transporter 1
GLUT5	Glucose Transporter 5
Gln	Glutamine
Glr	Glycerol
GlrTr	Glycerol Transporter
Glu	Glutamate

GTP	Guanosine Triphosphate
HEPES	4-(2-hydroxyethyl)piperazine-1-ethanesulfonic acid
HK	Hexokinase (E.C. 2.7.1.1)
kDa	kiloDalton
K_m	Michaelis constant
Lac	Lactate
LacTr	Lactate Transporter
l.o.d	Limit of detection
LDH	L-Lactate Dehydrogenase (E.C. 1.1.1.27)
MMV	Medicines for Malaria Venture
mRNA	Messenger RNA
MCT	Monocarboxylate Transporter
MDH	Malate Dehydrogenase
MCA	Metabolic Control Analysis
NAD^+	Oxidised Nicotinamide adenine dinucleotide
NADH	Reduced Nicotinamide adenine dinucleotide
$NADP^+$	Oxidised Nicotinamide dinucleotide phosphate
NADPH	Reduced Nicotinamide dinucleotide phosphate
NPO	Non profit organisation
ODN	Oligodeoxynucleotides
PDH	Pyruvate Dehydrogenase Complex
PEP	Phosphoenolpyruvate
PEPC	PEP carboxylase (E.C. 4.1.1.31)
PEPCK	PEP carboxy kinase (E.C. 4.1.1.32)
PfHT1	*Plasmodium falciparum* hexose transporter 1
PFK	Phosphofructokinase (E.C. 2.7.1.11)
PGI	Phosphoglucoisomerase (E.C. 5.3.1.9)
Pi	Inorganic Phosphate
Pyr	Pyruvate
PyrTr	Pyruvate Transporter
3PGA	3-Phosphoglycerate
2PGA	2-Phosphoglycerate
PGK	Phosphoglycerate Kinase (E.C. 2.7.2.3)
6PGL	6-Phosphogluconolactononase (E.C. 3.1.1.31)
PGM	Phosphoglycerate Mutase (E.C. 5.4.2.1)
PK	Pyruvate Kinase (E.C. 2.7.1.40)
PPP	Pentose Phosphate Pathway
R3PE	Ribulose-3-phosphate epimerase (E.C. 5.1.3.1)
PRPP	Phosphoriboyl-1-pyrophosphate
PRTases	Phosphoribosyl transferases
PvHT1	*Plasmodium vivax* hexose transporter 1
Pyr	Pyruvate
R5P	Ribulose 5-phosphate
ROS	Reactive Oxygen Species

TCA	Tricarboxylic Acid Cycle
TPI	Triosphosphate Isomerase (E.C. 5.3.1.1)
U	Enzyme Units
V_{max}	Maximal specific activity of an enzyme, normalised to total cell protein
WHO	World Health Organisation

Chapter 1

General Introduction

Malaria is a disease that infected an estimated 216 million individuals, with over 655 000 fatalities in 2010 (World Health Organisation (WHO) world malaria report 2011). The drive to eradicate malaria globally is slowly gaining ground with five regions being certified malaria free zones and mortality rate having decreased by 25% globally in the last decade. However, *Plasmodium* is gaining resistance to the current artemisinin combination therapies (WHO, world malaria report 2011) and this necessitates the development of novel therapeutics.

The causative agent, *Plasmodium*, is transmitted to the human host by the bite of an infected female *Anopheles* mosquito. Four species of *Plasmodium*:, *vivax*, *malariae*, *ovale* and *falciparum* are known to use a human host, although the simian *P. knowlesi* has also been shown to infect humans[43]. During the dual host life cycle of *Plasmodium*, the parasite has a number of physiologically different forms. In the human host, the transmitted parasite infects the liver hepatocytes, multiplies in a series of nuclear divisions followed by cytokinesis (schizogony)[213] and releases thousands of invasive merozoites into the blood stream[141]. The merozoites subsequently invade the host erythrocytes and this asexual phase is responsible for the clinical symptoms of malaria. *P. falciparum* develops from a merozoite into a young trophozoite (also known as the ring stage) and then into a mature trophozoite. After undergoing further schizogony and cellular division, each parasite may produce up to 32 merozoites[213]. Following erythrocyte lysis, the 48 hour cycle is repeated with the released merozoites invading new erythrocytes. Some of the merozoites during the asexual phase form male and female gametocytes. These precursors are dormant unless ingested by a female *Anopheles* mosquito during a blood meal,

after which they are activated to produce gametes[112]. Following fertilisation, a diploid zygote is formed in the mosquito midgut, which initiates the life cycle in the mosquito host[112].

The asexual bloodstream phase, which is the stage studied in this thesis, has access to the rich nutrient content of the host cell's haemoglobin and the host blood serum. Upon infection by *Plasmodium* the glucose uptake of the erythrocyte has been reported to increase up to 100-fold[123]. The asexual parasite does not have any reduced carbohydrate reserves and is largely dependent on glycolysis for generating ATP. The parasite's dependence on ATP makes the glycolytic pathway an attractive drug target and a high degree of inhibition of an enzyme within the pathway is expected to severely hamper parasite development. Several glycolytic enzymes in the *P. falciparum* have been biochemically characterised, inhibited *in vitro* and proposed as potential drug targets. These studies have been on isolated enzymes and have not considered the glycolytic pathway as a whole.

Kinetic models of metabolic pathways are useful for analysing systemic behaviour and identifying which enzymes are the most important in controlling the metabolic flux or metabolite concentrations. Kinetic models of yeast[205] and *Trypanosoma brucei*[7] glycolysis constructed from rate equations that described each of the glycolytic enzymes could successfully describe systemic behaviour (e.g. steady state fluxes and metabolite concentrations), enhance the understanding of the pathways, and, in the case of *T. brucei*, identified the pyruvate and glucose transporters as potential drug targets.
Numerous glycolytic enzymes of *P. falciparum* have been biochemically characterised and further characterisation is simplified by the wide availability of assay methods. This considered, a bottom up approach (i.e. using individual enzyme kinetics) to constructing a kinetic model for asexual *Plasmodium* glycolysis is feasible and forms part of this dissertation.

To examine a pathway as a whole, systems biology provides a variety of analytical methods such as metabolic control analysis (MCA), hierarchical regulation analysis, elementary mode analysis, metabolic flux analysis, flux balance analysis (these are reviewed by Geenen *et al.*[71]) and supply-demand analy-

sis[89]. MCA, developed independently by Kascer & Burns[107] and Heinrich & Rapoport[168,82], is a theoretical framework that defines coefficients that quantify a) the relative change in steady state systemic properties (e.g. steady state flux, J, or metabolite concentration, c) due to a small change in a reaction step (i.e. enzyme rate, v). This type of analysis has been utilised as a tool to improve our understanding of certain diseases (reviewed by Cascante *et al.*[33]), suggest new strategies to treat cancer[138] and among others identify drug targets in African sleeping sickness[8] and cancer[147].
The MCA approach to drug target identification has generally been to identify an enzyme or enzymes[138] with high flux control. These enzymes are expected to require a lower degree of inhibition to inhibit the pathway flux compared to an enzyme with low flux control. By also considering the host metabolic control profile, one can identify enzyme(s) with a high flux control in the parasite, whereas the equivalent reaction in the host has a low flux control[8,98]. This *differential control* approach has been proposed as a tool for drug target identification[8,98], but has yet to be demonstrated *in vivo*.

The overall goal of this thesis was to create a detailed kinetic model of asexual *P. falciparum* glycolysis, use it as a tool for drug target identification and experimentally investigate a drug target predicted by differential control analysis. In the pursuit of this goal, we also aimed to answer the following broader questions:

- Does a kinetic model constructed with a bottom up approach describe network behaviour sufficiently to be used as a heuristic tool for drug target identification?
- By analysing the glycolytic pathway in its entirety (i.e. using metabolic control analysis), which of the many enzymes that have been proposed as drug targets in *P. falciparum* glycolysis are feasible?
- Is differential control analysis of metabolic networks a relevant approach for drug target identification in general?

To address these questions the thesis is divided into a series of three research chapters designed as papers. This format has the advantage that each chapter

is independent, but I do apologise for the inevitable duplication of introductory material and materials and methods. **Chapter 3** presents i) the detailed biochemical characterisation of each of the enzymes in asexual *P. falciparum* glycolysis, ii) the integration of these enzyme kinetics into a detailed kinetic model and iii) the steady state prediction of the model.
In **Chapter 4** we investigate with validation experiments whether the kinetic model, as a function of the underlying biochemical kinetics, gives a fair representation of systemic behaviour (i.e. steady state fluxes, metabolite concentrations). We also use this validated kinetic model and MCA as tools for drug target identification in *P. falciparum* glycolysis.
In **Chapter 5** we identify drug targets in *P. falciparum* glycolysis using differential control analysis and investigate i) experimentally whether the predicted differential control occurs in the erythrocyte and the parasite and ii) if such an approach is relevant for drug target identification in general.
In addition to the three research chapters, in **Chapter 2** we review what is currently known about the central carbon metabolism of asexual *Plasmodium spp.* with specific focus on the glycolytic enzymes in terms of their kinetics and how these can be used for constructing a kinetic model. Finally, in **Chapter 6** we provide a general discussion of how the work in this dissertation addresses the general questions stated above.

Chapter 2

Introduction: Constructing a kinetic model of the central carbon metabolism of *P. falciparum*

2.1 Introduction

Malaria infects over 200 million individuals a year and results in the death of over 600 000 people (WHO, world malaria report 2011). In an attempt to eradicate malaria globally there is an internationally concerted effort in terms of funding, research, and implementation of preventative, diagnostic and treatment measures. The impact of these measures is evident considering the 25% reduction in mortality rate over the past decade. Artemisinin-based combination therapy treatment has proven highly effective to date, but of increasing concern is the development of drug resistance in Cambodia and possibly also in parts of Myanmar and Vietnam (WHO, world malaria report 2011). The continued development of novel antimalarial compounds is thus essential for maintaining the fight against the disease.

During the asexual erythrocyte phase, all *Plasmodium spp.* are entirely dependent on glycolysis for ATP production[193]. It is expected that inhibiting this pathway would severely reduce the growth rate of the parasite and as such several of the enzymes in the glycolytic pathway have been studied and proposed as drug targets. However, the enzymes have been studied in isolation

and their importance in terms of the entire glycolytic network has not been considered. Enzymes within the pentose phosphate pathway have also been proposed as drug targets, since the pathway's reduction of NADP is essential for the detoxification of free ferriprotoporphyrin IX (FP) and reactive oxygen species[11].

Identifying drug targets in these pathways is difficult, as many of the glycolytic enzymes of *Plasmodium spp.* share a degree of homology to the host enzymes. Crystal structures of some of the enzymes (e.g. lactate dehydrogenase[221,21,34] or triosephosphate isomerase[216]) aid drug target identification in this regard by highlighting structural differences between the parasite and host that may be exploited. What also needs to be considered, however, is the role of the target enzyme in the pathway as a whole. By examining the kinetics of the enzymes in isolation it is not possible to identify which enzymes are the most important for glycolytic flux. The field of systems biology has provided a number a tools, such as Metabolic Control Analysis (MCA), Hierarchical Regulation Analysis, Elementary Mode Analysis, Metabolic Flux Analysis, Flux Balance Analysis (reviewed by[71]) and supply-demand analysis[89] to investigate the behaviour of a system. MCA is particularly suited to identifying drug targets within a pathway, as it quantifies the relative importance of each enzyme in controlling the steady state flux and metabolite concentrations.

Pathway analysis necessitates a model describing the system. For several of the enzymes in the central carbon metabolism of *P. falciparum*, kinetic information is available, and the construction of a kinetic model is feasible[158]. To show how i) the individual enzyme kinetics can be used to construct a kinetic model of the entire pathway and ii) the relative importance of each enzyme in controlling the flux and metabolite concentration can be quantified, I describe

the process for a pathway consisting of two reactions:

Consider the following simple metabolic pathway where a substrate, S, is converted to a product, P, via an intermediate metabolite X (Eq. 2.1.1). In this pathway the two irreversible reactions (v_1 & v_2) are catalysed by two enzymes that follow Michaelis-Menten kinetics (Eq. 2.1.2), where K_x and K_s are the Michaelis constants for X and S respectively and V_{max_1} and V_{max_2} are the maximal rates for enzyme 1 and 2 respectively.

$$S \xrightarrow{v_1} X \xrightarrow{v_2} P \tag{2.1.1}$$

$$v_1 = \frac{V_{\max_1} \cdot S}{S + K_s} \qquad v_2 = \frac{V_{\max_2} \cdot X}{X + K_x} \tag{2.1.2}$$

Changes in the concentration of X over time, t, can be described by the difference in its rate of formation, v_1 and consumption, v_2 (Eq. 2.1.3).

$$\frac{dx}{dt} = v_1 - v_2 \tag{2.1.3}$$

To calculate the concentration of X at any time, this ordinary differential equation (ODE) can be integrated over time (Eq. 2.1.3). The results of such a numerical time integration can be compared to experimentally determined concentrations of X over time.

All metabolic pathways can be treated as open systems, where there is a constant influx of substrate and efflux of product. Assuming that the concentration of S remains constant (e.g. glucose in the human blood serum, which is homoeostatically buffered) and that P remains constant (e.g. immediately transported out of the cell as soon as it is formed) , the system would relax to a *steady state*. During steady state, i) the rate of X formation would be equal to the rate of X consumption, with this rate defined as the steady state flux, J, (i.e. $v_1 = v_2 = J$) and ii) the concentration of X (i.e. steady state concentration) would be constant over time (i.e. $X'[t] = 0$).

The steady state can be computed by solving for the conditions (i.e. metabolite concentration) where the ODE (which describes the change in metabolite concentrations over time) is equal to zero. This steady state analysis yields the steady state metabolite concentration, X, and flux of the pathway, J. This approach can be scaled-up to a multiple reaction pathway (e.g. glycolysis) by defining an ODE for each metabolite within the pathway.

A powerful tool for investigating the systemic properties (i.e. steady state fluxes and metabolite concentrations) of a pathway in terms of the local properties (i.e. enzyme rates and kinetic parameters) is Metabolic Control Analysis (MCA). MCA defines *elasticity coefficients, control coefficients* and *response coefficients*, which quantify the degree to which a change in a *local property* (e.g. enzyme rate, or an effector of enzyme activity) alters the *systemic property* of the pathway (i.e. metabolic fluxes and metabolite concentrations).

To demonstrate how these coefficients describe the local and systemic properties, consider a pathway of which a parameter, p, (e.g. an activator of an enzyme) is perturbed:
The small change in the parameter concentration (e.g. an activator) would lead to a change in the *local* enzyme activity, v. This change can be quantified by an *elasticity coefficient*, mathematically formulated as:

$$\epsilon_p^v = \frac{\partial \ln v}{\partial \ln p}$$

The change in the individual enzyme rate (due to the parameter perturbation) would result in the system reaching a new steady state (a *systemic property*). The change in the *systemic properties* can be quantified by *control coefficients*, which describe the percentage change in fluxes or metabolite concentrations (flux and concentration control coefficients, C_v^J & C_v^x) due to a small change in the local rate, v. Mathematically they can be formulated as:

$$C_v^J = \frac{d \ln J}{d \ln v} \quad \& \quad C_v^x = \frac{d \ln x}{d \ln v}$$

The change in the parameter, p, induced a change in the *local* enzyme rate, v, which in turn resulted in a new steady state. The combined *response* of the system (i.e. change in flux or metabolite concentration) to a change in the parameter, p, is defined as a *response coefficient*, R_p^J. The response coefficient

can also be expressed as the product of the control and elasticity coefficient:

$$R_p^J = \frac{d\ln J}{d\ln p} = C_v^J \cdot \epsilon_p^v \quad \& \quad R_p^x = \frac{d\ln x}{d\ln p} = C_v^x \cdot \epsilon_p^v \tag{2.1.4}$$

In summary, i) *elasticity* can be defined as the percentage change in a *local* enzyme rate, v, due to a 1% change in a *local* parameter, p ii) *control* is defined as the percentage change in a *systemic* property such as steady state flux or metabolite concentrations due to a 1% change in the *local* enzyme rate, v and lastly iii) The *response* is defined as the percentage change in a *systemic* property such as steady state flux or metabolite concentrations due to a 1% change in a parameter, p.

Although not discussed here, it should be noted that the control coefficients can be expressed in terms of the elasticity coefficients using connectivity and summation theorems[64,87]. Using these theorems and the coefficients discussed one can, among others, quantify i) the influence of parameters (e.g. kinetic parameters) on the steady state flux (i.e. response coefficients) and ii) the control each enzyme has on the steady state metabolite and flux concentrations. MCA thus allows the systemic properties to be understood in terms of the local properties.

The theory of MCA was developed independently by Kascer & Burns[107] and Heinrich & Rapoport[168,82] and further developed by others. For further detail on MCA and its mathematical formulation refer to Fell *et al*[64] and Hofmeyr[87].

It is relatively straightforward to calculate these coefficients computationally if a kinetic model for the system is available by making a small perturbation to an enzyme activity and analysing the effect on the steady state. However, experimentally measuring a control coefficient is difficult.
One method to measure a control coefficient is via a so-called inhibitor titration experiment. In this type of experiment the elasticity and response coefficient are measured, and the control coefficient is calculated from the ratio of the response coefficient and the elasticity (see Eq. 2.1.4).
To measure the *elasticity*, one could use an inhibitor that specifically inhibits a reaction step (e.g. glucose transporter) or enzyme (e.g. hexokinase). By

measuring the percentage decrease in enzyme rate, v, over a range of inhibitor concentrations and, one can calculate the *elasticity* (i.e. decrease in glucose transporter rate, v, due to a small increase in inhibitor concentration). In practice this elasticity is calculated as the slope on a ln (v) vs. ln ([inhibitor]) plot at zero inhibitor concentration.
In a separate experiment, the *response* on steady state *flux* could be measured. This could be determined by incubating cells in the presence of an inhibitor and determining the decrease in the steady state flux. From these data one can calculate the *response coefficient* (i.e. decrease in steady state *flux* due to a small increase in inhibitor concentration). Emphasis is placed on the difference between inhibiting the pathway *flux* (a global property) and the inhibition of the enzyme *rate* (a local property).
The flux control coefficients are particularly useful for identifying drug targets within a pathway. An ideal target would have a high flux control coefficient, which would mean that inhibition of this step would lead to a high degree of inhibition of the pathway flux.

Above we have described the process of creating a kinetic model on the basis of the enzyme kinetics and how the system can be analysed over time or in steady state. A number of the enzymes in the central carbon metabolism and especially glycolysis, of asexual *P. falciparum* have been biochemically characterised. An aim of this dissertation is to construct a detailed kinetic model of *P. falciparum* glycolysis and use the model as a tool to evaluate which of the proposed drug targets in the pathway are the most promising and also to identify new drug targets within the pathway. These aims required i) a broad knowledge of the network topology (i.e. which enzymes were present), ii) a number of kinetic parameters and iii) knowledge of which enzymes have been targeted or proposed as drug targets. The aim of the following review is to provide a detailed description of what is currently known about each enzyme in *P. falciparum* glycolysis, the pentose phosphate pathway and tricarboxylic acid cycle with particular focus on the biochemical characterisation of the enzymes.

2.2 Glycolysis

Plasmodium spp. infected erythrocytes rapidly utilise glucose from the host serum[156,190] and upon infection glucose uptake may increase as much as 100 fold[123]. Asexual parasites require glucose or fructose for growth[222,119] and are unable to utilise ribose, mannose or galactose as a carbohydrate source[123]

Plasmodium spp. has a classical Embden-Meyerhof pathway (Fig. 2.1) and nearly all glucose passes through the anaerobic glycolytic pathway, with a net yield of approximately two moles ATP and two moles lactate per mole glucose[190]. The almost complete conversion of glucose to lactate was initially thought to indicate that the pentose phosphate pathway (PPP) was inactive, although it is now known that there is a low flux (relative to glycolysis) through the PPP, as well as through a glycerol producing branch and a carbon dioxide fixating branch.

The considerable increase in glucose uptake rate and rapid production of lactate necessitates an efficient transport system. Sufficient glucose needs to be obtained from the host serum to support the rapidly multiplying parasite and since excessive lactate build-up in the cell is toxic, the parasite has an efficient monocarboxylate export system. Although, strictly speaking, hexose and lactate transport would not fall under the central carbon metabolism, these transport steps are an integral part of glycolysis and thus warrant their inclusion.

We broadly review the current knowledge of the *Plasmodium spp.* glycolytic enzymes - hexokinase (HK), phosphoglucoisomerase (PGI), phosphofructokinase (PFK), aldolase, triose phosphate isomerase (TIM), glyceraldehyde-phosphate dehydrogenase (G3PDH), phosphoglycerate kinase (PGK), phosphoglycerate mutase (PGM), enolase, pyruvate kinase (PK), lactate dehydrogenase (LDH) as well as the glucose and lactate transporters. Selected published kinetic parameters are tabulated at the end of the enzyme subsections in Table 2.1.

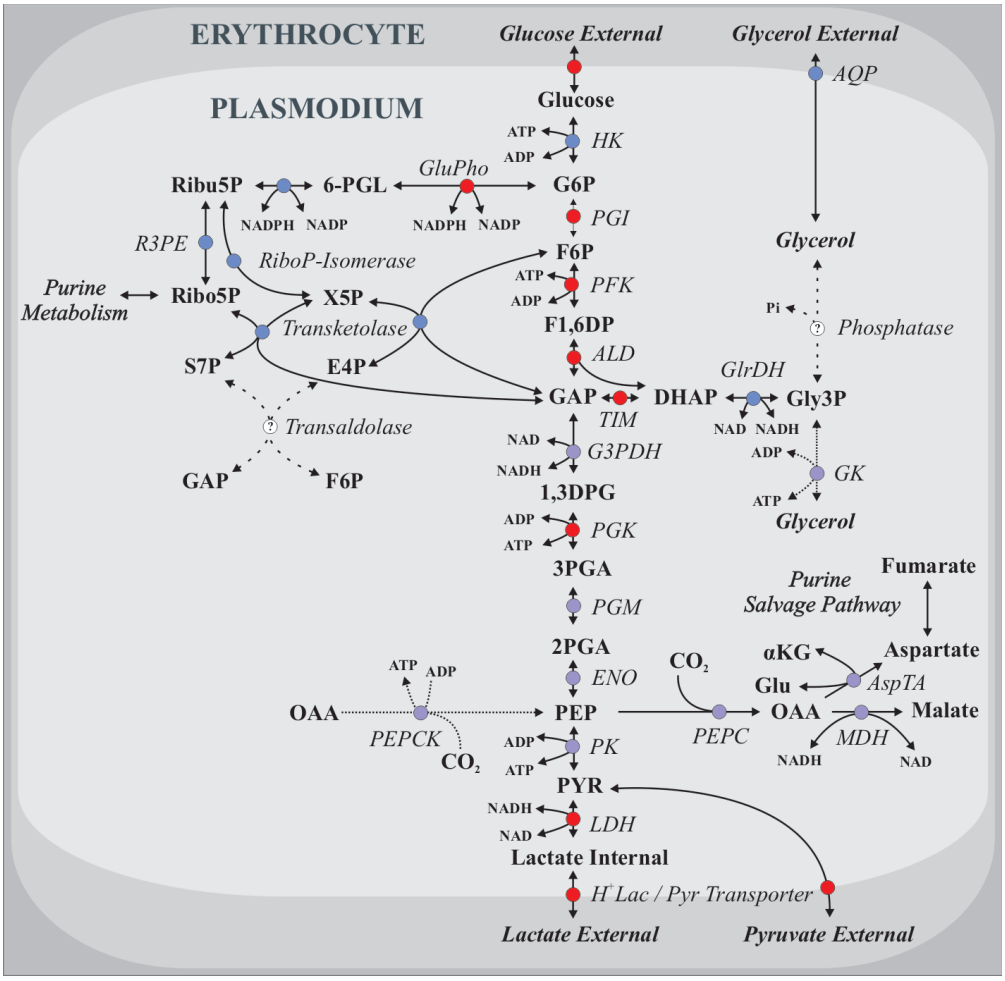

Figure 2.1: Overview of asexual *P. falciparum* central carbon metabolism. Asexual *P. falciparum*, which resides within the host erythrocyte, has a classic glycolytic pathway, a pentose phosphate pathway, a glycerol producing branch and a carbon dioxide fixation branch. Enzyme names are shown in italics and the metabolites and cofactors in bold. Red circles indicate enzymes that have been proposed in scientific literature as drug targets. Finely dashed reaction arrows (GK and PEPCK) represent reactions that do not occur during the asexual phase. The dashed reaction arrows with a question mark (inside a white circle), represent reactions that are thought to occur, but the enzymes that catalyse the reactions are currently unknown. HK, *hexokinase*, PGI, *phosphoglucoisomerase*, PFK, *phosphofructokinase*, ALD, *aldolase*, TIM, *triosephosphate isomerase*, G3PDH, *glyceraldehyde-3-phosphate dehydrogenase*, PGK, *phosphoglycerate kinase*, PGM, *phosphoglycerate mutase*, ENO, *enolase*, PK, *pyruvate kinase*, LDH, *lactate dehydrogenase*, GluPho, *Glucose-6-phosphate dehydrogenase-6-phosphogluconolactonase*, R3PE, *Ribulose-3-phosphate epimerase*, GlrDH, *glycerol-3-phosphate dehydrogenase*, GK, *glycerol kinase*, AspTA, *aspartate transaminase*, MDH, *malate dehydrogenase*, PEPC, *PEP carboxylase*, PEPCK, *PEP carboxy kinase*, AQP, *Aquaglyceroporin*

2.2.0.1 Hexose transport

Asexual *Plasmodium spp.* reside within the host erythrocyte and hexose transport from the serum to the parasite is obtained i) directly via 'new permeation pathways' induced by the parasite[115] and ii) by transporting glucose across the parasite plasma membrane via a hexose transporter, PHT1[222].
Within the erythrocyte, glucose and fructose cross the parasitophorous vacuolar membrane via high-capacity non-selective channels[49] and are then transported across the parasite plasma membrane via a hexose transporter, PHT1[222]. This passive transporter has been expressed in *Xenopus oocytes* and shown to be a saturable, sodium-independent, and a stereospecific transporter of both glucose and fructose[223]. The *P. vivax* and *P. falciparum* transporters, PvHT1 and PfHT1 respectively, have been kinetically characterised[100,101,222,223] as well as those from *P. knowlesi* (simian) and *P. yoelii* (murine)[102]. Immunofluorescence microscopy studies have shown that PfHT1 resides in the parasite plasma membrane and not in the erythrocyte membrane[223] and it has been established that PfHt1 is a single copy gene with no close homologues[223]. Expression of the single PfHt1 transcript varies throughout the *P. falciparum* life cycle with mRNA levels peaking 8-hour post invasion of the erythrocytes.[223].

Inhibition of PfHT1 immediately leads to a decrease in ATP levels[179]. This has prompted a great deal of research (reviewed by Patel *et al.*[155]) focussed on inhibiting the transporter, which has been found to kill asexual parasites as well as vector (mosquito) and liver stage parasites[102,179,100,101,198].

2.2.0.2 Lactate Transport

The parasite transports lactate and pyruvate across the parasite plasma membrane with a lactate-proton cotransporter[44,57]. This saturable transporter that shares many characteristics of the monocarboxylate transporter (MCT) family and also transports pyruvate[57]. The transport of lactate and pyruvate is proton linked with a 1:1 stoichiometry and has been biochemically characterised for *P. falciparum* in terms of its V_{max}, affinity for both pyruvate and lactate, which compete for the same binding site[44,57].

In uninfected erythrocytes, lactate is removed to the blood stream via three

major pathways: (i) a specific H^+ monocarboxylate transporter, (ii) the band 3 anion exchanger, and (iii) by diffusion of the protonated form across the lipid bilayer[115]. The capacity of these transport systems is considered to be insufficient for the removal of the lactate produced by *Plasmodium spp.* glycolysis in parasitised erythrocytes[109,115]. When these transport pathways are inhibited, however, there is still a high lactate flux across the erythrocyte membrane and this has been attributed to anion-selective diffusion pathways in the erythrocyte membrane[44,109,115].

2.2.0.3 Hexokinase

Hexokinase (HK), the first reaction in glycolysis, phosphorylates glucose in an ATP dependent reaction, producing glucose 6-phosphate (G6P) and ADP. In *P. falciparum* the 47 kDa hexokinase protein is coded by a gene on chromosome 8 that is only 26% homologous to human HK[121,143,190]. The total HK activity in *P. berghei* and *P. falciparum* infected erythrocytes is more than 25-fold greater than in uninfected erythrocytes[121,175]. The *P. berghei* enzyme has been biochemically characterised in terms of its affinity for ATP (K_m 2 mM) and glucose (K_m 0.431 mM). The enzyme has not been characterised in terms of its products, which may be relevant from a systems biology perspective as G6P is known to have feedback inhibition in mammalian cells[207] and act as an activator in the filarial roundworm, *Brugia malayi*[195].

2.2.0.4 Phosphoglucoisomerase

Phosphoglucoisomerase (PGI) catalyses the isomerisation of G6P to fructose-6-phosphate (F6P). Interestingly, *P. falciparum* has been reported to possess three or four PGI isozymes[202] with an apparent size of 66 kDa, but it is not known if these are expressed at different stages or differ in terms of their kinetics. A *P. falciparum* gene coding for PGI has been mapped to chromosome 14 and cloned and expressed in *Escherichia coli*[111]. The deduced amino acid sequence has a 34% identity to the human equivalent with the highest degree of similarity in the proposed active sites[111].

2.2.0.5 Phosphofructokinase

Phosphofructokinase (PFK) catalyses the ATP dependent phosphorylation of F6P to form fructose 1, 6-bisphosphate (F1,6BP) and ADP. In *P. berghei*, PFK activity has been found to be fairly insensitive to pH changes, compared to the host erythrocyte PFK which would indicate structural and kinetic differences[182]. Classically, PFK is highly regulated and is potentially inhibited by ATP, phosphoenolpyruvate (PEP), 2,3-bisphosphoglycerate, citrate and activated by AMP, F6P, ADP, F1,6BP and fructose 2,6-bisphosphate (F 2,6BP)[211,22]. Buckwitz *et al.* reported that *P. berghei* PFK is strongly inhibited by ATP and Mg^{2+} ions and is activated by PEP, F6P and inorganic phosphate[22,23,24,25]. Buckwitz *et al.* characterised the murine *P. berghei* enzyme extensively and could describe the kinetic behaviour with a Monod-Wyman-Changeaux type equation. In *P. falciparum*, Mony *et al.* identified putative genes coding for PFK on chromosome 9 and 11, although only the protein from chromosome 9, when expressed in *E. coli* exhibited the appropriate catalytic features[137]. This enzyme has domains that are homologous to a pyrophosphate dependent PFK found in plants. As in *P. berghei*, the *P. falciparum* enzyme is not activated by citrate or F2,6BP, but is insensitive to PEP[137].

2.2.0.6 Aldolase

Aldolase catalyses the aldol-cleavage of F1,6BP into dihydroxyacetone phosphate (DHAP) and glyceraldehyde-3-phosphate (GAP). In contrast to humans which have three aldolase isozymes, *Plasmodium spp.* only has a single gene coding for aldolase which is 50% homologous to its human equivalent.[39,117]. The *P. berghei* and *P. falciparum* genes have been cloned, sequenced and expressed in *E. coli*[51,136]. The homotetrameric enzyme has a molecular mass of 160 kDa[113] and has been kinetically characterised for its substrate F1,6BP[51].

Aldolase activity, which also correlated to mRNA expression levels, varies during the asexual phase, reaching peak activity between 32 and 36 hours (mature trophozoite stage)[99,142,143,219]. Aldolase has been the focus of some drug target discovery studies. Wanidworanun *et al.* reported 50% inhibition of parasitemia in the presence of nanomolar concentrations of phosphorothioate

antisense oligodeoxynucleotides that targeted several sites on the *P. falciparum* aldolase gene[219]. The crystal structure of *P. falciparum* aldolase[113] revealed two distinct differences between the parasite and human enzyme. i) A highly variable tail in the C-terminal region[156], which is essential for enzymatic catalysis[99,52] and i) the so called 290's loop, which forms part of the binding pocket in conjunction with two nearby loops[156]. There may be an interaction between the C-terminal tail and the binding pocket as they are located close together prompting Kim *et al.* to propose that small hydrophobic inhibitors that bind to the binding pocket, and interact with the lysine residues in the C-terminal tail may selectively inhibit the parasite enzyme[113]. The low genetic variation in *Plasmodium spp.* aldolase has been utilised in monoclonal antibody rapid diagnostic kits[114].

2.2.0.7 Triosephosphate isomerase

Triosephosphate isomerase (TIM) catalyses the isomerisation of DHAP to GAP. A single gene coding for TIM is located on chromosome 14. The coding region of the gene is 42 - 45% homologous to TIM genes from other sources, and has been cloned and expressed in *E. coli*[167]. In *P. falciparum* the gene codes for a 28 kDa protein, which has been crystallised and the crystal structure resolved to 2.2 Å [216] and at 1.1 Å in complex with 2-phosphoglycerate[154]. The crystal structures revealed several structural differences to the human enzyme and, for drug target identification, focus was placed on specific amino acid substitutions on the dimer interface[216]. Peptides designed to bind to the dimer interface have been shown to inhibit the enzyme at sub-micromolar concentrations[196] and anionic sulfonated dyes targeting this region have been shown to inhibit the enzyme at concentrations below 100 mM[106]. More detail of the strategies employed to inhibit this enzyme are reviewed in[169] and[156].

2.2.0.8 Glyceraldehyde-3-phosphate dehydrogenase

Glyceraldehyde-3-phosphate dehydrogenase (G3PDH) catalyses the conversion of GAP, P_i and NAD to 1,3-bisphosphoglycerate (1,3BPG) and NADH. In *P. falciparum* G3PDH has been cloned and expressed in *E. coli*[47]. The estimated 36.6 kDa protein has 63.5% identity to the erythrocyte G3PDH[47]. Typically G3PDH exists as a tetramer and is composed of four identical polypeptide

chains[26,47] and for *P. falciparum* the tetrameric enzyme has been crystallised and the crystal structure, with NAD^+ bound to each subunit, resolved to 2.5 Å [184] and 2.25 Å [171]. The asexual malaria parasite degrades haemoglobin during its development, which produces free ferriprotoporphyrin IX (FP) as a toxic product. Certain antimalarials such as chloroquine prevent FP detoxification and it was reported that free FP strongly inhibits *P. falciparum* G3PDH *in vitro* (K_i 0.2 μM)[29]. This finding indicated that in addition to other oxidative damage, metabolism itself may be halted by targeting FP detoxification mechanisms. *Plasmodium spp.* G3PDH has not been extensively biochemically characterised, although its affinity for GAP has been determined[29].

2.2.0.9 Phosphoglycerate Kinase

Phosphoglycerate kinase (PGK) is the first ATP producing enzyme in glycolysis and converts 1,3BPG and ADP to 3-phosphoglycerate (3PGA) and ATP. *P. falciparum* has two 45 kDa PGK isozymes that are distinct from the host enzyme with differing kinetic properties (i.e. K_m, V_{max}), isoelectric points and immunologic epitopes[75]. The gene coding for PGK is 60% homologous to other eukaryotic enzymes and is located on chromosome 9[190]. The enzyme has been biochemically characterised in terms of its substrates[75,148]. Crystal structures of the *P. falciparum* enzyme have been resolved to 3 Å [148] and in two different conformations at 3 Å and 2.7 Å respectively[199]. Some inhibitory studies have been performed and suramin was found to inhibit PGK expressed in *E. coli* with an IC_{50} of 7 μM[148].

2.2.0.10 Phosphoglycerate Mutase

Phosphoglycerate mutase (PGM) catalyses the conversion of 3PGA to 2-phosphoglycerate (2PGA). Two putative genes coding for PGM have been identified in *P. falciparum* and Hills *et al.* crystallised and characterised one of them, PGM2[85]. Interestingly the enzyme could not only utilise 3PGA as a substrate, but could also act as a phosphatase on F6P, F1,6BP, PEP, 3PGA, 2,3-bisphosphoglycerate (2,3BPG) and a number of amino acids[85].

2.2.0.11 Enolase

Enolase catalyses the inter-conversion of 2-phosphoglycerate and phosphoenolpyruvate. The enolase gene has been isolated, characterised and mapped to chromosome 10[151,170]. The gene is 60-70% homologous to other eukaryotic enolase enzymes[170]. The enzyme is a homodimer, with a molecular size of 100 kDa[151]. For activity, *P. falciparum* enolase requires the binding of two divalent cations (Mg^{2+} *in vivo*), per subunit[151]. The binding at site I leads to a conformational change within the enzyme, whereas binding at site II is essential for catalysis[62]. At high concentrations, bivalent cations inhibit enzyme activity[151]. *P. falciparum* enolase is strongly activated by Mg^{2+}, slightly by K^+ and inhibited by Na^+[151]. The enzyme has been dissociated into catalytically functional, but inefficient, monomers with distinct differences compared to the dimer in terms of kinetic behaviour and thermal stability.[149]. It was suggested that the monomeric form may play a role in moonlighting functions. *Plasmodium spp.* enolase, as in many organisms[153], appears to play a role in more than just metabolism. In *P. yoelii* enolase was found to be associated with nuclei, cell membranes and cytoskeletal elements[152] and in *P. falciparum* the enzyme was found localised to the merozoite cell surface[150]. The exact role of the moonlighting functions is unknown in *Plasmodium spp.*, but in other organisms it has been reported, among other functions, to act as a cell surface receptor for plasminogen, act as a heat-shock protein and also as a hypoxic stress protein (see[153] for a review).

2.2.0.12 Pyruvate Kinase

Pyruvate kinase catalyses the substrate level phosphorylation of ADP, using phosphoenolpyruvate and producing pyruvate and ATP. Pyruvate kinase activity was identified in the *P. falciparum* infected human erythrocytes[173] and *P. berghei* infected mice erythrocytes[22]. The enzyme activity appears to increase over 11-fold upon infection[173] and is highly regulated in protozoan parasites, such as *Toxoplasma gondii*, *Trypanosoma brucei* and *Leishmania mexicana*[58,59,131] and *Plasmodium spp.*[35].

P. falciparum has two PK isozymes (PK1 & PK2) and both are expressed during the asexual phase[36]. The isozymes differ in size (56 and 87 kDa), have low amino sequence identity (20%) and PK2 is unique to the Apicomplexans[36].

PK1 expression is continually high during the asexual phase as is thought to be part of the glycolytic pathway. PK2 expression levels peak at 20h post invasion, which coincides with lipid synthesis genes[36]. PK2 and lipid synthesis have been localised to the apicoplast[155,130]. *P. falciparum* PK has been cloned, isolated, kinetically characterised[35]. It is competitively inhibited by ATP with respect to PEP and non-competitively inhibited by citrate[35]. Pyruvate kinase appears not to be activated by F1,6BP[35], which is a common activator in other species[212].

2.2.0.13 Lactate dehydrogenase

Lactate dehydrogenase (LDH) is responsible for the recycling of NAD^+ from NADH by reducing the keto group of pyruvate to a hydroxyl group (lactate). The 33 kDa *P. falciparum* LDH is coded by a single gene on chromosome 13[28]. A wealth of structural and kinetic information is available for human and *Plasmodium spp.* LDH and differences between the enzymes have been highlighted as potential drug targets. The enzyme has been extensively biochemically characterised[21,34,194,221] and proposed to follow an ordered bi-bi mechanism with the coenzyme binding first[194].

The crystal structures of *P. berghei*, *P. vivax* (in complex with NADH and 3-acetylpyridine adenine dinucleotide (APADH)), *P. brucei* and *P. falciparum* LDH have all been determined[221,21,34]. The structures are all highly similar and it is thus likely that inhibitors targeting malarial LDH would be effective across the Plasmodia genus[34]. Structural differences between human and *Plasmodium spp.* LDH are few, but key differences are a shift in the positioning of the NADH cofactor and a larger active site due to a five amino acid extension of the substrate-binding loop[20,54,135].

Inhibition of LDH has been shown to kill the parasite[176] and numerous studies have focussed on inhibiting this enzyme. The cofactor binding site has been largely targeted. Gossypol, a polyphenolic binaphthyl disequiterpene found in cottonseed, binds competitively to LDH with respect to NADH and inhibits LDH *in vitro* at submicromolar (0.7 μM) levels[176] and displays anti-malarial activity *in vitro*[73], with an IC_{50} of 10 μM[20]. Napthoic acid based compounds, such as 2,6-dicarboxy naphthalene, have been shown to span across the LDH active site and NADH binding pocket[20]. Docking studies of compounds structurally similar to NADH, identified posaconazole as a potential drug, and it

inhibited *P. falciparum in vitro* and *P. berghei in vivo*[159].

2.2.0.14 Kinetic Parameters Present in Scientific Literature

Many of the glycolytic enzymes for *Plasmodium spp.* have been fully or partially characterised and the published kinetic parameters that were obtained during the scientific literature study are summarised below in Table 2.1.

Table 2.1: Summary of kinetic parameters present in scientific literature for the glycolytic enzymes of *Plasmodium spp.*.

Enzyme	Metabolite	K_m (mM)			Reference
Hexokinase	Glucose [1]	0.43	ATP	2.0	143,175
Phosphoglucoisomerase	F6P [2]	0.26	-		202
Phosphofructokinase	F6P	0.032	ATP	0.72	24,23,22
Aldolase	F1,6BP	0.020	-		51
Triosephosphate Isomerase	GAP	0.35	-		196
Triosephosphate Isomerase	GAP	0.39	-		70
Triosephosphate Isomerase	DHAP	0.59	-		196
Glyceraldehyde 3 PDH	GAP	1.0	-		29
Phosphoglycerate Kinase	3PGA	1.9			75
Phosphoglycerate Kinase	ADP	0.30	BPG	0.013	148,174
Phosphoglycerate Kinase	ATP	0.63	3PGA	0.52	148,174
Phosphoglycerate Mutase	3PGA	0.85	2,3BPG	4.2	85
Enolase	2PGA	0.041	PEP	0.25	151
Pyruvate Kinase	PEP	0.34	ADP	0.15	35
Lactate Dehydrogenase	PYR	0.030	NAD	0.086	73
Lactate Dehydrogenase	LAC	12	NADH	0.0070	73
Lactate Dehydrogenase	PYR	0.055	NAD	0.18	194
Lactate Dehydrogenase	LAC	47	NADH	0.011	194
Glucose Transporter, PfHT1	GLC	0.48	GLC	1.0	223,222,102
Monocarboxylate Transporter	LAC	3.8	PYR	16	57

[1] *Binding constant determined from lysed malaria parasite-infected erythrocytes and is a function of both Plasmodium and erythrocyte enzyme binding.*

[2] *Average value of three isozymes shown. Standard deviation of the mean is 0.026*

2.2.1 Tricarboxylic Acid Cycle

The classic TCA cycle occurs in the mitochondrion under aerobic conditions and utilises acetyl-CoA derived from glycolytic pyruvate. Acetyl-CoA combines with oxaloacetate, to produce citrate, which is subsequently catabolised in several reactions to produce CO_2, NADH, $FADH_2$, GTP, and ultimately regenerate oxaloacetate. NADH and $FADH_2$ are used as electron donors in the electron transport chain (ETC) to generate ATP. Experimentation and analysis of the *Plasmodium spp.* genome has revealed all classic or equivalent TCA enzymes (reviewed in[214]). However, in *asexual Plasmodium spp.* the cycle does not function in a typical fashion as there is not a direct link between glycolysis and the TCA cycle via the pyruvate dehydrogenase complex (PDH). Typically the PDH complex supplies the TCA cycle with acetyl-CoA derived from pyruvate, but in *Plasmodium spp.* the complex is located in the apicoplast[67]. This has been confirmed by reports that radioactive glucose fed to *P. falciparum* infected erythrocytes is converted predominantly to lactate with minimal conversion to TCA intermediates or acetyl-CoA[9,27,145]. The PDH complex in the apicoplast prevents the supply of acetyl-CoA to the TCA cycle and is thought to play a role in lipid biosynthesis[67] and acetylation of amino sugars[145]. Another possible source of acetyl-CoA is from the β-oxidation of fatty acids, but this does not appear to occur in *Plasmodium spp.*[214].

The architecture of the pathway appears to be unique in that it is branched rather than cyclic with a reductive (produces NADH) and an oxidative branch (produces NADPH). In *P. falciparum* it appears that several enzymes function in reverse to produce the large majority of acetyl-CoA from the amino acids glutamate and glutamine, which are deaminated to yield α-ketoglutarate[145]. A small fraction of acetyl-CoA is derived from glucose and is used to acetylate amino sugars[145,146]. This latter reaction occurs in the apicoplast where glycolytic PEP is converted to acetyl-CoA via PK2 and the PDH complex. In labelled uptake experiments that majority of acetyl-CoA was used for histone acetylation[145].

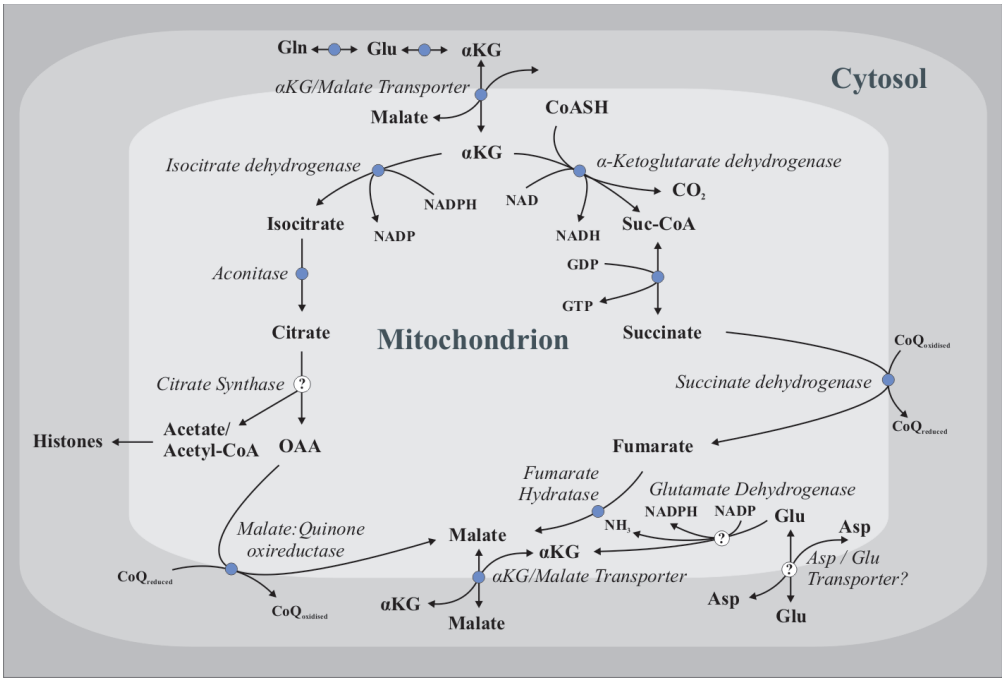

Figure 2.2: Overview of asexual *P. falciparum* tricarboxylic acid cycle. Asexual *P. falciparum* has a branched TCA cycle and obtains the carbon required for acetyl-CoA from glutamine and glutamate. Question marks inside a white circle represent reactions that are thought to occur, but it is not certain which enzymes catalyse them.

2.2.2 Pentose Phosphate Pathway

During the asexual phase, *Plasmodium spp.* is engaged in intensive nucleotide synthesis and is subjected to endogenously produced oxidative radicals, which necessitates the reducing potential of NADPH[18]. The pentose phosphate pathway (Fig. 2.1.) is essential for the production of NADPH, nucleotides and for the NADP dependent detoxification of oxidative radicals. The pathway can be divided into an oxidative and non-oxidative branch:

2.2.2.1 Oxidative Branch

The oxidative branch, which is the first part of the pathway, utilises G6P from glycolysis and produces two molecules of NADPH and ribulose-5-phosphate. Isomerisation of the latter, by ribose phosphate isomerase or ribulose-phosphate-3-epimerase, yields ribose-5-phosphate and xylulose-5-phosphate, respectively. The typical branch consists of three enzymes: glucose-6-phosphate-dehydrogenase (G6PD), 6-phosphogluconolactononase (6PGL) and 6-phosphogluconate de-

hydrogenase[18], but in *P. falciparum* the first two enzymes are combined in a single bifunctional G6PD-6PGL (GluPho) enzyme[38].

2.2.2.2 Non-oxidative Branch

The non-oxidative branch of PPP is primarily for the production of 3, 5 and 7-carbon sugars, that can be used for biosynthetic purposes, or form part of glycolysis for ATP production. Transketolase catalyses the first reaction of the non-oxidation branch, which is the conjunction of ribose-5-phosphate and a 2-carbon fragment from xylulose-5-phosphate. This reaction yields sedoheptulose-7-phosphate and GAP[18]. The second reaction, catalysed by transaldolase, involves the transfer of three carbons from sedoheptulose-7-phosphate to GAP, yielding erythrose-4-phosphate and fructose-6-phosphate[18]. Transketolase catalyses a further reaction where another molecule of xylulose-5-phosphate donates two carbon atoms to erythrose-4-phosphate, yielding an additional molecule of GAP and F6P.
The non-oxidative pathway can function in reverse, utilising GAP and F6P from the glycolytic pathway to produce ribose-5-phosphate (R5P) and this has been shown to occur in G6PD-deficient parasites by measuring the incorporation of [1-^{14}C] glucose into nucleotides[6].

2.2.2.3 Link to the Oxidative Defence

The PPP, and more specifically the production of NADPH, is essential for the parasite defence mechanisms against reactive oxygen species (ROS). During the asexual phase, haemoglobin is degraded, providing amino acids and sufficient space for parasite growth[11]. The degradation of haemoglobin occurs in the acidic food vacuole and produces a toxic free oxidised haem (ferri / ferro-protoporphyrin IX; FP) as well as ROS. The acidic environment oxidises the FP from the Fe (II) to Fe (III) state, which results in production of superoxide that dismutates to hydrogen peroxide and oxygen[11]. Both FP and H_2O_2 required detoxification and for FP this is facilitated by biomineralisation, a process where FP is converted into a crystalline form, known as haemozoin. Glutathione (GSH) and thioredoxin-dependent proteins play an integral role in the detoxification of peroxides. These proteins are oxidised by peroxides, which are converted to H_2O and O_2 in the process. The oxidised proteins are reduced again by NADPH, thus producing a continuous detoxification mech-

anism, as long as the PPP provides sufficient NADPH.

Despite the importance of the PPP for the survival of the parasite, research aimed at inhibiting enzymes in the pathway is limited and in comparison to the vast amount of information existing for the glycolytic pathway, structural and kinetic data for the PPP is sparse.

2.2.3 Pentose Phosphate Pathway Enzymes

2.2.3.1 Glucose-6-phosphate dehydrogenase-6-phospho-glucono-lactonase

Early reports suggested that asexual malaria parasites did not possess a glucose 6-phosphate dehydrogenase (G6PD) and that they depended on the host erythrocyte for NADPH. However, G6PD was found in *P. berghei* and the parasite enzyme was found to account for 5% of the total G6DP present in infected cells[25]. Yoshida and Roth partially purified and biochemically characterised *P. falciparum* in G6PD deficient erythrocytes[226] and the enzyme was also later purified by others[122,127]. The *P. falciparum* gene coding for G6PD, located on chromosome 14, was cloned and expressed[140,189]. The enzyme with an estimated molecular mass of 450 kDA[140] exists as a homodimer or homotetramer[9].

Compared with the human enzyme, the N-terminal region of the parasite protein has an additional 286 to 310 amino acid extension, which is rich in hydrophilic and charged residues[38]. This extension had no homology to other G6PD enzymes, but was homologous to a protein that is encoded near to the G6PD gene in *Haemophilus influenzae*, which suggested that it might encode an alternative PPP enzyme[23,187]. The homologous human cDNA was shown to encode for 6-phospho-glucono-lactonase (6PGL) activity[40], which led Clarke *et al.*[38] to test for 6PGL. It was shown in *P. berghei* that the N-terminal has 6PGL activity, while the C-terminal region has G6PD activity[38].

The bifunctional enzyme is unique and the G6PD-6PGL (GluPho) enzyme oxidises the first carbon of G6P to a lactone, which is linked to the reduction of $NADP^+$ to NADPH. The resulting glucono-1,5-lactone-6 is converted to 6-phospho-gluconate by the PGL activity of the N-terminal. The 6-phospho-

gluconate is decarboxylated and oxidised by G6PD, yielding R5P, a molecule of CO_2 and NADPH. Jortzik *et al.*[104] cloned, overexpressed and kinetically characterised the G6PD and 6PGL activity of the complete purified enzyme in detail. The bifunctional enzyme was reported to follow a random order bi-bi mechanism[104].

GluPho presents a favourable drug target, as its inhibition would prevent the production of NADPH, which is expected to induce severe oxidative stress in the parasite[166]. It has been shown that RNA mediated silencing of the GluPho gene arrested the parasite in the trophozoite stage and promoted the formation of gametocytes[46]. Preuss *et al.*[162,161] specifically targeted GluPho in a high throughput approach and tested over 34 000 compounds *in vitro*. A lead compound[162,161] was identified that achieved submicromolar inhibition and also has good drug-like qualities in terms of solubility and stability.

2.2.3.2 6-Phosphogluconate dehydrogenase

6-Phosphogluconate dehydrogenase (6PGDH) catalyses the decarboxylation and oxidation of 6-phospho-gluconate, yielding R5P, a molecule of CO_2 and NADPH. The activity of 6PGDH has been detected indirectly and presumed to be present in *Plasmodium spp.*[66,206]. A putative gene coding for the enzyme was identified in *P. falciparum*[18], and it was shown that chloroquine induced accumulation of FP inhibits the enzyme[63].

2.2.3.3 Transketolase

Transketolase catalyses two reactions, i) where xylulose 5-phosphate donates 2 carbon atoms to erythrose-4-phosphate, yielding GAP and F6P and ii) where xylulose-5-phosphate and ribulose-5-phosphate are converted to GAP and sedoheptulose-7-phosphate. The gene coding for transketolase has been identified in *P. falciparum*[18] and the enzyme has been expressed, purified and biochemically characterised[105]. The hexameric enzyme has low homology to the host enzyme and consists of subunits with a molecular mass of approximately 70 kDa. Confocal microscopy results indicate that the enzyme is located in both the cytoplasm and nucleus of the asexual parasite[105]. The enzyme can utilise both F6P and hydroxypyruvate as substrates and is strongly inhibited by p-hydroxyphenylpyruvate.

2.2.3.4 Transaldolase

Typically the transaldolase reaction involves the transfer of 3 carbons from sedoheptulose-7-phosphate to GAP, yielding erythrose-4-phosphate and F6P. Surprisingly, the gene that codes for transaldolase could not be found in the genome of any *Plasmodium spp.* species, although biochemical evidence suggests the presence of a functional non-oxidative branch[18]. It may be possible that a novel enzyme performs the same function or as Joshi *et al.* suggested, perhaps transketolase produces erythrose 4-phosphate alone or in conjunction with another enzyme .

2.2.3.5 Ribose-phosphate isomerase

Ribose-phosphate isomerase catalyses the interconversion of ribose-5-phosphate and ribulose-5-phosphate. The gene coding for ribose phosphate isomerase has been identified in *P. falciparum*[18] and the enzyme has a low (35%) sequence identity to the human enzyme. The crystallised enzyme suggested a dimer, although in eukaryotes it exists as a tetramer[92]. The enzyme has not been biochemically characterised.

2.2.3.6 Ribulose-phosphate 3-epimerase

Ribulose-phosphate-3-epimerase catalyses the isomerisation of ribulose-5-phosphate and xylulose-5-phosphate. In *P. falciparum* the ribulose-phosphate 3-epimerase gene[18] codes for a dimeric protein with a classic TIM-barrel fold[32]. The *P. falciparum* enzyme has been crystallised and the crystal structure with a co-ordinated Zn^{2+} and sulphate ion bound in the active site was resolved to 2 Å [32].

2.2.4 Ancillary pathways

The malarial parasite has several supplementary pathways, such as glycerol production, carbon dioxide fixation and purine salvage pathways. The role of glycerol production and carbon fixation is unclear at present, but they are essential for parasite survival. The purine salvage pathways supply free amino acids, keto acids and organic acids to the parasite, but are not discussed in this review.

2.2.4.1 Glycerol Production

The production of glycerol by asexual *P. falciparum* was discovered by Lian *et al.*[125], indicating the presence of a glycerol producing pathway where presumably glycerol is produced from DHAP. Lian *et al.* suggested the existence of a shuttle consisting of a cytosolic glycerol-3- phosphate dehydrogenase and mitochondrial glycerol-3-phosphate:ubiquinone oxidoreductase, which would convert DHAP to glycerol 3-phosphate (G3P) and in the process oxidise NADH. It is not known, however, how glycerol is produced from G3P. In *P. falciparum* glycerol kinase is expressed, but not during the asexual stage; disruption of this gene does not inhibit growth and development of the asexual parasite[186]. Furthermore, no putative genes for glycerol 3- phosphatase have been identified in the *P. falciparum* genome[69]. The ability of the *P. falciparum* PGM isozyme to act as a phosphatase (discussed previously) on a wide variety of substrates may provide an alternative enzyme[85] to produce glycerol. The role of glycerol in asexual *Plasmodium spp.* is unclear, but what has not been considered previously is that asexual *Plasmodium spp.* glycolysis is not redox neutral. Both lactate and more importantly pyruvate are transported out of the parasite via the same monocarboxylate transporter[57]. The loss of pyruvate, prevents the oxidation of NADH via lactate dehydrogenase and consequently the parasite requires an alternative pathway such as the production of glycerol and consequent oxidation of NADH to maintain redox balance.

2.2.4.2 Carbon dioxide fixation

P. lophurae[208,191], *P. knowlesi*[192], *P. falciparum*[188] and *P. berghei*[139] have all been shown to incorporate $^{14}CO_2$ into oxaloacetate, α-ketoglutarate, glutamate, aspartate, malate and citrate. Phosphoenolpyruvate carboxylase (PEPC) and PEP carboxy kinase (PEPCK) are present in *P. berghei*[197].

PEPCK is normally involved in gluconeogenesis and converts oxaloacetate and ATP to PEP and ADP. Compared to asexual stages, the enzyme has been shown to be highly expressed in gametocytes and zygotes, suggesting that during these stages gluconeogenesis is initiated in preparation for conditions experienced in the mosquito host[81]. Further evidence that the enzyme is not active during the asexual phase is provided by the observation that

parasites supplied with ^{13}C labelled aspartate do not produce labelled PEP, pyruvate or lactate[146,145].

Activity of PEPC, which carboxylates PEP to form oxaloacetate and inorganic phosphate results in the loss of 1 mol ATP per mol glucose incorporated into glycolysis. This enzyme is active during the asexual phase as evidenced by the incorporation of $^{14}CO_2$ into a variety of amino and keto-acids[146,145]. A 280 kDa PEPC has been purified and characterised for *P. berghei* in terms of its affinity for PEP (K_m 2.6 mM), bicarbonate (K_m 2.0 mM) and Mg^{2+} (K_m 1.3 mM)[134].

The role of carboxylation in *Plasmodium spp.* central carbon metabolism is unclear. It does utilise some of the glycolytic intermediates (i.e. PEP) and cost 1 mol ATP per mol carbon dioxide fixated. However, the finding of an almost 2:1 ratio of mol lactate[190] produced to mol glucose consumed indicates that the flux through the pathway is low and probably does not have much influence on the energy metabolism, but may be important for anabolism.

2.3 Summary

This review has summarised what is currently known in the scientific literature about the central carbon metabolism in asexual *Plasmodium spp.* with specific focus on i) network topology and information that may be useful in constructing a kinetic model of the central carbon metabolism and ii) studies focussed on the inhibition of the individual enzymes.

The network structure of the central carbon metabolism of *Plasmodium spp.* is different from many organisms in that, although gylcolysis and the TCA cycle are present, the TCA cycle does not contribute towards ATP production. The localisation of the PDH complex to the apicoplast prevents the formation of acetyl-CoA derived from glycolytic pyruvate. Consequently the parasite is entirely dependent on glycolysis for ATP and makes the pathway an attractive drug target. The TCA cycle instead follows a branched structure and utilises amino acids (glutamine and glutamate) to generate acetyl-CoA. The pentose phosphate pathway is similar to the structure found in other organisms, al-

though the enzyme that catalyses the transaldolase reaction is unknown. The role of the glycerol production branch is unknown, although we hypothesise it to be essential for balancing the redox imbalance produced by the transport of pyruvate out of the parasite. The reason why the carbon dioxide fixation pathway is essential for the asexual parasite is unclear, as it does not contribute much to the TCA cycle and the majority of carbon channelled from glycolysis through this pathway is exported in the form of malate[146,145].

The distinct separation of glycolysis and the TCA cycle would suggest that a kinetic model aimed at identifying drug targets in the parasite energy (i.e. ATP) metabolism would not need to include the TCA cycle or carbon dioxide fixation branch, although the integration of each of these pathways may provide insight into the function of the TCA cycle.

Many of the glycolytic enzymes have been biochemically characterised in part (i.e. for one substrate or product), but apart from PFK, which has been extensively biochemically characterised in *P. berghei* in terms of its allosteric regulation, none of the glycolytic enzymes have been characterised in detail for allosteric regulation. The incomplete kinetic data set for glycolysis is a starting point for the construction of a kinetic model and could be supplemented with kinetic data obtained for enzymes in other organisms. For a kinetic model, constructed as a tool for analysing pathway behaviour *in vivo*, the enzyme parameter values should reflect those found in the parasite (i.e. kinetic parameters should have been determined under conditions similar to those found in the parasite). In the scientific literature, however, most of the enzymes were biochemically characterised in the presence of contaminating erythrocyte enzymes, or in a purified form under ideal conditions (e.g. pH, ionic strength). Thus it was decided that for the study presented in this thesis, kinetic parameters (and assay methods) in scientific literature for *P. falciparum* glycolysis would be used as reference values for further experimental characterisation. By following the approach of van Eunen *et al.*[215] who characterised each of the glycolytic enzymes in yeast lysates under the same conditions (set to reflect intracellular conditions *in vivo*), a more complete set of kinetic data for *P. falciparum* can be obtained. In Chapter 3 we describe the kinetic characterisation of the glycolytic enzymes and integrate the kinetic rate equations

into a kinetic model for *P. falciparum* glycolysis.

Many of the glycolytic and some of the PPP enzymes have been proposed as drug targets. A kinetic model constructed from some of the kinetic data obtained from this scientific literature study as well as from additional experimental characterisation studies, may provide insight into which of these drug targets are the most favourable.

Chapter 3

Construction of a detailed kinetic model of asexual *Plasmodium falciparum* glycolysis, Part 1: Enzyme Kinetics & Construction

Penkler, G.P[1]., Rautenbach, M., Snoep, J.L.

3.1 Introduction

The central carbon metabolism of *Plasmodium* has been intensely studied to understand the metabolic link between host and parasite and to discover potential drug targets. *P. falciparum* is dependent on glycolysis for ATP[193] and the parasite does not store any reduced carbon reserves[156,190]. Because of the essential role of ATP in the energy metabolism, glycolysis and numerous enzymes within it have been suggested as targets for novel antimalarials. However, the enzymes have been studied and examined in isolation, not taking into account the metabolic pathway as a whole.

One may think that it is not important which of the glycolytic enzymes is inhibited, because as long as the enzyme is inhibited strongly enough it will block glycolysis effectively. However, for such an inhibitor to be a good drug it is important that it does not significantly inhibit the host's glycolysis. As such it would be important to identify reaction steps in the parasite whose inhibition leads to a drastic decrease in glycolysis (i.e. enzymes with a high flux control). Additionally, if the homologous step in the host has a low flux control it would be possible to selectively inhibit the parasite's glycolysis, even if the drug does not differentiate between the parasite and host target enzyme.

[1]Part of the biochemical characterisation of the glycolytic enzymes was presented in my M.Sc. thesis.[158]. Here we present a full characterisation, which includes completely new analysis of HK, PFK, TPI, G3PDH and PGK.

To identify which of the enzymes in glycolysis have a high flux control it is necessary to analyse the system as a whole. In this study we outline the construction of a detailed kinetic model of *P. falciparum* glycolysis, which would enable the analysis of the entire system.

The central carbon metabolism of *Plasmodium falciparum* consists of glycolysis, the pentose phosphate pathway and a glycerol production pathway. The tricarboxylic acid cycle is not directly linked to glycolysis as the pyruvate dehydrogenase complex is localised in the apicoplast and does not contribute much acetyl-coA to the tricarboxylic acid cycle. Instead the TCA cycle utilises primarily glutamine and glutamate as carbon sources[145]. Although a modified form of the TCA cycle exists, it is not considered as part of the central carbon metabolism. It was initially thought that *P. falciparum* glycolysis was homolactic, which supported the finding of an almost 2:1 ratio of mole lactate produced per mole glucose[190]. However, this is inconsistent with several findings, such as pyruvate being transported out of the cell[57], which prevents the recycling of NADH to NAD^+. The production of glycerol by asexual *P. falciparum* was reported by Lian *et al.*[125], which indicates the presence of a glycerol producing pathway. The presence of this oxidative pathway could counter the redox imbalance caused by pyruvate excretion. The pentose phosphate pathway flux is low in asexual *P. falciparum*, although it is thought to play an essential role in the oxidative defence system[190,11].

Some of the glycolytic enzymes have been kinetically characterised for a variety of *Plasmodium* species, with many characterised as pure enzymes (after cloning, expression and isolation) under optimal conditions. Ideally, all of the kinetic parameters should be determined under physiologically relevant conditions. In order to examine the glycolytic pathway as a whole, we employed the bottom up approach of van Eunen *et al.*[215] in yeast, where each of the glycolytic enzymes were characterised under conditions (e.g. pH, ionic strength, temperature) which mimicked those found in the yeast cytosol.

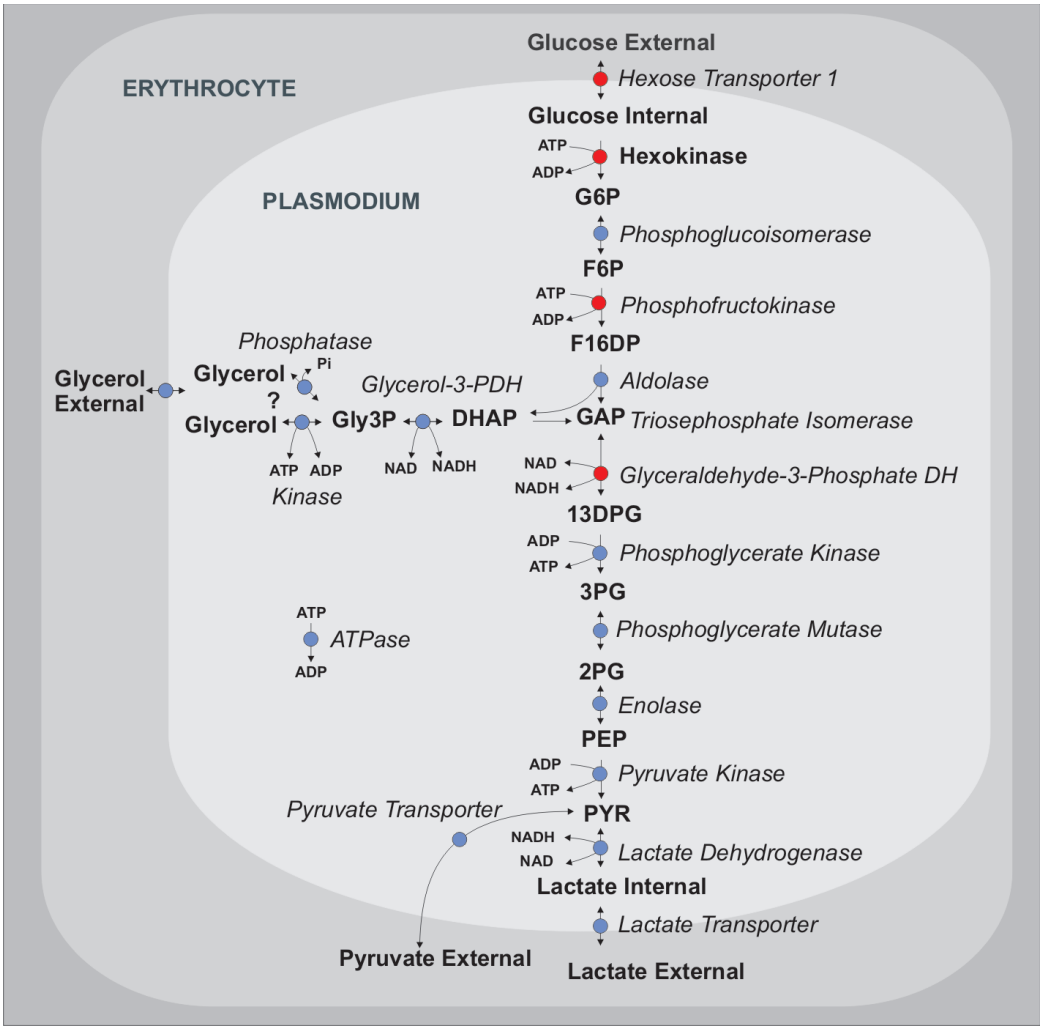

Figure 3.1: Overview of asexual *P. falciparum* glycolysis. The asexual parasite has a classic glycolytic pathway as well as a glycerol producing branch. The enzyme names are in italics and the metabolites shown in bold font. Red circles indicate enzymes that have been proposed as drug targets in scientific literature. It is not certain which enzyme produces glycerol during the asexual phase and this is indicated by a question mark.

In this study we test if our biochemical knowledge (i.e. enzyme kinetics) of *P. falciparum* glycolysis can describe the pathway in terms of fluxes and metabolite concentrations found in the parasite. We follow an approach that is similar to a study on yeast by Teusink *et al*[205]. Firstly we present the biochemical characterisation of each of the glycolytic enzymes and describe the

kinetic behaviour with a mechanistic kinetic equation. Each of these equations is integrated into an ordinary differential equation (ODE) based model. The steady state (i.e. fluxes and metabolite concentrations) of the kinetic model is analysed. This systematic bottom up approach to modelling a metabolic pathway provides a strong foundation for constructing a kinetic model to improve our understanding the pathway and for drug target identification. We also present the model on an open source database (JWS Online[144,201]), which allows users to analyse the model and have access to the kinetic datasets and rate equations.

3.2 Methods

3.2.1 Culturing and synchronisation of *P. falciparum*

Packed human erythrocytes (A^+, obtained from the Western Province Blood Bank, South Africa) were infected with *P. falciparum* D10 and incubated with 3% oxygen, 4% carbon dioxide and 93% nitrogen at 37 °C in RPMI 1640 culture medium supplemented with 0.5% *m/v* Albumax II $^{(R)}$, 22 mM glucose, 25 mM HEPES, 3 mM hypoxanthine, 25 mM sodium bicarbonate and 50 μg/mL gentamycin sulphate as described elsewhere[45,209].

Parasite cultures were synchronised by suspending pelleted infected erythrocytes (750 $\times$ *g*, 3 min), in a 5% *m/v* sorbitol solution and incubating the suspension at 37°*C* for 5 min as described by Hoppe *at al.*[97]. Following further centrifugation the infected erythrocytes were cultured as described above. Sorbitol treatment leaves the erythrocytes intact, but destroys all but ring stage parasites. After sorbitol treatment, the suspensions were centrifuged and cultured as described above.

3.2.2 Trophozoite Isolation and Lysate Preparation

Trophozoites (36 - 40 hours post invasion) were isolated from the erythrocyte using a saponin lysis protocol[178]. Saponin permeabilises the erythrocyte and parasitophorous vacuolar membranes by interacting with cholesterol found in these membranes[3,4], but leaves the parasite plasma membrane intact and able to maintain a transmembrane ion gradient and a substantial membrane po-

tential[178,177]. Greater than 95% of parasites ,isolated in this manner, maintain the ability to exclude 0.04% *v/v* trypan blue[177].

After washing isolated trophozoites twice in assay buffer, lysates were prepared by three freeze - thaw cycles between liquid nitrogen and room temperature. The lysis protocol was optimised by the inclusion of a 30 second sonication step between freeze-thaw cycles. After centrifugation (10 000 ×g , 10 min), the supernatant was retained and used for kinetic determinations. Lysates were prepared before enzyme kinetic assays and kept on ice.

3.2.3 Enzyme Characterisation

For reference each of the enzyme abbreviations are defined as follows: HK, *hexokinase*; PGI, *phosphoglucoisomerase*; PFK, *phosphofructokinase*; ALD, *aldolase*; TIM, *triosephosphate isomerase*; G3PDH, *glyceraldehyde 3-phosphate dehydrogenase*; PGK, *phosphoglycerate kinase*; PGM *phosphoglycerate mutase*; ENO, *enolase*; PK, *pyruvate kinase*; LDH, *lactate dehydrogenase*; αGlyPDH, *glycerol 3-phosphate dehydrogenase*; G6PDH, *glucose 6-phosphate dehydrogenase*

Each of the metabolites is abbreviated as follows: G6P, *glucose 6-phosphate*; F6P, *fructose 6-phosphate*; F1,6BP *fructose 1,6-bisphosphate*; DHAP, *dihydroxy acetone phosphate*; GAP, *glyceraldehyde 3-phosphate*; B1,3PG, *bis 1,3-phosphoglycerate*; 3PGA, *3-phosphoglycerate*; 2PGA, *2-phosphoglycerate*; PEP, *phosphoenolpyruvate*; PYR*pyruvate*; LAC*lactate*; GLC*glucose*

Each of the glycolytic enzymes were characterised in cell lysates in terms of their maximal specific activity (V_{max}) and affinity for each substrate and product. The NADH/NAD^+/$NADP^+$ linked enzyme assays used were adapted from Teusink *et al.*[205]. These oxidation/reduction assays were measured at 340 nm in 96-well plates (*Greiner* bio-one Flat Bottom microplate) on a spectrophotometer (VarioSkan microplate reader, *Thermo Electron Corporation*). The assay buffer, 20 mM HEPES, 20 mM MgCl, 10 mM KCl and 20 mM NaCl, included a high magnesium concentration to ensure that ATP was predominantly in the active MgATP form. The pH of the assay buffer was set to 7.17, matching the cytosolic pH of *P. falciparum* D10[224]. All of the link-

ing enzymes were used at a final concentration of 5 U/mL. For each assay a control was used to ensure that the linking reactions were not rate limiting. For bisubstrate reactions, saturating concentrations of one substrate was maintained while varying the concentration of the other in the presence or absence of product. All reagents and enzymes were obtained from *Sigma-Aldrich*.

HEXOKINASE (HK): The enzyme was characterised in the forward direction in terms of glucose (0 -10 mM) and ATP (0 - 10 mM) and inhibition by ADP (0 - 20 mM) by linking the production of G6P to the reduction of $NADP^+$ (0.8 mM) via G6PDH. Product inhibition by G6P (0 - 30 mM) was characterised by linking the production of ADP to the oxidation of NADH (0.8 mM) via LDH and PK in the presence of PEP (2 mM).

PHOSPHOGLUCOISOMERASE (PGI): The conversion of G6P (0 - 35 mM) to F6P was linked to the oxidation of NADH (0.8 mM) via αGlyPDH, ALD, TPI, PFK in the presence of ATP (2 mM). The reverse isomerisation of F6P (0 - 2.5 mM) to G6P was linked to reduction of $NADP^+$ (0.8 mM) via G6PDH.

PHOSPHOFRUCTOKINASE (PFK): The phosphorylation of F6P (0 - 30 mM) by ATP (0 - 10 mM) as well as inhibition by ADP (0 - 5 mM) was linked to the oxidation of NADH (0.8 mM) via αGlyPDH, ALD, TPI. Product inhibition by F1,6BP (0 - 60 mM) was assayed by linking the production of ADP to the oxidation of NADH (0.8 mM) via LDH, PK in the presence of PEP (2 mM). Since PFK exhibited substrate inhibition, the enzyme rates could not be normalised to maximal specific activity at saturating substrate concentrations. A control rate was determined at 1.25 mM ATP and 1 mM F6P.

ALDOLASE (ALD): The reaction was characterised in terms of its substrate F1,6BP (0 - 0.8 mM) by linking the production of DHAP to the oxidation of NADH (0.8 mM) via αGlyPDH in the presence of excess TPI.

TRIOSEPHOSPHATE ISOMERASE (TPI): The isomerase reaction was assayed in both directions via αGlyPDH or G3PDH in the presence of NADH (0.8 mM) and GAP (0 - 1.2 mM) or NAD^+ (0.8 mM), KH_2PO_4 (10 mM) and DHAP (0 - 15 mM) respectively.

GLYCERALDEHYDE 3-PHOSPHATE DEHYDROGENASE (G3PDH): The forward assay included NAD^+ (0 - 2.5 mM), GAP (0 - 5 mM) and KH_2PO_4 (10 mM) and the reverse reaction included NADH (0 - 0.8 mM) and 3PGA (0 - 2.5 mM). Since the product B1,3PG is chemically unstable with a short half-life and not commercially available, 3-phosphoglycerate was used together with PGK and ADP to produce B1,3PG. Complete and immediate conversion by PGK is assumed to validate the B1,3PG concentration.

PHOSHOGLYCERATE KINASE (PGK): The kinase reaction was assayed in the reverse direction by linking the production of B1,3PG from ATP (0 - 5 mM) and 3PGA (0 - 10 mM) in the presence of ADP (0 - 10 mM) to the oxidation of NADH (0.8 mM) via G3PDH.

PHOSHOGLYCERATE MUTASE (PGM): The conversion of 3PGA (0 - 10 mM) to 2PGA was linked to the oxidation of NADH (0.8 mM) via LDH, PK, ATP (2 mM) and ENO. The reverse reaction (2PGA 0 - 20 mM) was linked to NADH (0.8 mM) oxidation by G3PDH via PGK and ATP (2 mM).

ENOLASE (ENO): The forward conversion of 2PGA (0 - 5 mM) to PEP was linked to NADH oxidation by LDH via PK and ADP (2mM) and reverse conversion of PEP (0 - 12 mM) to 2PGA was linked to NADH (0.8 mM) oxidation by G3PDH via PGM, PGK and ATP (2 mM).

PYRUVATE KINASE (PK): The phosphorylation of ADP (0 - 5 mM) by PEP (0 - 5 mM) was characterised in the presence of ATP (0 - 5 mM) by linking the reaction to NADH oxidation by LDH and in the presence of pyruvate (0 - 100 mM) by linking the production of ATP to the reduction of $NADP^+$ (0.8 mM) via G6PDH, HK and glucose (10 mM). Since PK exhibited substrate inhibition, the enzyme rates could not be normalised to maximal specific activity at saturating substrate concentrations. A control rate was determined at 1.25 mM PEP and 0.625 mM ADP.

LACTATE DEHYDROGENASE (LDH): The enzyme was characterised for the forward oxidation of NADH (0 - 0.8 mM) by pyruvate (0 - 2.5 mM) and

the reverse reduction of NAD^+ (0 - 2 mM) by lactate (0 - 80 mM).

3.2.4 Glucose transport characterisation

The rate of glucose uptake over 2 s was measured using a modification of the method by Walsh *et al.*[217,218], which was based on a method by Bisson and Fraenkel[12]. Isolated trophozoites were washed and suspended in glucose free incubation modified Ringer buffer (25 mM HEPES, 1 mM $MgCl_2$, 10 mM KCl, 120 mM NaCl, pH 7.1) similar to that described by Wünsch *et al.*[224] and stored on ice before the assay. In this buffer the parasites were able to exclude 0.04% *v/v* trypan blue. An aliquot of this suspension was incubated at 37°C in a petri dish. Glucose solutions (1 - 20 mM, specific radioactivity 700 to 10 Bq $nmol^{-1}$) were incubated separately in a water bath. An equal volume of radiolabelled D-[1-^{14}C] glucose was mixed with the incubated trophozoites and incubated for 2 s. Uptake was halted by quenching with 10 mL of quench buffer (500 mM Glucose, 25 mM HEPES, 1 mM $MgCl_2$, 10 mM KCl, 120 mM NaCl, pH 7.1), maintained at -5°C on a salt-ice mixture. The trophozoites were immediately transferred to a filter (covered with a thin layer of filter aid Celite 545, *Sigma-Aldrich*, to prevent clogging) and washed with 10 mL of ice-cold quenching solution. Filters were transferred immediately to scintillation vials containing 5 mL scintillation fluid.

For uptake rates under 2 s, a simple programmable quench-flow device was utilised (see Appendix B for a detailed description of the device design, construction and calibration). The apparatus used the same method as above, where glucose and trophozoites were loaded into temperature controlled sample chambers and allowed to reach 37°C. Upon triggering the device, the samples were injected through a mixing chamber into a collection vial and at the pre-programmed quench time, pre-chilled quenching solution was injected. The cells were washed as described above. The control in each method was the addition of the quench fluid prior to the addition of labelled glucose.

3.2.5 Fitting rate equations

For each glycolytic enzyme we wanted to describe the complete experimental data set with a single rate equation. For this the independent kinetic data

(i.e. for all substrate and product concentrations) were normalised to their respective V_{max} values and combined into a single data array for fitting. Fitting of the entire combined multidimensional dataset was achieved using *Wolfram Mathematica 8.0*® and its NonlinearModelFit function. For PFK and PK, independent data were normalised to enzymes rates measured under standardised substrate concentrations as described in their respective enzyme assay methods. Subsequently the rate equations were fitted to the combination of these normalised datasets, with the difference that the V_{max} was also fitted and not set to 1. This fitted V_{max} was used to scale the apparent V_{max} accordingly.

3.2.6 Computational Modelling

The kinetic model was constructed using *Wolfram Mathematica 8.0*®. The set of ordinary differential equations was solved using the NDSolve function. Steady state was calculated using the FindRoot function. The mathematical model was also constructed in Copasi[96].

3.3 Results and Discussion

3.3.1 Kinetic Characterisation

3.3.1.1 Hexokinase

Hexokinase, the first step in glycolysis, phosphorylates glucose using ATP to form glucose 6-phosphate (G6P) and ADP. The enzyme was characterised in terms of both its substrates (glucose and ATP) and products (G6P and ADP) as shown in Figure 3.2. The saturation curve for glucose shows a classical Michaelis-Menten type curve and product inhibition of G6P and ADP showed simple monotonous behaviour, but ATP exhibits inhibitory behaviour at concentrations above 3 mM. Mg^{2+} concentrations were maintained at least twice the concentration of ATP at all times, so inhibition is attributed to the activated Mg-ATP complex. For simplicity, in this study, ATP refers to the complexed Mg-ATP form. Inhibition was not competitive with respect to glucose (data not shown). The inhibitory effect of ATP is not expected to play an important role *in vivo* due to the relatively high concentration at which it

occurs.

$$vHK = \frac{V_{HK} \cdot \frac{ATP}{K_{ATP}} \cdot \frac{glucose_{int}}{K_{Glc_{int}}} \cdot \left(1 - \frac{ADP \cdot G6P}{ATP \cdot glucose_{int} \cdot K_{eq}}\right)}{\left(1 + \frac{ADP}{K_{ADP} \cdot V_{Pf}} + \frac{ATP}{K_{ATP}}\right) \cdot \left(1 + \frac{G6P}{K_{G6P}} + \frac{glucose_{int}}{K_{Glc_{int}}}\right) + \sum_{n=1}^{4} \left(\frac{ATP}{K_{i_{ATP}}}\right)^n} \quad (3.3.1)$$

A *B*

C *D*

Figure 3.2: Biochemical characterisation of *P. falciparum* hexokinase. HK catalyses the ATP-dependent phosphorylation of glucose to form G6P and ADP. Saturation of the enzyme with glucose (A) and ATP (B) is shown in addition to the inhibition of ADP (C) and G6P (D). Equation 3.3.1 was fitted to the entire normalised dataset and describes the data well (adjusted $R^2 = 0.97$). The fitted lines (adjusted $R^2 = 0.96$) are shown in the figures above and the parameters values obtained from the fitting are presented in Table 3.1. The error bars represent SEM, where n = 3 (C), n = 2 (D), n = 3 (A) and n = 4 (B) independent experiments.

Table 3.1: Summary of the kinetic parameters for *P. falciparum* hexokinase. The combined hexokinase kinetic data were normalised to V_{max} (Fig. 3.2) and fitted simultaneously to Eq. 3.3.1. The fitted parameters (± asymptotic standard error) are compared to the affinities determined for infected erythrocyte lysate (i.e. kinetics are the combination of erythrocyte and parasite HK). The maximal specific activity, V_{HK} was determined independently (see Table 3.15 and Section 3.3.2 for discussion).

Parameter	Fitted Value	Literature Value	Reference
K_{Glc} (mM)	0.076 ± 0.019	0.43 ± 0.021[1]	[175]
K_{ATP} (mM)	0.75 ± 0.030	3.1 ± 1.4[1]	[175]
K_{ADP} (mM)	1.1 ± 0.22	-	-
K_{G6P} (mM)	0.021 ± 0.0064	-	-
Ki_{ATP} (mM)	1.2 ± 0.087	-	-
V_{HK} (μmol·min^{-1}·mg^{-1})	0.34 ± 0.058	-	
K_{eq}		1310	[17]

[1] Determined in *P. falciparum* infected erythrocyte lysates and includes the affinity of the native erythrocyte enzymes (see text for discussion).

Erythrocyte hexokinase: K_{ATP} (mM) = 2.5 ± 1.0 [175] and K_{Glc} (mM) = 0.098 ± 0.0010 [175]

Equation 3.3.1 was derived assuming a rapid equilibrium random ordered bi-bi mechanism. The inhibitory mechanism of ATP is not known and we assumed a non-competitive mechanism where up to four ATP molecules can bind to the enzyme. This equation could describe the kinetics quite well (Fig. 3.2) although the Michaelis constants for glucose and ATP are lower than those determined by Roth *et al.*[175]. However, their Michaelis constants were determined in infected erythrocyte lysates and these parameters are thus the combination of parasite and erythrocyte HK kinetics[175].

3.3.1.2 Phosphoglucoisomerase

Phosphoglucoisomerase catalyses the conversion of glucose 6-phosphate to fructose 6-phosphate. Srivastava *et al.* identified and characterised three PGI isoenzymes from *P. falciparum* each with a similar K_m for fructose 6-phosphate[202].

The expression profile of the three isozymes during the asexual development phase of the *P. falciparum* life cycle is not known and in this work we characterised the average of the three isozymes during the asexual phase. The data of five independent experiments (two for the forward reaction and three for the reverse) were normalised to their respective maximal activities (V_{max}) and combined, followed by fitting to a reversible Michaelis-Menten equation (Eq. 3.3.2), which described the data well (Fig. 3.3). Fitted parameter values are shown in Table 3.2.

$$v\mathrm{PGI} = \frac{V_{\mathrm{PGI}} \cdot \frac{\mathrm{g6p}}{K_{\mathrm{g6p}}} \left(1 - \frac{\mathrm{f6p}}{\mathrm{g6p \cdot Keq}}\right)}{1 + \frac{\mathrm{f6p}}{K_{\mathrm{f6p}}} + \frac{\mathrm{g6p}}{K_{\mathrm{g6p}}}} \tag{3.3.2}$$

A *B*

Figure 3.3: Biochemical characterisation of *P. falciparum* phosphoglucoisomerase. *P. falciparum* PGI was characterised in terms of its substrate, glucose 6-phosphate (A) and product fructose 6-phosphate (B). The fitted curve of a reversible Michaelis-Menten equation, which was used to determine the Michaelis constants is shown (adjusted $R^2 = 0.99$). The forward reaction is a combination of two independent experiments and the reverse reaction is a combination of three independent experiments, each normalised to their maximal activity. Error bars represent SEM ($n \geq 3$).

Table 3.2: Summary of the average kinetic parameters for the three *P. falciparum* PGI isozymes. The kinetic data were fitted to a reversible Michaelis-Menten equation (Eq. 3.3.2). The fitted curves are shown in Fig. 3.3 and the fitted parameters are indicated with asymptotic standard error. The forward and reverse maximal specific activities ($V_{f_{PGI}}$ and $V_{r_{PGI}}$, respectively) were determined in separate experiments (Table 3.15, Fig. 3.15).

Parameter	Fitted Value	Literature Value	Reference
K_{G6P} (mM)	1.0 ± 0.056	-	-
K_{F6P} (mM)	0.097 ± 0.0053	0.26 ± 0.026[1]	[202]
$V_{f_{PGI}}$ (μmol·min^{-1}·mg^{-1})	3.7 ± 0.37	-	-
$V_{r_{PGI}}$ (μmol·min^{-1}·mg^{-1})	1.4 ± 0.26	-	-
K_{eq}	0.17 - 0.38[2]	0.33	[203,72]

[1] Average value of three *P. falciparum* isoenzymes with SEM.

[2] Lower and upper range determined from the Haldane relationship and error on the fitted parameters.

3.3.1.3 Phosphofructokinase

PFK catalyses the ATP-dependent phosphorylation of F6P to form F1,6BP and ADP. In this work we characterised PFK in terms of its substrates and products, and also tested for its regulation by PEP and F1,6BP found in *P. berghei*[22,23,24,25]. We found substrate inhibition by ATP, product inhibition by both ADP and F1,6BP and a classical Michaelis-Menten saturation curve for F6P (Fig. 3.4). To describe the kinetic data (Fig. 3.4) and regulatory effects of ATP, a variety of equations were tried. Neither competitive, noncompetitive nor uncompetitive models of substrate inhibition, as described by[124] were sufficient in describing the inhibition exhibited by ATP. Furthermore, a reversible Hill equation[90] with ATP as an independent modifier, could also not describe the data (results not shown).

A Monod-Wyman-Changeux (MWC) equation for bisubstrate reactions (Eq. 3.3.3) as derived by Hess and Pletter[84] was successfully used to describe the kinetic behaviour after making certain assumptions (see below).
Equation 3.3.3 describes a bi-substrate reaction describing tense (T) and relaxed (R) enzymatic states, with j number of allosteric effectors. V_{max_r} and V_{max_t} describe the maximal rate of the R and T state respectively. Further-

more, g_r and g_t are affinity coefficients for two substrates at the R and T state in absence of modifiers. Modifier behaviour is determined by c_{ij} which is defined as ratio of modifier binding to the R and T state. Thus if $c_{ij} > 1$, γ acts as an inhibitor and if $0 < c_{ij} < 1$, γ is an activator. L_o describes the equilibrium ratio between the R and the T state. c_1 and c_2 are binding coefficients for the two substrates and defined as the ratio of the Michaelis constants for each substrate in the R and the T state. Binding of an inhibitor results in the favouring of the T-state and conversely binding of an activator favours the R state.

$$v = \frac{\left(V_{\max_r} \cdot g_r \cdot \alpha_1 \cdot \alpha_2 \cdot R^{(n-1)} + V_{\max_t} \cdot L \cdot g_t \cdot c_1 \cdot \alpha_1 \cdot c_2 \cdot \alpha_2 \cdot T^{(n-1)}\right)}{(R^n + L \cdot T^n)} \tag{3.3.3}$$

Where i independent binding sites per protomer (n) gives:

$$L = L_o \prod_{j=1}^{i} \left(\frac{1 + c_{\mathrm{ij}} \cdot \gamma_j}{1 + \gamma_j}\right)^n$$

And :

$$\gamma_j = \frac{I_j}{K_{I_r}} \quad ; \quad \alpha_j = \frac{S_j}{K_{j_r}}$$

$$R = (1 + \alpha_1 + \alpha_2 + g_r \cdot \alpha_1 \cdot \alpha_2)$$

$$T = (1 + c_1 \cdot \alpha_1 + c_2 \cdot \alpha_2 + g_t \cdot c_1 \cdot \alpha_1 \cdot c_2 \cdot \alpha_2)$$

The following assumptions were made with regards to *P. falciparum* PFK:

- Fructose 6-phosphate does not bind to the T-state, such that $c_2 = 0$
- ATP, F1,6BP and ADP are modelled as allosteric inhibitors and regulate the ratio of the R to T state.
- The reaction was assumed to be irreversible at physiological concentrations of substrate and product, due to the high equilibrium constant (K_{eq} = 2290[79]) of the PFK catalysed reaction.

Using these assumptions, Eq. 3.3.3 reduces to Eq. 3.3.4, where $V_{\max_r}$ is the maximal rate of the R-state, K_{atp_r} and K_{f6p_r} are dissociation constants for ATP and F6P and Ki_{atp}, Ki_{fbp}, Ki_{adp} are inhibitory constants for ATP, F1,6BP and ADP, respectively. The ratios of the dissociation constants for the R and T-states for ATP, F1,6BP and ADP are given by c_{atp}, c_{fbp} and c_{adp} respectively.

$$v\mathrm{PFK} = \frac{V_{\max_r} \cdot \frac{\mathrm{atp}}{K_{\mathrm{atp}_r}} \cdot \frac{\mathrm{f6p}}{K_{\mathrm{f6p}_r}} \cdot g_r \left(1 + \frac{\mathrm{atp}}{K_{\mathrm{atp}_r}} + \frac{\mathrm{f6p}}{K_{\mathrm{f6p}_r}} + \frac{\mathrm{atp} \cdot \mathrm{f6p} \cdot g_r}{K_{\mathrm{atp}_r} \cdot K_{\mathrm{f6p}_r}}\right)^{n-1}}{\left(1 + \frac{\mathrm{atp}}{K_{\mathrm{atp}_r}} + \frac{\mathrm{f6p}}{K_{\mathrm{f6p}_r}} + \frac{\mathrm{atp} \cdot \mathrm{f6p} \cdot g_r}{K_{\mathrm{atp}_r} \cdot K_{\mathrm{f6p}_r}}\right)^{n} + L} \tag{3.3.4}$$

$$L = L_o \left(1 + \frac{\mathrm{atp} \cdot c_1}{K_{\mathrm{atp}_r}}\right)^n \left(\frac{1 + \frac{c_{\mathrm{atp}} \cdot \mathrm{atp}}{\mathrm{Ki}_{\mathrm{atp}}}}{1 + \frac{\mathrm{atp}}{\mathrm{Ki}_{\mathrm{atp}}}}\right)^n \left(\frac{1 + \frac{c_{\mathrm{fbp}} \cdot \mathrm{fbp}}{\mathrm{Ki}_{\mathrm{fbp}}}}{1 + \frac{\mathrm{fbp}}{\mathrm{Ki}_{\mathrm{fbp}}}}\right)^n \left(\frac{1 + \frac{c_{\mathrm{adp}} \cdot \mathrm{adp}}{\mathrm{Ki}_{\mathrm{adp}}}}{1 + \frac{\mathrm{adp}}{\mathrm{Ki}_{\mathrm{adp}}}}\right)^n$$

Figure 3.4: Biochemical characterisation of *P. falciparum* phosphofructokinase. The enzyme was characterised in terms of its substrates, ATP and F6P as well as its products ADP and F1,6BP. A MWC equation (Eq. 3.3.4) was fitted simultaneously to all the data and the equation gives a good description the data (adjusted $R^2 = 0.95$). Parameter values obtained from the fitting are shown in Table 3.3. The data are a combination of 8 independent experiments and error bars represent SEM (n >3).

Table 3.3: Summary of kinetic parameter values for *P. falciparum* phosphofructokinase. The parameters were obtained by simultaneously fitting Eq. 3.3.4 to the kinetic data (Fig. 3.4). The parameters are listed below ± asymptotic standard error.

Parameter	Fitted Value
$V_{\max_r}$ (μmol·min^{-1}·mg^{-1})	0.68 ± 0.13
K_{atp_r} (mM)	1.0 ± 3.7
K_{f6p_r} (mM)	0.11 ± 0.72
Ki_{atp} (mM)	7.0 ± 8.8
Ki_{fbp} (mM)	25 ± 18
Ki_{adp} (mM)	3.0 ± 5.0
g_r	1.9 ± 6.6
c_1	4.9 ± 5.8
c_{atp}	60 ± 0.12
c_{fbp}	16 ± 9.2
c_{adp}	5.0 ± 7.7
n	1.0 ± 0.19
L_o	0.58 ± 6.8

Buckwitz *et al.*[22,23,24,25] characterised PFK from *P. berghei* in detail and showed it to be inhibited by ATP, and Mg^{2+} ions and activated by PEP, F6P and inorganic phosphate. *P. falciparum* PFK is similar to *P. berghei* PFK in terms of inhibition by ATP. However, in this study and others[137], it is not activated by F1,6BP or PEP

The MWC equation described the combined datasets fairly well (Fig. 3.4), and could also account for kinetic behaviour at both saturating and non-saturating concentrations of substrates and products. Interestingly the equation fitted best when $n = 1$. This is consistent with the results shown by Money *et al.*[137], which indicated the existence of an α and β subunit, fused into a single protein 200kDa protein, where the β subunit contains the catalytic domain with the alpha subunit showing almost no enzymatic activity.

3.3.1.4 Aldolase

Aldolase catalyses the aldol cleavage of F,16BP into GAP and DHAP. The forward reaction for *P. falciparum* aldolase was characterised in terms of its substrate, F1,6BP (Fig 3.5). The kinetic data were described by a random order uni-bi rapid equilibrium rate equation (Eq. 3.3.5), and the fitted parameters are summarised in Table 3.4. In lysate the presence of triosephosphate isomerase prevents the characterisation of product inhibition by its products GAP and DHAP. Characterising the reaction in reverse via glucose 6-phosphate dehydrogenase was also not possible as phosphofructokinase has a high K_{eq}. The Michaelis constants for the products, K_{GAP} and K_{DHAP} were estimated by averaging the Michaelis constants found for *T. brucei*, *Lactococcus lactis* and human erythrocytes[83,86,93] (Table 3.4).

$$v\mathrm{ALD} = \frac{V_{\mathrm{ALD}} \cdot \frac{\mathrm{f16bp}}{K_{\mathrm{F1,6BP}}} \cdot \left(1 - \frac{\mathrm{dhap \cdot gap}}{K_{\mathrm{eq}} \cdot \mathrm{f16bp}}\right)}{1 + \frac{\mathrm{dhap}}{K_{\mathrm{DHAP}}} + \frac{\mathrm{f16bp}}{K_{\mathrm{F1,6BP}}} + \frac{\mathrm{gap}}{K_{\mathrm{GAP}}} + \frac{\mathrm{dhap \cdot gap}}{K_{\mathrm{DHAP}} . K_{\mathrm{GAP}}}} \tag{3.3.5}$$

Figure 3.5: Kinetic characterisation of *P. falciparum* aldolase. The enzyme was assayed to determine its affinity for F1,6BP. The fitted curve (adjusted $R^2 = 0.98$) was obtain using a uni - bi rate equation (Eq. 3.3.5) and the fitted parameters are shown in Table 3.4. The data are a combination of two independent experiments, normalised to their respective V_{max} values. Error bars represent SEM ($n \geq 3$).

Table 3.4: Summary of kinetic parameters for *P. falciparum* aldolase, The enzyme was characterised in terms of its affinity for its substrate, F1,6BP and maximal specific activity V_{ALD} (Fig. 3.5). The data were fitted to a uni-bi rate equation (Eq. 3.3.5) and the fitted parameter values are summarised below. The product affinities could not be determined in lysates and these parameters were estimated by averaging the values of the affinities determined for *L. lactis*, *T. brucei* and human erythrocytes. The data are the combination of two independent experiments with each point measured in triplicate.

Parameter	Fitted Value	Literature Value	Reference
V_{ALD} (μmol·min^{-1}·mg^{-1})	0.27 ± 0.049	-	
$K_{F_{1,6}BP}$ (mM)	0.067 ± 0.0046	0.025 ± 0.0060	[51]
K_{GAP} (mM)	-	0.046 ± 0.019[1]	[83,86,93]
K_{DHAP} (mM)	-	0.11 ± 0.089[1]	[83,86,93]
K_{eq} (mM^{-1}	-	0.090	[128]

[1] Estimated by averaging value of affinities in *Trypanosoma brucei*, *Lactococcus lactis* & human erythrocytes (Mean ± SEM).

3.3.1.5 Triosephosphate Isomerase

Triosephosphate isomerase (TIM) catalyses the isomerisation of DHAP and GAP and was characterised in terms of it substrate (DHAP) and product (GAP) as well as the inhibition by PEP (Fig. 3.6).

$$v\mathrm{TIM} = \frac{V_{\mathrm{TIM}} \cdot \frac{\mathrm{dhap}}{K_{\mathrm{DHAP}}} \left(1 - \frac{\mathrm{gap}}{K_{\mathrm{eq}} \cdot \mathrm{dhap}}\right)}{1 + \frac{\mathrm{dhap}}{K_{\mathrm{DHAP}}} + \frac{\mathrm{gap}}{K_{\mathrm{GAP}}} + \frac{\mathrm{pep}}{\mathrm{Ki}_{\mathrm{PEP}}}} \tag{3.3.6}$$

Figure 3.6: Kinetic characterisation of *P. falciparum* triosephosphate isomerase. *P. falciparum* triosephosphate isomerase exhibits Michaelis-Menten kinetics with regard to both its substrate (DHAP) and product (GAP), as well as being inhibited competitively by PEP. The data shown was combined and fitted simultaneously to a reversible Michaelis-Menten equation with a competitive inhibitor term (Eq. 3.3.6). The equation describes the data well (adjusted $R^2 = 0.93$) and the fitted parameters are displayed in Table 3.5. Each saturation curve is the combination of two independent experiments and error bars represent SEM (n = 6)

The data were described by a reversible Michaelis-Menten equation, with PEP as a competitive inhibitor (Eq. 3.3.6), where V_{TIM} is the maximal rate, K_{gap} and K_{dhap} are the Michaelis constant for GAP and DHAP, and Ki_{PEP} is the Michaelis inhibition constant for the competitive inhibitor, PEP. K_{eq} is the equilibrium constant of the reaction. The fitted parameters for the equation are shown in Table 3.5.

Table 3.5: Summary of Kinetic parameters for *P. falciparum* triosephosphate isomerase. The kinetic behaviour of triosephosphate isomerase was characterised in terms of its substrate, product and inhibition by PEP (Fig. 3.6). The combined data were fitted to a reversible Michaelis-Menten equation with a competitive inhibitor (Eq. 3.3.6) and the parameters obtained for the fit are displayed below with asymptotic standard error. The forward ($V_{f_{TIM}}$) and reverse ($V_{r_{TIM}}$) maximal specific activities were determined separately (see Fig. 3.15 and text for discussion.)

Parameter	Fitted Value	Literature Value	Reference
$V_{f_{TIM}}$ (μmol·min^{-1}·mg^{-1})	7.0 ± 1.0	-	-
$V_{r_{TIM}}$ (μmol·min^{-1}·mg^{-1})	15 ± 0.74	-	-
K_{GAP} (mM) 0.34 ± 0.039	0.35 ± 0.16	[196,132]	
K_{DHAP} (mM) 2.0 ± 0.33	0.59	[196]	
Ki_{PEP} (mM)	0.47 ± 0.053	-	-
K_{eq}	0.050 - 0.13[1]	0.046	[13]

[1] Lower and upper range as determined from the Haldane relationship within the error range of the parameters.

TIM is generally viewed as a near equilibrium reaction and was not thought to contribute to the regulation of glycolysis. However, TIM was proposed to have a regulatory role in yeast when PEP was discovered as an inhibitor of the enzyme in yeast and rabbit muscle[77]. In *P. falciparum* TPI is strongly inhibited by PEP (see Fig 3.6) and is almost entirely inhibited at concentrations > 5 mM, which may have implications regarding the regulation of flux towards glycerol (see discussion).

3.3.1.6 Glyceraldehyde 3- Phosphate Dehydrogenase

Glyceraldehyde 3-phosphate dehydrogenase (G3PDH) catalyses the conversion of GAP, P_i and NAD^+ to 1,3 -bisphosphoglycerate and NADH. G3PDH has not been previously characterised for *P. falciparum*. For the forward reactions, the phosphate concentration was fixed at 10 mM and either GAP or NAD^+ varied at saturating concentrations of the other (Fig. 3.7). The reverse reaction was also characterised by varying either B1,3PG (indirectly via 3PGA and PGK) or NADH under saturating concentrations of the other (Fig. 3.7).

$$v\text{G3PDH} = \frac{V_{f_{\text{G3PDH}}} \cdot \frac{\text{gap}\cdot\text{nad}}{K_{\text{GAP}} \cdot K_{\text{NAD}}} - V_{r_{\text{G3PDH}}} \cdot \frac{\text{nadh}\cdot\text{b1,3pg}}{K_{\text{NADH}} \cdot K_{\text{B1,3PG}}}}{\left(1 + \frac{\text{nad}}{K_{\text{NAD}}} + \frac{\text{nadh}}{K_{\text{NADH}}}\right)\left(1 + \frac{\text{gap}}{K_{\text{GAP}}} + \frac{\text{b1,3pg}}{K_{\text{B1,3PG}}}\right)} \tag{3.3.7}$$

A random order bi-bi equilibrium binding equation (Eq. 3.3.7) was fitted to all of the normalised kinetic data simultaneously (Fig. 3.7). The fitted parameters are summarised in Table 3.6.

Figure 3.7: Biochemical characterisation of *P. falciparum* glyceraldehyde 3-phosphate dehydrogenase. The enzyme was characterised in the forward (NAD^+, GAP) and the reverse (NADH, B1,3PG) direction. The rates were normalised to maximal specific activity and the combined data are well described by Eq. 3.3.7 (adjusted $R^2 = 0.96$). The fitted parameter values are summarised in Table 3.6. Each saturation curve is the combination of two independent experiments and data points represent the mean ± SEM, $n \geq 3$.

Table 3.6: Summary of kinetic parameters for *P. falciparum* glyceraldehyde 3-phosphate dehydrogenase. G3PDH was characterised in terms of GAP and NAD^+ under high phosphate concentrations as well as for NADH and B1,3PG (Fig. 3.7). The normalised data were fitted simultaneously to a random order bi-bi equilibrium equation (Eq. 3.3.7) and the fitted parameters are displayed below with asymptotic standard error. The maximal forward and reverse specific activities were determined independently (See Fig 3.15 and text for discussion).

Parameter	Fitted Value	Literature Value	Reference
$V_{f_{G3PDH}}$ (μmol·min^{-1}·mg^{-1})	1.2 ± 0.25	-	-
$V_{r_{G3PDH}}$ (μmol·min^{-1}·mg^{-1})	3.1 ± 0.23	-	-
K_{GAP} (mM)	0.92 ± 0.11	1.0	[29]
K_{NAD} (mM)	0.54 ± 0.058	-	-
K_{NADH} (mM)	0.029 ± 0.0038	-	-
$K_{B1,3PG}$ (mM)	1.1 ± 0.094	-	-

It should be noted that $K_{B1,3PG}$ obtained from the fitted G3PDH curve (Fig. 3.7) is in all likelihood an overestimation. Since 1,3 BPG is chemically unstable with a short half-life, 3PGA is used together with PGK and ADP to produce B1,3PG. Complete conversion is assumed for the calculation of the B1,3PG concentration, although this is unlikely, especially as the K_{eq} for PGK is relatively high. The apparent sigmoidality seen in the saturation curve (Fig. 3.7) is attributed to the assay method. The method is not expected to result in a linear correlation between the concentrations of B1,3PG produced at high and low concentrations of 3PGA. Due to the assumption of complete conversion, it is expected that the Michaelis constant is overestimated.

3.3.1.7 Phosphoglycerate kinase

PGK is the first ATP producing reaction of glycolysis and converts B1,3PG and ADP to 3PGA and ATP. *P. falciparum* phosphoglycerate kinase was characterised in the reverse direction with ATP and 3-phosphoglycerate as substrates as well for the product inhibition of the reverse reaction by ADP (Fig. 3.8). As stated before, determining a Michaelis constant for B1,3PG was not possible, as it is chemically unstable and not commercially available. The kinetic data (Fig. 3.8) was described by a random order bi-bi rapid equilibrium equation (Eq. 3.3.8) and the fitted parameters are displayed in Table 3.7. The Michaelis constant for B1,3PG was used from the work of Roth *et al.*[174].

$$v\mathrm{PGK} = \frac{V_{r_{\mathrm{PGK}}} \cdot \frac{3\mathrm{pg}\cdot\mathrm{atp}}{K_{3\mathrm{PGA}}\cdot K_{\mathrm{ATP}}} \cdot \left(\frac{\mathrm{adp}\cdot\mathrm{b13pg}\cdot K_{\mathrm{eq}}}{\mathrm{atp}\cdot 3\mathrm{pg}} - 1\right)}{\left(1 + \frac{\mathrm{adp}}{K_{\mathrm{ADP}}} + \frac{\mathrm{atp}}{K_{\mathrm{ATP}}}\right)\left(1 + \frac{\mathrm{b13pg}}{K_{\mathrm{B1,3PG}}} + \frac{3\mathrm{pg}}{K_{3\mathrm{PGA}}}\right)} \tag{3.3.8}$$

Equation 3.3.8 is not in the standard Haldane relationship form, as the maximal forward rate (defined as the ATP forming direction) is unknown. By using the Haldane relationship the forward maximal rate, $\mathrm{V}_{f_{PGK}}$ can be defined in terms of the Michaelis constants, K_{eq} and $\mathrm{V}_{r_{PGK}}$. Substituting this into the standard Haldane relationship form of the equation, gives Eq. 3.3.8 and describes the forward rate as a function of the reverse maximal specific activity.

Two isoenzymes of PGK have been isolated from *P. falciparum*[190], but the role of these isoenzymes and, whether they are expressed during the different life stages is not known. The kinetic parameters determined here would therefore be apparent Michaelis constants representing both isoenzymes.

Figure 3.8: Biochemical characterisation of *P. falciparum* phosphoglycerate kinase. PGK was assayed for its products and one of its substrates, ADP. The reaction was characterised in the reverse direction, hence ADP inhibiting the reaction and ATP and 3-phosphoglycerate increasing the reaction rate. The fitted curves (adjusted R^2 = 0.99) were obtained using a random order bi-bi equation (Eq. 3.3.8) and the fitted parameters are presented in Table 3.7. Each saturation curve is the combination of two independent experiments where error bars represent SEM (n $\geq$ 3).

Table 3.7: A summary of kinetic parameters for *P. falciparum* phosphoglycerate kinase. PGK was biochemically characterised in the reverse direction for ATP, ADP and 3PGA and the combined data fitted (Fig. 3.8 to a random order bi-bi rate equation (Eq. 3.3.8). Michaelis constants are shown ± asymptotic standard error.

Parameter	Fitted Value	Literature Value	Reference
V_{rPGK} (μmol·min^{-1}·mg^{-1})	1.7 ± 0.36	-	
V_{fPGK} (μmol·min^{-1}·mg^{-1})	30[1]	-	
K_{ADP} (mM)	0.15 ± 0.0095	0.30[2]	[174]
K_{ATP} (mM)	0.78 ± 0.027	0.68[2], 0.63[3]	[174], [148]
K_{3PGA} (mM)	0.27 ± 0.013	0.17[2], 0.52[3]	[174], [148]
K_{B13PG} (mM)	-	0.013[2]	[174]
K_{eq}	-	1890	[61]

[1] Calculated using the Haldane relationship.

[2] Determined for PGK-deficient erythrocytes infected with *P. falciparum*.

[3] Determined for recombinant *P. falciparum* PGK.

3.3.1.8 Phosphoglycerate Mutase

Phosphoglycerate mutase (PGM) converts 3PGA to 2PGA. In this work *P. falciparum* PGM was biochemically characterised in both the forward and reverse directions. The saturation curves (Fig. 3.9) were fitted to a reversible Michaelis-Menten equation (Eq. 3.3.9) and the fitted parameters are shown in Table 3.8.

$$v\mathrm{PGM} = \frac{V_{\mathrm{PGM}} \cdot \frac{3\mathrm{pga}}{K_{3\mathrm{PGA}}}\left(1 - \frac{2\mathrm{pga}}{3\mathrm{pga}\cdot K_{\mathrm{eq}}}\right)}{1 + \frac{2\mathrm{pga}}{K_{2\mathrm{pga}}} + \frac{3\mathrm{pga}}{K_{3\mathrm{PGA}}}} \tag{3.3.9}$$

Figure 3.9: Biochemical characterisation of *P. falciparum* phosphoglycerate mutase. The enzyme was characterised in terms of its substrate, 3PGA and product, 2PGA. The combined and normalised data were fitted (adjusted $R^2 = 0.99$) to a Michaelis-Menten equation (Eq. 3.3.8) and the fitted parameters are shown in Table 3.7. For 2PGA, the rate becomes negative and denotes the enzyme functioning in reverse. Each saturation curve is the combination of three independent experiments and error bars represent SEM ($n \geq 3$).

Table 3.8: Summary of kinetic parameters for *P. falciparum* phosphoglycerate mutase. PGM was biochemically characterised in the forward (3PGA) and reverse (2PGA) direction and the combined data fitted (Fig. 3.9) to a Michaelis-Menten equation (Eq. 3.3.9). The fitted parameters are displayed below ± asymptotic standard error.

Parameter	Fitted Value	Literature Value	Reference
$V_{f_{PGM}}$ (μmol·min^{-1}·mg^{-1})	0.87 ± 0.072	-	-
$V_{r_{PGM}}$ (μmol·min^{-1}·mg^{-1})	0.22 ± 0.050	-	-
K_{3PGA} (mM)	1.7 ± 0.091	0.85	[85]
K_{2PGA} (mM)	0.32 ± 0.016	0.041	[85]
K_{eq}	0.14 - 0.45[1]	0.10	[128]

[1] Lower and upper range as determined from the Haldane relationship and error on the parameters.

3.3.1.9 Enolase

Enolase catalyses production of PEP from 2PGA and was kinetically characterised in both the forward and reverse direction (Fig 3.10). The forward and reverse reactions follow classical Michaelis-Menten kinetics and are well described by a reversible Michaelis-Menten equation (Eq. 3.3.10). The fitted curves are shown in Figure 3.10 and the fitted parameters listed in Table 3.9.

$$v\mathrm{ENO} = \frac{V_{\mathrm{ENO}} \frac{2\mathrm{pga}}{K_{2\mathrm{PGA}}} \left(1 - \frac{\mathrm{pep}}{2\mathrm{pga} K_{\mathrm{eq}}}\right)}{1 + \frac{2\mathrm{pga}}{K_{2\mathrm{PGA}}} + \frac{\mathrm{pep}}{K_{\mathrm{PEP}}}} \tag{3.3.10}$$

A

Figure 3.10: Biochemical characterisation of *P. falciparum* enolase. The enzyme was characterised in the forward (2PGA) and reverse (PEP) direction. The curve (adjusted $R^2 = 0.96$) is the description of the data by Eq. 3.3.10 and the fitted parameters are summarised in Table 3.9. The data are the combination of two independent experiments. Error bars represent SEM ($n \geq 3$).

Table 3.9: Summary of the kinetic parameters of *P. falciparum* enolase. The enzyme was assayed in the forward and reverse direction (Fig. 3.10) and the data were fitted to a reversible Michaelis-Menten equation (Eq. 3.3.10). Values are listed as the mean ± asymptotic standard error.

Parameter	Fitted Value	Literature Value	Reference
$V_{f_{ENO}}$ (μmol·min^{-1}·mg^{-1})	1.3 ± 0.41	-	-
$V_{r_{ENO}}$ (μmol·min^{-1}·mg^{-1})	0.94 ± 0.44	-	-
K_{2PGA} (mM)	0.53 ± 0.055	0.041 ± 0.0040[2]	[151]
K_{PEP} (mM)	1.3 ± 0.13	0.25 ± 0.030[2]	[151]
K_{eq}	1.8 - 9.6[1]	4.6	[128]

[1] Lower and upper range as determined from the Haldane relationship and the error on the parameters.

[2] *P. falciparum* enolase expressed in *E. coli* and characterised in its purified form.

The affinities for PEP and 2PGA determined in this work are between 6 and 10 fold weaker than determined by Pal-Bhowmick *et al.*[151], but these were determined for a cloned and purified enzyme, at optimal pH (Table 3.9).

3.3.1.10 Pyruvate Kinase

Pyruvate kinase catalyses the substrate level phosphorylation of ADP, using phosphoenolpyruvate and producing pyruvate and ATP. *P. falciparum* PK was characterised in the forward direction for substrates, PEP and ADP and product inhibition by ATP and pyruvate (Fig. 3.11). From the saturation curves (Fig. 3.11) it is apparent that the PK is under kinetic regulation, inhibited by both of its substrates at higher concentrations and inhibited cooperatively by its product ATP. The enzyme is fairly insensitive to pyruvate and inhibition is only observed at more than 20 mM.

A variety of rate equations were evaluated in an attempt to capture the overall kinetic behaviour in a single equation. Reversible Hill equations, with PEP and ADP as allosteric inhibitors could not describe the bi-substrate inhibition, although it did describe the cooperative inhibition by ADP (data not shown).

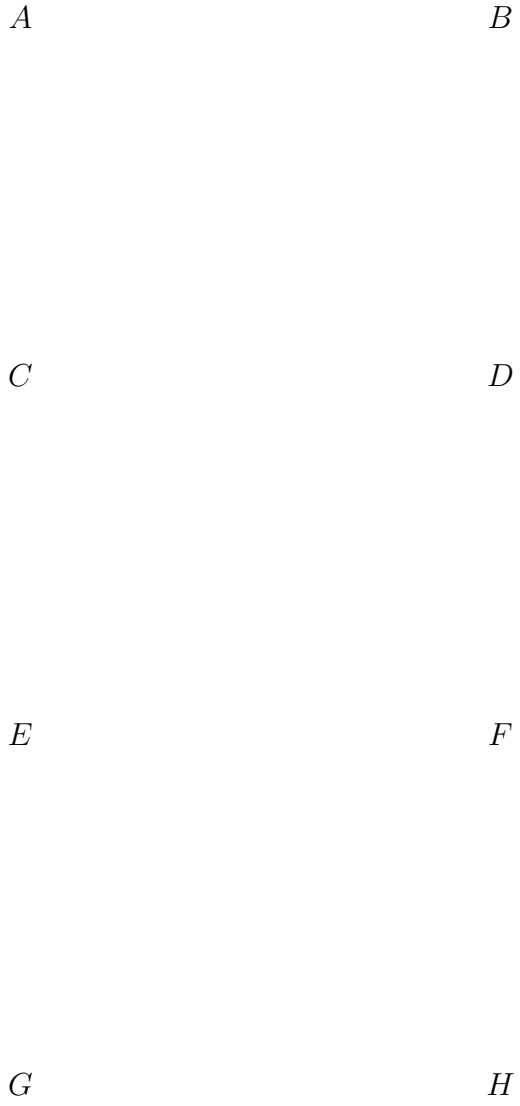

Figure 3.11: Kinetic characterisation of *P. falciparum* pyruvate kinase. PK was characterised in terms of its substrates (ADP and PEP) and products (ATP and pyruvate). A) Indicates the allosteric inhibition of the enzyme by ADP. B,C& D) PEP inhibition at varying concentrations of ADP. E,F & G) Strong cooperative inhibition shown by ATP. F) Slight product inhibition by pyruvate. The fitted curve (adjusted $R^2 = 0.97$) through each of the datasets was obtained by simultaneously fitting all the kinetic data to Equation 3.3.12. Parameter values are shown in Table 3.10. The data are representative of seven independent experiments and errors bars represent SEM ($n \geq 3$).

An MWC equation, which assumes an irreversible reaction, rapid equilibrium binding and independent binding of substrates (Eq. 3.3.11) and described by Buckwitz *et al.*[24] was used to describe the observed kinetic behaviour. The equation describes the reaction rate as a function of two substrates (S_1 & S_2), where K_{S_1} and K_{S_2} are Michaelis constants for the first and second substrate, L_o describes the equilibrium constant between the R and the T-state, n is the number of subunits and K_i is the inhibition constant of an inhibitor, i.

$$v = \left(\frac{V_f \cdot \frac{S_1}{K_{S_1}} \cdot \frac{S_2}{K_{S_2}}}{1 + \frac{S_1 \cdot S_2}{K_{S_1} \cdot K_{S_2}} + \frac{S_1}{K_{S_1}} + \frac{S_2}{K_{S_2}}} \right) \cdot \left(\frac{1}{1+L} \right) \qquad (3.3.11)$$
$$L = L_o \cdot \left(1 + \frac{i}{K_i}\right)^n$$

Using Eq. 3.3.11 for PK with the additional assumption that only a tetrameric form (n = 4) is active ($(1 + (\frac{i}{K_i})^n)$ with atp, pep, adp and PYRacting as inhibitors yields (Eq. 3.3.12). This equation could describe the bi-substrate inhibition, the cooperativity of ATP and the inhibition by pyruvate in a single rate equation (Fig. 3.11) and the fitted parameters are shown in Table 3.10.

$$v\mathrm{PK} = \left(\frac{V_{\mathrm{PK}} \cdot \frac{\mathrm{adp}}{K_{\mathrm{ADP}}} \cdot \frac{\mathrm{pep}}{K_{\mathrm{PEP}}}}{1 + \frac{\mathrm{adp} \cdot \mathrm{pep}}{K_{\mathrm{ADP}} \cdot K_{\mathrm{PEP}}} \cdot \frac{\mathrm{pep}}{K_{\mathrm{PEP}}} + \frac{\mathrm{adp}}{K_{\mathrm{ADP}}}} \right) \cdot \left(\frac{1}{1+L} \right) \qquad (3.3.12)$$

$$L = L_o \left(\left(1 + \left(\frac{\mathrm{adp}}{K_{i_{\mathrm{ADP}}}}\right)^n\right) \cdot \left(1 + \left(\frac{\mathrm{atp}}{K_{i_{\mathrm{ATP}}}}\right)^n\right) \cdot \left(1 + \left(\frac{\mathrm{pep}}{K_{i_{\mathrm{PEP}}}}\right)^n\right) \cdot \left(1 + \left(\frac{\mathrm{pyr}}{K_{i_{\mathrm{PYR}}}}\right)^n\right) \right)$$

Plasmodium possesses two homotetrameric pyruvate kinases (PK1 and PK2). Both are expressed during the asexual phase[36], but PK1 expression is constant and continually high throughout the asexual phase and thought to be part of glycolysis, whereas PK2 correlates with the expression of lipid synthesis genes. Since the enzyme characterisation is in trophozoite lysates, both isozymes would be present and the characterisation would represent the combined behaviour and kinetics. The interpretation of this data thus has to consider the relative contribution of the two enzymes. In this work, it is assumed that the relative contribution of the apicoplast PK2 compared to PK1 is minimal. This assumption is based on i) that cDNA levels are far higher for PK1[36] and ii) the reasoning that rate of lipid synthesis would be far less than the glycolytic rate

Table 3.10: Summary of kinetic parameters for *P. falciparum* pyruvate kinase. PK is inhibited by both of its substrates, as well as cooperatively by ATP and inhibited at high concentrations of pyruvate. The kinetic data shown in Figure 3.11, were fitted simultaneously to a MWC type equation (Eq. 3.3.12). The fitted parameters and the respective asymptotic standard error for each parameter are indicated below.

Parameter	Fitted Value	Literature	Reference
$V_{f_{PK}}$ (μmol·min^{-1}·mg^{-1})	2.3		
K_{ADP} (mM)	0.30 ± 0.050	0.13 ± 0.043	[36]
K_{PEP} (mM)	0.39 ± 0.047	0.19 ± 0.028	[36]
$K_{i_{Pyr}}$ (mM)	69 ± 6.7	-	-
$K_{i_{ATP}}$ (mM)	1.4 ± 0.12	-	-
$K_{i_{ADP}}$ (mM)	1.9 ± 0.15	-	-
$K_{i_{PEP}}$ (mM)	2.8 ± 0.24	-	-
L_o	0.198 ± 0.0877	-	-
n	4		

and with the small apicoplast volume, not much enzyme would be required to fulfil the flux requirement. It is also assumed that the regulation of the two enzymes is the same, although this may not be the case.

3.3.1.11 Lactate Dehydrogenase

P. falciparum lactate dehydrogenase (LDH) is essential for maintaining the redox balance of the cell by recycling NAD^+ from NADH by reducing the keto group of pyruvate to a hydroxyl group (lactate). In this work, the enzyme was characterised in the forward and reverse directions (Fig. 3.11). Pyruvate has been shown to inhibit the enzyme as high concentrations with a K_i of 140 mM[194], but this inhibition is negligible at physiological concentrations of pyruvate and thus excluded. The combined kinetic data were described successfully (Fig. 3.11) with a random order bi-bi rapid equilibrium equation (Eq. 3.3.13) and the fitted parameters are indicated in Table 3.12.

$$vLDH = \frac{V_{f_{LDH}} \cdot \frac{nadh \cdot pyr}{K_{NADH} \cdot K_{Pyr}} - V_{r_{LDH}} \cdot \frac{lac \cdot nad}{K_{Lac} \cdot K_{NAD}}}{\left(1 + \frac{nad}{K_{NAD}} + \frac{nadh}{K_{NADH}}\right)\left(1 + \frac{lac}{K_{Lac}} + \frac{pyr}{K_{Pyr}}\right)} \tag{3.3.13}$$

Figure 3.12: Kinetic characterisation of *P. falciparum* lactate dehydrogenase. LDH was assayed in both the forward (NADH & pyruvate) and reverse directions (NAD^+ & lactate). The curve (adjusted $R^2 = 0.97$) shows the fit obtained for a random order bi-bi equation (Eq. 3.3.13). The fitted parameters are displayed in Table 3.12. Each saturation curve is the combination of three biological repeats with n $\geq$ 3 technical repeats. Error bars indicate SEM.

Table 3.11: Summary of kinetic parameters determined for *P. falciparum* lactate dehydrogenase. LDH was biochemically characterised for asexual *P. falciparum* (Fig. 3.11) and the kinetic data fitted simultaneously to Eq. 3.3.13 to obtain the below parameters (± asymptotic standard error).

Parameter	Fitted Value	Literature Value	Reference
$V_{f_{LDH}}$ (μmol·min^{-1}·mg^{-1})	2.5 ± 0.23	-	-
$V_{r_{LDH}}$ (μmol·min^{-1}·mg^{-1})	1.4 ± 0.18	-	-
K_{Pyr} (mM)	0.13 ± 0.0080	0.030, 0.055	[73,194]
K_{NADH} (mM)	0.046 ± 0.0031	0.0070, 0.011	[73,194]
K_{Lac} (mM)	3.6 ± 0.30	12, 47	[73,194]
K_{NAD} (mM)	0.23 ± 0.020	0.086, 0.18	[73,194]
K_{eq}	150 - 430[1]	227 - 7194	[165,48]

[1] Lower and upper range as determined using the Haldane relationship and error in the parameters.

3.3.1.12 Glycerol Production and Transport

The experimental finding of a 2:1 ratio of lactate produced per mole glucose consumed supported the hypothesis that *P. falciparum* glycolysis was homolactic[190]. However, this is inconsistent with several findings, such as pyruvate being transported out of the cell[57], which would prevent the recycling of NADH to NAD^+ . The production of glycerol by asexual *P. falciparum* was discovered by Lian *et al.*[125], which indicates the presence of a glycerol shunt pathway where presumably glycerol is produced from DHAP combined with the important oxidation of NADH to balance pyruvate excretion. The enzyme(s) used to produce glycerol in *P. falciparum* during the asexual phase have yet to be identified. We measured glycerol 3-phosphate dehydrogenase activity (converts DHAP to G3P combined with the oxidation of NADH to form NAD^+) in trophozoite lysates (results not shown). However, the reaction that converts G3P to glycerol (if this is the pathway for glycerol production in asexual *P. falciparum*) is unknown. In *P. falciparum* studies have shown the existence of a gene that codes for glycerol kinase, but it is not expressed during the asexual stage and disruption of this gene does not inhibit growth and development of the parasite[186]. Furthermore, no putative genes for glycerol-3-phosphatase have been identified in the *P. falciparum* genome[69]. There is however, a PGM isozyme, PGM2[85], which has phosphatase activity and it may be able to utilise G3P as a substrate to produce glycerol.

Since the pathway for glycerol production is not clear, a single rate equation (Eq. 3.3.14) was used to describe the production of glycerol, NAD^+ and orthophosphate from DHAP combined with the oxidation of NADH. The orthophosphate concentration was not included in the rate equation. For simplicity it was also assumed that all glycerol produced is transported out of the trophozoite. The parameters for the reaction (assumed to be the same as for glycerol-3-phosphate dehydrogenase) were obtained from the Brenda enzyme database[185] (Table. 3.12).

$$v\mathrm{GlrDH} = \frac{V_{f_{\mathrm{GlrDH}}} \cdot \frac{\mathrm{dhap}\cdot\mathrm{nadh}}{K_{\mathrm{DHAP}}\cdot K_{\mathrm{NADH}}} \cdot \left(1 - \frac{\mathrm{gly}_{\mathrm{external}}\cdot\mathrm{nad}}{K_{\mathrm{eq}}\cdot\mathrm{dhap}\cdot\mathrm{nadh}}\right)}{\left(1 + \frac{\mathrm{nad}}{K_{\mathrm{NAD}}} + \frac{\mathrm{nadh}}{K_{\mathrm{NADH}}}\right)\cdot\left(\frac{\mathrm{gly}_{\mathrm{external}}}{K_{\mathrm{Gly}}} + \frac{\mathrm{dhap}}{K_{\mathrm{DHAP}}}\right)} \tag{3.3.14}$$

Table 3.12: Summary of the kinetic parameters obtained for the glycerol producing enzyme. The enzymatic pathway for the production of glycerol in *P. falciparum* has yet to be identified. The production of glycerol was described by a single rate equation (Eq. 3.3.14). The first step in the pathway is assumed to be glycerol-3-phosphate dehydrogenase and parameters for this enzyme were obtained from the Brenda Enzyme database[185] for a number of organisms. The maximal specific activity, $V_{f_{Glr}}$, was fitted to obtain experimentally measured flux rates.

Parameter	Literature Value	Reference
$V_{f_{Glr}}$ (μmol·min^{-1}·mg^{-1})	0.020[1]	Fitted (This work)
K_{DHAP} (mM)	0.23 ± 0.16[2]	[185]
K_{NADH} (mM)	0.023 ± 0.025[3]	[185]
$K_{Glycerol}$ (mM)	5.0 [4]	-
K_{NAD} (mM)	0.25 ± 0.19[5]	[185]
K_{eq}	32600[6]	[227]

[1] Fitted to obtain experimentally measured flux.

[2] Mean ± SD of 18 independent values for Gly3PDH across 13 different organisms)

[3] Mean ± SD of 22 independent values for Gly3PDH across 18 different organisms)

[4] Assumed to be fairly insensitive to external glycerol.

[5] Mean ± SD of 17 independent values for Gly3PDH across 13 different organisms)

[6] K_{eq} for Gly3PDH reaction.

3.3.1.13 Glucose Transporter, PfHT1

Asexual *Plasmodium* relies on the erythrocyte GLUT1 and GLUT5 enzymes for glucose and fructose transport respectively. The rapid transport facilitated by these enzymes far exceeds the demands of the parasite[115] and uptake of both glucose and fructose into the parasite has been shown to be a passive process[116]. Glucose and fructose are thought to first cross the parasitophorous vacuolar membrane via high-capacity non-selective channels[116,74,119] after which they are transported across the parasite plasma membrane via a specialised saturable, sodium-independent and stereo-specific hexose transporter[223,222]. The *P. vivax* and *P. falciparum* hexose transporters (PvHT1 and PfHT1 respectively) as well as those for *P. knowlesi* and *P. yoelli* have been biochemically characterised[223,222,100,101,102]. The potential of PfHT1 as a drug target has been examined with inhibitors in several studies[100,101,102,179] and reviewed by Patel

et al.[155].

During this study the glucose transporter, PfHT1 was characterised using ^{14}C labelled D-glucose uptake experiments (Fig. 3.14) in isolated *P. falciparum* trophozoites. Many studies have looked at uptake rates of glucose derivatives or L-glucose by the transporter when expressed in *Xenopus laevis* oocytes[223,102,133], but this does not reflect the expression of the transporter *in vivo*. It is also difficult to obtain the specific activity of the parasite glucose transporter from data describing the uptake of labelled glucose in infected erythrocytes[116,74]. In isolated parasites Saliba *et al.*[179] investigated the uptake of 2-deoxy-D-glucose(2DOG), at times greater than 20 seconds, which may not reflect zero-trans influx kinetics. Goodyer *et al.*[74] estimated that the V_{max} of the parasite transporter was a factor of 2 to 4 less than the RBC transporter rate, which is in agreement with the observations that uptake for 2DOG into *P. falciparum* was extremely rapid[116,179]. In erythrocytes, it has recently been shown that unless uptake is measured in less than 30 ms, the rate is underestimated and does not reflect zero-trans influx kinetics[15].

To determine the maximal uptake rate of glucose into the parasite, we investigated the uptake of ^{14}C D-glucose into isolated trophozoites with a simple quench flow device (Appendix B). This device enabled us to observe uptake rates within 0.25 s, which was essential for measuring zero-trans flux kinetics. Knowing the concentration of internal ^{14}C label after a specific sample time makes it possible to determine the uptake rate (i.e. change in internal glucose per time). However, the sampling time has a large influence on the perceived uptake rate. It is expected that at sufficiently short sampling times, the change in internal label is expected to reflect only an increase in internal glucose and not metabolised glucose (i.e. labelled intermediate metabolites). The transport rate determined under these short sampling times would represent a zero-trans flux rate. At longer sampling times, as glucose is metabolised, the change in ^{14}C label concentration would include labelled glycolytic metabolites. Uptake rates calculated at these longer time intervals would consequently be lower than the zero-trans uptake rate. To ascertain the sampling time required to measure zero-trans uptake in *P. falciparum* trophozoites, we determined the glucose uptake rate within a range (0.2 - 60 s) of sampling times. The calculated uptake rates were normalised to total protein and are shown in

semi-logarithmic space (Fig. 3.13). The uptake rate increases almost exponentially (linear region within semi-logarithmic plot) as the sample time decreases below 5.1 s (Fig. 3.13). To obtain the y-intercept value, which represents the transporter maximal carrying capacity, v, ($v = \frac{V_{max} \cdot s}{s+K_s}$) a linear regression was performed on the data between 0.25 and 5.1 s. This time range was selected as it falls within the linear region on the semi-logarithmic plot. The two data points below this time were excluded from the regression as they were determined near the dead time of the quench flow device, and are expected to have a larger degree of error. The data points above 5.1 s were excluded as the uptake rate is no longer reflecting zero-trans uptake. During the assay, the substrate concentration,s, is 5 mM and the K_s is 1.8 mM (Table 3.13). By taking the antilogarithm of the fitted y-intercept value (-0.819 $\pm$ 0.157), v, and substituting the aforementioned parameters into the equation, the V_{max} value is determined to be 0.207 (0.143, 0.296) μmol·min^{-1}·mg^{-1} with the lower and upper limits indicated in parentheses. The lower and upper limits were obtained by taking into account the standard error of the linear regression when solving for V_{max}. The uptake rates determined below 0.25 s are expected to have a high degree of experimental error, but do indicate that the maximal uptake rate may indeed by higher than determined from the linear regression. To ensure that this does not bias model predictions, the model simulations (e.g. steady fluxes) in this thesis include an upper and lower boundary value obtained by also performing the simulations with the glucose transporter V_{max} set to 1.0 and 0.1 μmol·min^{-1}·mg^{-1}, respectively.

It should be noted that Kirk *et al.*[116] found that for *P. falciparum* infected erythrocytes, the internal and external concentrations of "non-metabolisable" 2-deoxy D-glucose (2DOG) equilibrated within a minute. In our studies where the labelled glucose is metabolised by hexokinase and subsequent enzymatic reactions, it is not expected that internal and external glucose concentrations would equilibrate. In our assays, the internal concentration of label (i.e sum of a labelled metabolites) attained 1.6 mM over a period of 10 min, compared to the 5 mM external glucose concentration.

Figure 3.13: The specific activity of the glucose transporter PfHT1 as a function of quench time. A simple quench flow device allowed the study of labelled D-glucose uptake into isolated trophozoites. The rate of uptake (change in internal ^{14}C label concentration per time and normalised to total protein) was determined at sampling times ranging between 0.2 and 60 s and presented in a semi-logarithmic form. To calculate the carrying capacity of the glucose transporter a linear regression was performed on the data between 0.25 and 5.1 s and the y-intercept value was used to determine the V_{max} (see text for details). The data are the combination of four biological repeats. Individual data points that are shown were determined in singleton. Error bars represent the mean ± SEM (n >2).

Due to error in measuring the uptake rate at low quench times, the K_m of the transporter was determined by assaying the change in rate as a function of external glucose at a 2 second sampling time (Fig. 3.14). The kinetic data were fitted to a reversible Michaelis-Menten equation (Eq. 3.3.15) and binding was assumed to be symmetrical, where the Michaelis constant for external glucose ($K_{Glc_{ext}}$) is the same as for internal glucose ($K_{Glc_{int}}$). The K_m of 1.8 mM ± 0.99 mM is higher than determined by others, but comparable considering the high degree of error (Table 3.13).

$$v\mathrm{GlcTr} = \frac{V_{\mathrm{GlcTr}} \cdot \mathrm{glucose}_{\mathrm{ext}} \left(1 - \frac{\mathrm{glucose}_{\mathrm{int}}}{\mathrm{glucose}_{\mathrm{ext}} \cdot K_{\mathrm{eq}}}\right)}{K_{\mathrm{Glc}_{\mathrm{ext}}} \left(1 + \frac{\mathrm{glucose}_{\mathrm{ext}}}{K_{\mathrm{Glc}_{\mathrm{ext}}}} + \frac{\mathrm{glucose}_{\mathrm{int}}}{K_{\mathrm{Glc}_{\mathrm{int}}}}\right)} \tag{3.3.15}$$

Table 3.13: Summary of the kinetic parameters for *P. falciparum* hexose transport. The *P. falciparum* hexose transporter was been characterised in terms of its maximal specific activity and affinity for glucose. V_{GlcTr} is calculated from Fig. 3.13 (see text for details) and displayed with the lower and upper limit in parentheses.

Parameter	Fitted Value	Literature Value	Reference
$K_{Glc_{ext}}$ (mM)	1.8 ± 0.99	0.48, 1.0, 0.97	[223,222,102]
V_{GlcTr} (μmol·min^{-1}·mg^{-1})	0.21 (0.14 - 0.30)	-	-
K_{eq}	1.0	-	-

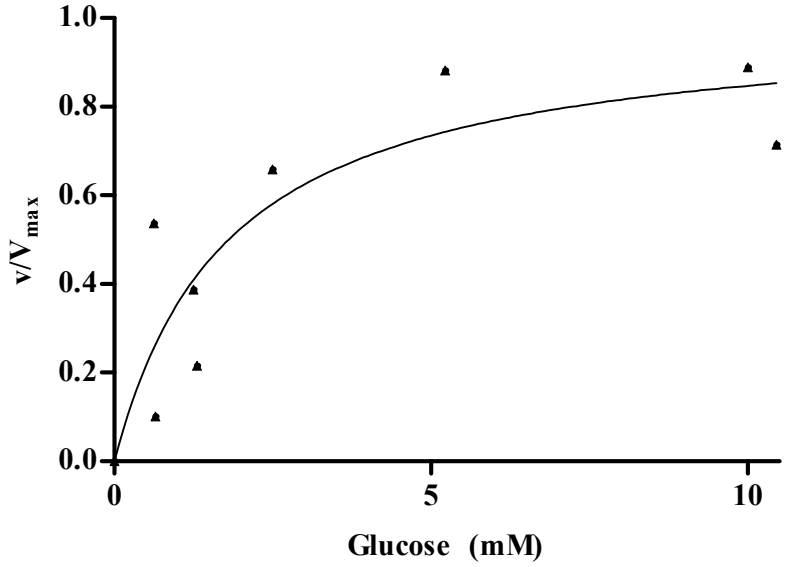

Figure 3.14: Kinetic characterisation of *P. falciparum* PfHT1. The glucose transporter was biochemically characterised for glucose uptake in isolated trophozoites. Individual data points are presented for the rate of glucose transport determined in two independent experiments (sampled at 2 s) each normalised to their respective V_{max} values. The data follows Michaelis-Menten kinetics with a K_m of 1.8 ± 0.99 mM.

3.3.1.14 Lactate and pyruvate transporters

Human erythrocytes facilitate the removal of internal lactate into the blood stream via i) a specific H^+ monocarboxylate transporter, ii) the band 3 an-

ion exchanger, and iii) by diffusion of the protonated form across the lipid bilayer[115]. The capacity of these pathways, however, is calculated to be insufficient for the increased production of lactate by *Plasmodium* during infection[109,115]. Lactate is transported from the parasite into the host cytosol via a pyruvate/lactate-proton cotransporter, which shares many characteristics of the monocarboxylate transporter (MCT) family[57]. The transport of pyruvate or lactate is H^+ linked with a 1:1 stoichiometry and saturable[57].

Elliot *et al.*[57] characterised the *P. falciparum* transporter in terms of both lactate and pyruvate influx and to a lesser degree, efflux. The transport kinetics are summarised in Table 3.14. They fitted the transporter kinetics to Eq. 3.3.17, where monocarboxylate refers to the concentration of either lactate or pyruvate, K_m is the Michaelis constant, V_{max} is the maximal specific activity and K_d was included as a linear component to fit their data.
The V_{max} is in the units (mmol $H^+ min^{-1}$ ·L cell $water^{-1}$). Using the conversion factor of 4.67 μL cytosol·mg total $protein^{-1}$ determined in this work, the V_{max} for lactate and pyruvate influx become 0.44 ± 0.028 and 0.16 ± 0.037 (μmol·min^{-1} · mg^{-1} respectively. These rates were determined at an assay temperature of 4 °C, and as such the rates are expected to be substantially faster at 37 °C. The V_{max} rates were assumed to be 8 fold greater, based on the rule of thumb that the rate doubles for every increase of 10 °C. This rough rule is based on the Arrhenius equation (Eq. 3.3.16), where k is the rate constant, E_A is the activation energy, R is the universal gas constant, T is the temperature in kelvin and A is the pre-exponential factor. If one assumes that A and E_A remain constant with temperature and that the activation energy is between 10 and 50 kJ/mol, the rate would increase between 2 and 10 fold respectively for a 33 °C change in temperature.

$$k = A \cdot e^{\frac{E_A}{R \cdot T}} \tag{3.3.16}$$

To model the reversible transport of pyruvate and lactate, Eq. 3.3.17 extended to a reversible random order bi-bi equation with the addition of the mass action linear component (Eq. 3.3.18). The affinity of protons for the transporter has not been determined and for simplicity it is assumed that they have an almost infinite affinity, which reduces Eq. 3.3.18 to the simpler form of Eq. 3.3.19. Although the kinetic component of protons is removed from the equation, the thermodynamic component of the pH gradient is still taken into account by

the disequilibrium ration, Γ. The intracellular pH of *P. falciparum* strains has been shown to vary between 7.17 and 7.4[178,224,16,80,225]. The average pH was taken as 7.2 and the erythrocyte cytosolic pH set to 6.9. The erythrocyte pH is generally considered to be 7.1[224,16,225], but it has been shown that immediately adjacent to the parasite, the pH is a fraction lower at 6.9[80]. The ratio of extracellular to intracellular proton concentration is thus two and incorporated into the disequilibrium ratio. Lactate and pyruvate bind competitively to the monocarboxylate transporter and Cranmer *et al.*[44] showed that the transport rate was inhibited by 44 ± 10% (mean ± SEM, n = 4) at 0.5 mM lactate and 2.5 mM pyruvate. To incorporate this into the rate equation, two competitive inhibition terms are included into Eq. 3.3.19, yielding Eq. 3.3.20. Binding of protons, lactate and pyruvate was assumed to symmetrical and the inhibition constants for pyruvate and lactate, Ki_{lac} and Ki_{pyr}, were fitted (Table 3.14), such that equations 3.3.20 & 3.3.21) are inhibited by 44% at 0.5 mM lactate and 2.5 mM pyruvate.

$$H^{+}\text{influx} = \frac{V_{max} \cdot [\text{monocarboxylate}]}{K_m + [\text{monocarboxylate}]} + k_d \cdot [\text{monocarboxylate}] \tag{3.3.17}$$

$$v\text{LacTr} = \frac{\text{Vf} \cdot \frac{H^{+}_{\text{int}}}{K_{H^{+}_{\text{int}}}} \cdot \frac{\text{Lac}_{\text{int}}}{K_{\text{Lac}_{\text{int}}}} \cdot \left(1 - \frac{\Gamma}{\text{Keq}}\right)}{\left(1 + \frac{H^{+}_{\text{int}}}{K_{H^{+}_{\text{int}}}} + \frac{H^{+}_{\text{ext}}}{K_{H^{+}_{\text{ext}}}}\right)\left(1 + \frac{\text{Lac}_{\text{int}}}{K_{\text{Lac}_{\text{int}}}} + \frac{\text{Lac}_{\text{ext}}}{K_{\text{Lac}_{\text{ext}}}}\right)} + k_d \cdot (\text{Lac}_{\text{int}} - \text{Lac}_{\text{ext}}) \tag{3.3.18}$$

Assuming $K_{H^{+}_{\text{int}}}$ and $K_{H^{+}_{\text{int}}} \to 0$,

$$\begin{aligned} \lim_{K_{H^{+}_{\text{int \& ext}}} \to 0} & \frac{\text{Vf} \cdot \frac{H^{+}_{\text{int}}}{K_{H^{+}_{\text{int}}}} \cdot \frac{\text{Lac}_{\text{int}}}{K_{\text{Lac}_{\text{int}}}} \cdot \left(1 - \frac{\Gamma}{\text{Keq}}\right)}{\left(1 + \frac{H^{+}_{\text{int}}}{K_{H^{+}_{\text{int}}}} + \frac{H^{+}_{\text{ext}}}{K_{H^{+}_{\text{ext}}}}\right)\left(1 + \frac{\text{Lac}_{\text{int}}}{K_{\text{Lac}_{\text{int}}}} + \frac{\text{Lac}_{\text{ext}}}{K_{\text{Lac}_{\text{ext}}}}\right)} + k_d \cdot (\text{Lac}_{\text{int}} - \text{Lac}_{\text{ext}}) \\ = \; & v\text{LacTr} \frac{\text{Vf} \cdot \frac{\text{Lac}_{\text{int}}}{K_{\text{Lac}_{\text{int}}}} \cdot \left(1 - \frac{\Gamma}{\text{Keq}}\right)}{\left(1 + \frac{\text{Lac}_{\text{int}}}{K_{\text{Lac}_{\text{int}}}} + \frac{\text{Lac}_{\text{ext}}}{K_{\text{Lac}_{\text{ext}}}}\right)} + k_d \cdot (\text{Lac}_{\text{int}} - \text{Lac}_{\text{ext}}) \end{aligned} \tag{3.3.19}$$

$$\text{Where } \Gamma = \frac{H^{+}_{\text{ext}} \cdot \text{Lac}_{\text{ext}}}{H^{+}_{\text{int}} \cdot \text{Lac}_{\text{int}}} \text{ and } H^{+} = 10^{-\text{pH}}$$

Including competitive inhibition by pyruvate gives:

$$v\text{LacTr} = \frac{V_{\text{LacTr}} \cdot \frac{\text{Lac}_{\text{int}}}{K_{\text{Lac}_{\text{int}}}} \cdot \left(1 - \frac{\Gamma}{\text{Keq}}\right)}{\left(1 + \frac{\text{Lac}_{\text{int}}}{K_{\text{Lac}_{\text{int}}}} + \frac{\text{Lac}_{\text{ext}}}{K_{\text{Lac}_{\text{ext}}}} + \frac{\text{Pyr}_{\text{int}}}{K_{i_{\text{Pyr}_{\text{int}}}}} + \frac{\text{Pyr}_{\text{ex}}}{K_{i_{\text{Pyr}_{\text{ex}}}}}\right)} + k_{d_{Lac}} \cdot (\text{Lac}_{\text{int}} - \text{Lac}_{\text{ext}}) \tag{3.3.20}$$

Similarly :

$$v\text{PyrTr} = \frac{V_{\text{PyrTr}} \cdot \frac{\text{Pyr}_{\text{int}}}{K_{\text{Pyr}_{\text{int}}}} \cdot \left(1 - \frac{\Gamma}{\text{Keq}}\right)}{\left(1 + \frac{\text{Pyr}_{\text{int}}}{K_{\text{Pyr}_{\text{int}}}} + \frac{\text{Pyr}_{\text{ext}}}{K_{\text{Pyr}_{\text{ext}}}} + \frac{\text{Lac}_{\text{int}}}{K_{i_{\text{Lac}_{\text{int}}}}} + \frac{\text{Lac}_{\text{ex}}}{K_{i_{\text{Lac}_{\text{ex}}}}}\right)} + k_{d_{Pyr}} \cdot (\text{Pyr}_{\text{int}} - \text{Pyr}_{\text{ext}}) \tag{3.3.21}$$

Table 3.14: Summary of kinetic parameters for *P. falciparum* lactate and pyruvate transport obtained from scientific literature. In *P. falciparum* lactate and pyruvate are transported by the same monocarboxylate transporter, which has been biochemically characterised by Cranmer *et al.*[44] and Elliot *et al.*[57]. Eqs. 3.3.20 & 3.3.21 are used to describe the reversible transport and competitive inhibition between pyruvate and lactate. The parameters for these equations are tabulated below. Symmetrical binding (internal/external) is assumed for pyruvate and lactate as denoted by the *int/ext* subscript. The inhibition constants were obtained by fitting these equations to data reported by Cranmer *et al.*[44].

Parameter	Parameter Value	Reference
V_{LacTr} (mmol H^+min^{-1}L cell water^{-1})	94 ± 6.0^1	[57]
V_{PyrTr} (mmol H^+min^{-1}L cell water^{-1})	34 ± 8.0^1	[57]
$K_{Pyr_{int/ext}}$ (mM)	16 ± 3.3	[57]
$K_{Lac_{int/ext}}$ (mM)	3.8 ± 0.80	[57]
$k_{d_{Pyr}}$ (min^{-1})	0.11 ± 0.010	[57]
$k_{d_{Lac}}$ (min^{-1})	0.80 ± 0.30	[57]
$K_{i_{Pyr_{int/ext}}}$ (mM)	1.6^2	This study
$K_{i_{Lac_{int/ext}}}$ (mM)	0.36^2	This study

[1] In the model these rates are normalised to μmol·mg^{-1}·mg^{-1} total protein using a conversion factor of 4.67 μL cytosol·mg total protein^{-1} .

[2] Eqs. 3.3.20 & 3.3.21 were fitted to obtain 44% inhibition at 0.5 mM lactate and 2.5 mM pyruvate as determined by Cranmer *et al.*[44].

3.3.1.15 ATPase

P. falciparum utilises the nett ATP produced during glycolysis in a variety of biosynthetic and homeostatic processes. This rate of ATP consumption, however, cannot be measured experimentally, since ATP is used for a variety of biosynthetic and homeostatic reactions. For simplicity we define a single 'ATPase' reaction, which includes all of the cellular ATP demand. In the model this ATP demand is described by simple mass action kinetics (Eq. 3.3.22), where V_{ATPase} is the reaction rate constant. The intracellular ATP:ADP has been experimentally measured to be between 1 (glucose starved) and 5.7[178,37,68,204]. To obtain an ATPase rate for the model (see Model Descrip-

tion), we fitted the V_{ATPase} (0.035 min^{-1}) to obtain a steady state ATP:ADP ratio of 3.

$$v\text{ATPase} = V_{\text{ATPase}} \cdot \text{atp} \tag{3.3.22}$$

3.3.2 Maximal Specific Activities

Asexual *Plasmodium* develops over 48 hours, with glycolytic flux peaking during the trophozoite stage. When *Plasmodium* is isolated from the infected erythrocyte, the degree of synchrony and the exact point in the developmental cycle is expected to vary between isolates. This would alter total protein, and if the enzymes are expressed to different degrees, it would have an impact on the V_{max}[2] determinations. In order to counter this variation, specific activities were determined for a large number of different trophozoite isolations at saturating or near saturating concentrations of substrate. Total protein was determined using the method of Bradford[19] and bovine serum albumin as a standard. These specific activities were adjusted to V_{max} by substituting the substrate concentrations into the fitted rate equations and dividing the specific activity by corresponding $\frac{v}{V_{max}}$ ratio. The V_{max} values for each of the enzymes characterised in this work are shown in Table 3.15 and Figure 3.15.

[2]The V_{max} values presented in this study were determined in trophozoite lysates and are normalised to mg total protein. These are thus not true V_{max} values, which are instead normalised to mg pure enzyme protein.

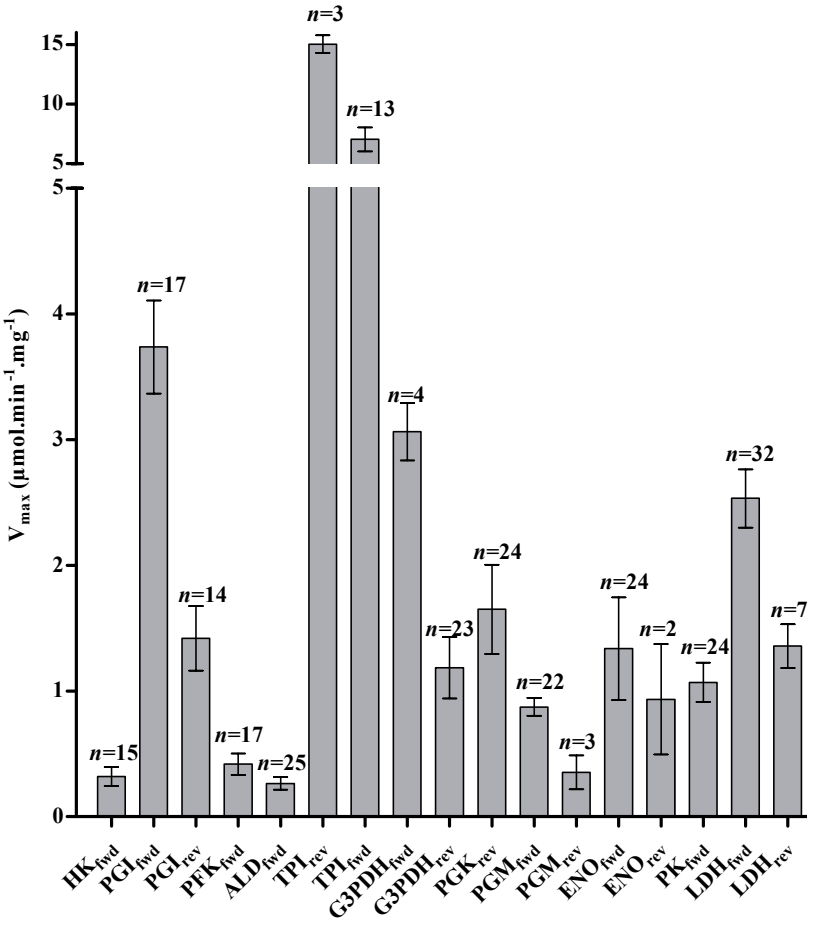

Figure 3.15: Comparison of the V_{max} values of the *P. falciparum* glycolytic enzymes. The maximal specific activities for each of the glycolytic enzymes of *P. falciparum* were determined from numerous trophozoite isolations to ensure a good representation of the enzyme activities at this stage of parasite development. Each V_{max} includes the values obtained during the biochemical characterisation (saturation curves). In addition, the enzymes were assayed in several independent isolations (n displayed in figure) at near saturating concentrations of substrate and these were adjusted to represent V_{max}. The error bars represent SEM, where n is displayed for each enzyme. The subscript *fwd* and *rev*, refer to the forward and reverse rates respectively.

Table 3.15: Maximal specific activity for each of the glycolytic enzymes in *P. falciparum* as measured in this study. Both the forward and reverse reaction activities are indicated. Error is given as SEM, n is displayed below.

Enzyme	Maximal Specific Activity (μmol·min^{-1}·mg^{-1})			
	Forward	*n*	*Reverse*	*n*
HK	0.32 ± 0.076	15	-	-
PGI	3.7 ± 0.37	17	1.4 ± 0.26	14
PFK	0.42 ± 0.084	17	-	-
ALD	0.70 ± 0.049	25	-	-
TIM	7.0 ± 1.0	13	15 ± 0.74	3
G3PDH	4.0 ± 0.23	4	1.2 ± 0.25	23
PGK	-	-	1.7 ± 0.36	24
PGM	0.87 ± 0.072	22	0.35 ± 0.14	3
ENO	1.3 ± 0.41	24	0.94 ± 0.44	2
PK	1.1 ± 0.16	24	-	-
LDH	2.5 ± 0.23	32	1.4 ± 0.18	7
Transport Steps	Maximal Specific Activity (μmol·min^{-1}·mg^{-1})			
	Forward	*n*		
*v*LacTr	3.5[1]			
*v*PyrTr	1.3[1]			
*v*GlrDH	0.014[2]			
*v*GlcTr	0.21 (0.14 - 0.30)[3]	4		

[1] Obtained from[57]. See Section 3.3.1.14 for details.

[2] Fitted to the glycerol flux. See Section 3.3.1.12.

[3] Lower - Upper Limit

3.3.3 Model Description

3.3.3.1 Rate Equations, Moieties and Parameters Values

The model consists of eighteen reaction steps (Fig. 3.1), which describe the glycolytic conversion of glucose to its end products, lactate, pyruvate and glycerol with the concomitant production of ATP, as well as the transport of these metabolites in and out of the *P. falciparum* trophozoite. In the above results, each reaction step has been described by a kinetic rate equation obtained by fitting to experimental data or from scientific literature in the case of monocarboxylate transport (pyruvate and lactate). Only two reactions were fitted, the first being the ATPase rate as it cannot be measured experimentally and the second reaction being the V_{max} for the GlrDH enzyme in the glycerol pathway

as this pathway has yet to be elucidated.

The transport rates of glucose, pyruvate and lactate are described by vGlcTr, vPyrTr and vLacTr respectively (Eqs. 3.3.23,3.3.37 & 3.3.38). Glycerol production and transport is described by vGlrDH (Eq. 3.3.35). The glycolytic enzyme rates are described by vHK (hexokinase, Eq. 3.3.24), vPGI (phosphoglucoisomerase, Eq. 3.3.25), vPFK (phosphofructokinase, Eq. 3.3.26), vALD (aldolase, Eq. 3.3.27), vTIM (triosephosphate isomerase, Eq. 3.3.28), vG3PDH (glyceraldehyde 3-phosphate dehydrogenase, Eq. 3.3.29), vPGK (phosphoglycerate kinase, Eq. 3.3.30), vPGM (phosphoglycerate mutase, Eq. 3.3.31), vENO (enolase, Eq. 3.3.32), vPK (pyruvate kinase, Eq. 3.3.33) and vLDH (lactate dehydrogenase, Eq. 3.3.34). ATP consumption is described by vATPase (Eq. 3.3.36). The parameter values obtained for each rate equation are described above and are summarised in Tables 3.15 & 3.16.

Asexual *P. falciparum* resides within the erythrocyte and to model the *P. falciparum* "compartment", two changes were made to the rate equations. Firstly, the V_{max} values were in the units μmol·min^{-1} · mg^{-1} total protein and these were changed to mmol·min^{-1} · L cytosol^{-1} by multiplying each V_{max} by the parasite volume and by the factor α (4.67 μL cytosol·mg^{-1} total protein, which was determined assuming a trophozoite cytosolic volume of 28 fL). The second change to the rate equations was to explicitly include the compartment volume for each metabolite. Thus in each rate equation, the *P. falciparum* metabolites are divided by the *P. falciparum* trophozoite cytosolic volume (V_{Pf}) and for the external metabolites (i.e. in the erythrocyte), are divided by the external volume (V_{RBC}). The volume of the trophozoite has been measured to be between 21 and 30 fL[2] and in this study, is assumed to be 28 fL. These changes were made in order to model in terms of mole quantity and not concentration (e.g. mM) and has the advantage that the model can easily be integrated as a separate compartment into a model of erythrocyte glycolysis. The external concentrations (subscript *ext* in the rate equations) of glucose, lactate, pyruvate and glycerol were fixed (Table 3.17) for steady state analysis. The remaining metabolites were always variables as a function of time, denoted in the rate equations by *metabolite[t]*.

Table 3.16: Summary of the kinetic parameters used for model construction. Most of the kinetic parameters were determined in this work, but some were obtained from scientific literature.

Enzyme	E.C. Number	Parameter	Experimental (mM)	Literature (mM)	Parameter	Experimental (mM)	Literature (mM)
HK	2.7.1.1	K_{Glc}	0.076 ± 0.019	0.43 ± 0.021 [175]	K_{ATP}	0.75 ± 0.030	3.1 ± 1.4 [175]
		K_{ADP}	1.1 ± 0.22	-	K_{G6P}	0.021 ± 0.0064	-
		Ki_{ATP}	1.2 ± 0.087	-	n	4	
PGI	5.3.1.9	K_{G6P}	1.0 ± 0.056	-	K_{F6P}	0.097 ± 0.0053	0.26 ± 0.026 [202]
PFK	2.7.1.11	K_{F6P}	0.11 ± 0.72	0.034	K_{ATP}	1.0 ± 3.7	0.028
		$K_{i_{F16BP}}$	25 ± 18	-	$K_{i_{ADP}}$	3.0 ± 5.0	0.17
		$K_{i_{ATP}}$	7.0± 8.8	-	gr	1.9 ± 6.6	-
		c_1	4.9 ± 5.8	-	c_{atp}	60 ± 0.12	-
		c_{fbp}	16 ± 9.2	-	c_{adp}	5.1 ± 7.7	-
		n	1.0 ± 0.19	-	L_o	0.58 ± 6.8	
ALD	4.1.2.13	K_{F16BP}	0.067 ± 0.0046	0.025 ± 0.0060 [51]	K_{GAP}	-	0.046 ± 0.089 [83,86,93]
		K_{DHAP}	-	0.11 ± 0.089 [83,86,93]			
TIM	5.3.1.1	K_{GAP}	0.34 ± 0.039	0.35 ± 0.16 [196,132]	K_{DHAP}	2.0 ± 0.33	0.59 [196]
		Ki_{PEP}	0.47 ± 0.053	-			
G3PDH	1.2.1.12	K_{GAP}	0.92 ± 0.11	1.0 [29]	K_{NAD}	0.54 ± 0.058	-
		K_{NADH}	0.029 ± 0.0038	-	K_{B13PG}	1.1 ± 0.095	-
PGK	2.7.2.3	K_{ADP}	0.15 ± 0.0095	0.30 [174]	K_{ATP}	0.78 ± 0.027	0.68-0.63 [174,148]
		K_{3PGA}	0.27 ± 0.0132	0.17 - 0.52 [174,148]	K_{B13PG}	-	0.013 [174]
PGM	5.4.2.1	K_{3PGA}	1.7 ± 0.091	0.85 [85]	K_{2PGA}	0.32 ± 0.016	0.041 [85]
ENO	4.2.1.11	K_{2PGA}	0.53 ± 0.055	0.041 ± 0.0040 [151]	K_{PEP}	1.3 ± 0.13	0.25 ±0.030 [151]
PK	2.7.1.40	K_{PEP}	0.39 ± 0.047	0.19 ± 0.028 [36]	K_{ADP}	0.30 ± 0.050	0.13 ± 0.043 [36]
		$K_{i_{ATP}}$	1.4 ± 0.12	-	$K_{i_{Pyr}}$	69 ± 6.7	-
		$K_{i_{PEP}}$	2.8 ± 0.24	-	L_o	0.20 ± 0.088	-
		n	4	-			
LDH	1.1.1.27	K_{Pyr}	0.13 ± 0.0080	0.030 - 0.055 [73,194]	K_{NADH}	0.046 ± 0.0031	0.0070 - 0.011 [73,194]
		K_{Lac}	3.6 ± 0.30	12 - 47 [73,194]	K_{NAD}	0.23 ± 0.020	0.086 - 0.18 [73,194]
GlrDH	Unknown	K_{DHAP}	-	0.23 ± 0.16 [185]	K_{NADH}	-	0.023 ± 0.025 [185]
		K_{NAD}	-	0.25 ± 0.19 [185]	K_{Gly}	5.0	-
GLCTransporter		$K_{Glc_{int}}$	1.8 ± 0.99	0.48 - 1.0 [222,223,102]	1.8 ± 0.99	0.48 - 1.0 [222,223,102]	
LACTransporter		$K_{Lac_{int/ext}}$	-	3.8 ± 0.80 [57]	$k_{d_{Lac}}$ (min^{-1})	-	0.80 ± 0.30 [57]
		$K_{i_{Pyr_{int/ext}}}$	1.6	Fitted to [44]			
PYRTransporter		$K_{Pyr_{int/ext}}$	-	16 ± 3.3 [57]	$k_{d_{Pyr}}$ (min^{-1})	-	0.11 ± 0.010 [57]
		$K_{i_{Lac_{int/ext}}}$	0.36	Fitted to [44]			

$$v\text{GlcTr} = \frac{V_{\text{GlcTr}} \cdot \alpha \cdot V_{\text{Pf}} \cdot \frac{\text{glucose}_{\text{ext}}}{K_{\text{Glc}_{\text{ext}}} \cdot V_{\text{RBC}}} \cdot \left(1 - \frac{\text{glucose}_{\text{int}}[t]}{\text{glucose}_{\text{ext}} \cdot K_{\text{eq}}}\right)}{\left(1 + \frac{\text{glucose}_{\text{ext}}}{K_{\text{Glc}_{\text{ext}}} \cdot V_{\text{RBC}}} + \frac{\text{glucose}_{\text{int}}[t]}{K_{\text{Glc}_{\text{int}}} \cdot V_{\text{Pf}}}\right)} \tag{3.3.23}$$

$$v\text{HK} = \frac{V_{\text{HK}} \cdot \alpha \cdot V_{\text{Pf}} \cdot \frac{\text{ATP}[t]}{K_{\text{ATP}} \cdot V_{\text{Pf}}} \cdot \frac{\text{glucose}_{\text{int}}[t]}{K_{\text{Glc}_{\text{int}}} \cdot V_{\text{Pf}}} \cdot \left(1 - \frac{\text{ADP}[t] \cdot \text{G6P}[t]}{\text{ATP}[t] \cdot \text{glucose}_{\text{int}}[t] \cdot K_{\text{eq}}}\right)}{\left(1 + \frac{\text{ADP}[t]}{K_{\text{ADP}} \cdot V_{\text{Pf}}} + \frac{\text{ATP}[t]}{K_{\text{ATP}} \cdot V_{\text{Pf}}}\right) \cdot \left(1 + \frac{\text{G6P}[t]}{K_{\text{G6P}} \cdot V_{\text{Pf}}} + \frac{\text{glucose}_{\text{int}}[t]}{K_{\text{Glc}_{\text{int}}} \cdot V_{\text{Pf}}}\right) + \sum_{n=1}^{4} \left(\frac{\text{ATP}[t]}{K_{i_{\text{ATP}}}}\right)^n} \tag{3.3.24}$$

$$v\text{PGI} = \frac{V_{\text{PGI}} \cdot V_{\text{Pf}} \cdot \alpha \cdot \frac{\text{G6P}[t]}{K_{\text{G6P}} \cdot V_{\text{Pf}}} \cdot \left(1 - \frac{\text{F6P}[t]}{\text{G6P}[t] \cdot K_{\text{eq}}}\right)}{1 + \frac{\text{F6P}[t]}{K_{\text{F6P}} \cdot V_{\text{Pf}}} + \frac{\text{G6P}[t]}{K_{\text{G6P}} \cdot V_{\text{Pf}}}} \tag{3.3.25}$$

$$v\text{PFK} = \frac{V_{\text{PFK}} \cdot V_{\text{Pf}} \cdot \alpha \cdot \frac{\frac{\text{ATP}[t] \cdot \text{F6P}[t]}{V_{\text{Pf}} \cdot V_{\text{Pf}}}}{K_{\text{ATP}} \cdot K_{\text{F6P}}} \cdot g_r}{\left(1 + \frac{\text{ATP}[t]}{K_{\text{ATP}} \cdot V_{\text{Pf}}} + \frac{\text{F6P}[t]}{K_{\text{F6P}} \cdot V_{\text{Pf}}} + \frac{\text{ATP}[t] \cdot \text{F6P}[t] \cdot g_r}{K_{\text{ATP}} \cdot K_{\text{F6P}} \cdot V_{\text{Pf}} \cdot V_{\text{Pf}}}\right) + L \cdot \left(1 + \frac{c_1 \cdot \text{ATP}[t]}{V_{\text{Pf}} \cdot K_{\text{ATP}}}\right) \cdot \left(\frac{1 + \frac{c_{\gamma 1} \cdot \text{ATP}[t]}{V_{\text{Pf}} \cdot K_{i_{\text{ATP}}}}}{1 + \frac{\text{ATP}[t]}{V_{\text{Pf}} \cdot K_{i_{\text{ATP}}}}}\right) \cdot \left(\frac{1 + \frac{c_{\gamma 2} \cdot \text{F1,6BP}[t]}{V_{\text{Pf}} \cdot K_{i_{\text{F1,6BP}}}}}{1 + \frac{\text{F1,6BP}[t]}{V_{\text{Pf}} \cdot K_{i_{\text{F1,6BP}}}}}\right) \cdot \left(\frac{1 + \frac{c_{\gamma 3} \cdot \text{ADP}[t]}{V_{\text{Pf}} \cdot K_{i_{\text{ADP}}}}}{1 + \frac{\text{ADP}[t]}{V_{\text{Pf}} \cdot K_{i_{\text{ADP}}}}}\right)} \tag{3.3.26}$$

$$v\text{ALD} = \frac{V_{\text{ALD}} \cdot V_{\text{Pf}} \cdot \alpha \cdot \frac{\text{F1,6BP}[t]}{K_{\text{F1,6BP}} \cdot V_{\text{Pf}}} \cdot \left(1 - \frac{\text{DHAP}[t] \cdot \text{GAP}[t]}{K_{\text{eq}} \cdot \text{F1,6BP}[t]}\right)}{1 + \frac{\text{DHAP}[t]}{K_{\text{DHAP}} \cdot V_{\text{Pf}}} + \frac{\text{F1,6BP}[t]}{K_{\text{F1,6BP}} \cdot V_{\text{Pf}}} + \frac{\text{GAP}[t]}{K_{\text{GAP}} \cdot V_{\text{Pf}}} + \frac{\text{DHAP}[t] \cdot \text{GAP}[t]}{K_{\text{DHAP}} \cdot V_{\text{Pf}} \cdot K_{\text{GAP}} \cdot V_{\text{Pf}}}} \tag{3.3.27}$$

$$v\text{TIM} = \frac{V_{\text{TIM}} \cdot V_{\text{Pf}} \cdot \alpha \cdot \frac{\text{DHAP}[t]}{K_{\text{DHAP}} \cdot V_{\text{Pf}}} \cdot \left(1 - \frac{\text{GAP}[t]}{K_{\text{eq}} \cdot \text{DHAP}[t]}\right)}{1 + \frac{\text{DHAP}[t]}{K_{\text{DHAP}} \cdot V_{\text{Pf}}} + \frac{\text{GAP}[t]}{K_{\text{GAP}} \cdot V_{\text{Pf}}} + \frac{\text{PEP}[t]}{\text{Ki}_{\text{PEP}} \cdot V_{\text{Pf}}}} \tag{3.3.28}$$

$$v\text{G3PDH} = \frac{V_{f_{\text{G3PDH}} \cdot V_{\text{Pf}} \cdot \alpha \cdot} \frac{\text{GAP}[t] \cdot \text{NAD}[t]}{K_{\text{GAP}} \cdot V_{\text{Pf}} \cdot K_{\text{NAD}} \cdot V_{\text{Pf}}} - V_{r_{\text{G3PDH}} \cdot} \frac{\text{NADH}[t] \cdot \text{B1,3PG}[t]}{K_{\text{NADH}} \cdot V_{\text{Pf}} \cdot K_{\text{B1,3PG}} \cdot V_{\text{Pf}}}}{\left(1 + \frac{\text{NAD}[t]}{K_{\text{NAD}} \cdot V_{\text{Pf}}} + \frac{\text{NADH}[t]}{K_{\text{NADH}} \cdot V_{\text{Pf}}}\right) \cdot \left(1 + \frac{\text{GAP}[t]}{K_{\text{GAP}} \cdot V_{\text{Pf}}} + \frac{\text{B1,3PG}[t]}{K_{\text{B1,3PG}} \cdot V_{\text{Pf}}}\right)} \tag{3.3.29}$$

$$v\text{PGK} = \frac{V_{r_{\text{PGK}}} \cdot V_{\text{Pf}} \cdot \alpha \cdot \frac{\text{PGA3}[t] \cdot \text{ATP}[t]}{K_{\text{PGA3}} \cdot V_{\text{Pf}} \cdot K_{\text{ATP}} \cdot V_{\text{Pf}}} \cdot \left(\frac{\text{ADP}[t] \cdot \text{B1,3PG}[t] \cdot K_{\text{eq}}}{\text{ATP}[t] \cdot \text{PGA3}[t]} - 1\right)}{\left(1 + \frac{\text{ADP}[t]}{K_{\text{ADP}} \cdot V_{\text{Pf}}} + \frac{\text{ATP}[t]}{K_{\text{ATP}} \cdot V_{\text{Pf}}}\right) \cdot \left(1 + \frac{\text{B1,3PG}[t]}{K_{\text{B1,3PG}} \cdot V_{\text{Pf}}} + \frac{\text{PGA3}[t]}{K_{\text{PGA3}} \cdot V_{\text{Pf}}}\right)} \tag{3.3.30}$$

$$v\text{PGM} = \frac{V_{\text{PGM}} \cdot V_{\text{Pf}} \cdot \alpha \cdot \frac{\text{PGA3}[t]}{K_{\text{PGA3}} \cdot V_{\text{Pf}}} \cdot \left(1 - \frac{\text{PGA2}[t]}{\text{PGA3}[t] \cdot K_{\text{eq}}}\right)}{1 + \frac{\text{PGA2}[t]}{K_{\text{PGA2}} \cdot V_{\text{Pf}}} + \frac{\text{PGA3}[t]}{K_{\text{PGA3}} \cdot V_{\text{Pf}}}} \tag{3.3.31}$$

$$v\text{ENO} = \frac{V_{\text{ENO}} \cdot V_{\text{Pf}} \cdot \alpha \cdot \frac{\text{PGA2}[t]}{K_{\text{PGA2}} \cdot V_{\text{Pf}}} \cdot \left(1 - \frac{\text{PEP}[t]}{\text{PGA2} K_{\text{eq}}}\right)}{1 + \frac{\text{PGA2}[t]}{K_{\text{PGA2}} \cdot V_{\text{Pf}}} + \frac{\text{PEP}[t]}{K_{\text{PEP}} \cdot V_{\text{Pf}}}} \tag{3.3.32}$$

$$v\text{PK} = \frac{V_{\text{PK}} \cdot V_{\text{Pf}} \cdot \alpha \cdot \frac{\text{ADP}[t]}{K_{\text{ADP}} \cdot V_{\text{Pf}}} \cdot \frac{\text{PEP}[t]}{K_{\text{PEP}} \cdot V_{\text{Pf}}}}{\left(1 + \frac{\text{ADP}[t]}{V_{\text{Pf}} \cdot K_{\text{ADP}}} \cdot \frac{\text{PEP}[t]}{V_{\text{Pf}} \cdot K_{\text{PEP}}} + \frac{\text{pyruvate}_{\text{int}}[t]}{V_{\text{Pf}} \cdot K_{\text{Pyr}_{\text{int}}}}\right) + L_o \cdot \left(1 + \left(\frac{\text{ADP}[t]}{V_{\text{Pf}} \cdot K_{i_{\text{ADP}}}}\right)^4\right) \cdot \left(1 + \left(\frac{\text{ATP}[t]}{V_{\text{Pf}} \cdot K_{i_{\text{ATP}}}}\right)^4\right) \cdot \left(1 + \left(\frac{\text{PEP}[t]}{V_{\text{Pf}} \cdot K_{i_{\text{PEP}}}}\right)^4\right) \cdot \left(1 + \left(\frac{\text{Pyr}_{\text{ext}}[t]}{V_{\text{Pf}} \cdot K_{i_{\text{Pyr}_{\text{ext}}}}}\right)^4\right)} \tag{3.3.33}$$

$$v\text{LDH} = \frac{V_{f_{\text{LDH}}} \cdot V_{\text{Pf}} \cdot \alpha \cdot \frac{\text{NADH}[t] \cdot \text{pyruvate}_{\text{int}}[t]}{K_{\text{NADH}} \cdot V_{\text{Pf}} \cdot K_{\text{pyr}} \cdot V_{\text{Pf}}} - V_{r_{\text{LDH}}} \cdot V_{\text{Pf}} \cdot \alpha \cdot \frac{\text{lactate}_{\text{int}}[t] \cdot \text{NAD}[t]}{K_{\text{lac}} \cdot V_{\text{Pf}} \cdot K_{\text{NAD}} \cdot V_{\text{Pf}}}}{\left(1 + \frac{\text{NAD}[t]}{K_{\text{NAD}} \cdot V_{\text{Pf}}} + \frac{\text{NADH}[t]}{K_{\text{NADH}} \cdot V_{\text{Pf}}}\right) \cdot \left(1 + \frac{\text{lactate}_{\text{int}}[t]}{K_{\text{lac}} \cdot V_{\text{Pf}}} + \frac{\text{pyruvate}_{\text{int}}[t]}{K_{\text{pyr}} \cdot V_{\text{Pf}}}\right)} \tag{3.3.34}$$

$$v\text{GlrDH} = \frac{V_{\text{GlrDH}} . V_{\text{Pf}} \cdot \alpha \cdot \frac{\text{DHAP}[t] \cdot \text{NADH}[t]}{K_{\text{DHAP}} \cdot V_{\text{Pf}} \cdot K_{\text{NADH}} \cdot V_{\text{Pf}}} \cdot \left(1 - \frac{\frac{\text{glycerol}_{\text{ext}}[t] \cdot \text{NAD}[t]}{\text{VRBC} \cdot V_{\text{Pf}}}}{\frac{\text{DHAP}[t] \cdot \text{NADH}[t]}{V_{\text{pf}} \cdot V_{\text{pf}}} \cdot K_{\text{eq}}}\right)}{\left(1 + \frac{\text{DHAP}[t]}{K_{\text{DHAP}} \cdot V_{\text{Pf}}} + \frac{\text{glycerol}_{\text{ext}}[t]}{K_{\text{g3p}} \cdot V_{\text{RBC}}}\right) \cdot \left(1 + \frac{\text{NAD}[t]}{K_{\text{NAD}} \cdot V_{\text{Pf}}} + \frac{\text{NADH}[t]}{K_{\text{NADH}} \cdot V_{\text{Pf}}}\right)} \tag{3.3.35}$$

$$v\text{ATPase} = V_{\text{ATPase}} \cdot V_{\text{Pf}} \cdot \alpha \cdot \text{ ATP}[t] \tag{3.3.36}$$

$$v\text{PyrTr} = \frac{V_{\text{PyrTr}} \cdot \alpha \cdot V_{\text{Pf}} \cdot \frac{\text{pyr}_{\text{int}}[t]}{K_{\text{Pyr}_{\text{int}}} \cdot V_{\text{pf}}} \cdot \left(1 - \frac{\frac{10^{-6.9} \cdot V_{\text{RBC}} \cdot \text{pyr}_{\text{ext}}[t]}{V_{\text{RBC}} \cdot V_{\text{RBC}}}}{\cdot \frac{10^{-7.2} \cdot V_{\text{Pf}} \cdot \text{pyr}_{\text{int}}[t]}{V_{\text{Pf}} \cdot V_{\text{Pf}}} \cdot K_{\text{eq}}}\right)}{\left(1 + \frac{\text{pyr}_{\text{ext}}[t]}{K_{\text{Pyr}_{\text{ext}}} \cdot V_{\text{RBC}}} + \frac{\text{pyr}_{\text{int}}[t]}{K_{\text{Pyr}_{\text{int}}} \cdot V_{\text{Pf}}} + \frac{\text{lac}_{\text{ext}}[t]}{\text{Ki}_{\text{Lac}_{\text{int}}} \cdot V_{\text{RBC}}} + \frac{\text{lac}_{\text{int}}[t]}{\text{Ki}_{\text{Lac}_{\text{int}}} \cdot V_{\text{Pf}}}\right)} + k_d \cdot \left(\frac{\text{pyr}_{\text{int}}[t]}{V_{\text{Pf}}} - \frac{\text{pyr}_{\text{ext}}[t]}{V_{\text{RBC}}}\right) \tag{3.3.37}$$

$$v\text{LacTr} = \frac{V_{\text{LacTr}} \cdot \alpha \cdot V_{\text{Pf}} \cdot \frac{\text{lactate}_{\text{int}}[t]}{K_{\text{Lac}_{\text{int}}} \cdot V_{\text{pf}}} \cdot \left(1 - \frac{\frac{10^{-6.9} \text{lactate}_{\text{ext}}[t]}{V_{\text{RBC}} \cdot V_{\text{RBC}}}}{\frac{10^{-7.2} \cdot \text{lactate}_{\text{int}}[t]}{V_{\text{Pf}} \cdot V_{\text{Pf}}} \cdot K_{\text{eq}}}\right)}{\left(1 + \frac{\text{lac}_{\text{ext}}[t]}{K_{\text{Lac}_{\text{ext}}} \cdot V_{\text{RBC}}} + \frac{\text{lac}_{\text{int}}[t]}{K_{\text{lac}_{\text{int}}} \cdot V_{\text{Pf}}} + \frac{\text{pyr}_{\text{int}}[t]}{\text{Ki}_{\text{pyr}_{\text{int}}} \cdot V_{\text{Pf}}} + \frac{\text{pyr}_{\text{ext}}[t]}{\text{Ki}_{\text{pyr}_{\text{int}}} \cdot V_{\text{RBC}}}\right)} + k_d \cdot \left(\frac{\text{lac}_{\text{int}}[t]}{V_{\text{Pf}}} - \frac{\text{lac}_{\text{ext}}[t]}{V_{\text{RBC}}}\right) \tag{3.3.38}$$

The model has two conserved moieties, where the concentration of NAD^+ + NADH and ATP + ADP remains constant (Eqs. 3.3.39 & 3.3.40). The total concentration of the adenosine phosphate moiety was set to 3.0 mM and the NAD^+ moiety set to 3 mM (Table 3.17). The total ATP + ADP moiety concentration has been measured experimentally to be between 3 and 4 mM[178,204], although Choi and Mikkelsen[37] reported a value of 0.9 mM. For the model we use the value of 3 mM, which is in agreement with the aforementioned studies. Typically the cytosolic concentration of unbound NAD^+ greatly exceeds that of NADH[65], and for instance in rat liver cytoplasm, an NAD^+:NADH ratio of approximately 700 has been measured[220]. In *P. falciparum* NAD^+ has been measured to be approximately 3 mM[204], and assuming a high NAD^+:NADH ratio, this concentration is representative of the total moiety concentration and is used as such.

$$\mathrm{NAD^+} + \mathrm{NADH} = [\text{Total NADH Moiety}] \tag{3.3.39}$$

$$\mathrm{ADP} + \mathrm{ATP} = [\text{Total ATP Moiety}] \tag{3.3.40}$$

3.3.3.2 Ordinary Differential Equations and Starting Conditions

The model consists of 18 ODEs (Eqs. 3.3.41 - 3.3.56), which describe the change in concentration of external metabolites ($\text{glucose}_{external}$, $\text{lactate}_{external}$, $\text{pyruvate}_{external}$ and $\text{glycerol}_{external}$ (Eqs. 3.3.41, 3.3.56-3.3.58) and as well as each of the internal metabolites (Eqs. 3.3.42-3.3.53) and ADP (Eq. 3.3.54) and NAD^+ (Eq. 3.3.55) as a function of time and enzyme rates. ATP and NADH are not modelled explicitly, as they form part of moiety conserved cycles (Eqs. 3.3.39 & 3.3.40). As such, the concentration of ATP and NADH

can be calculated from the total moiety sum.

$$\text{Glucose}_{external}'[t] = -v\text{GlcTr} \tag{3.3.41}$$
$$\text{Glucose}_{internal}'[t] = v\text{GlcTr} - v\text{HK} \tag{3.3.42}$$
$$\text{G6P}'[t] = v\text{HK} - v\text{PGI} \tag{3.3.43}$$
$$\text{F6P}'[t] = v\text{PGI} - v\text{PFK} \tag{3.3.44}$$
$$\text{F1,6BP}'[t] = v\text{PFK} - v\text{ALD} \tag{3.3.45}$$
$$\text{DHAP}'[t] = v\text{ALD} - v\text{TIM} - v\text{GlrDH} \tag{3.3.46}$$
$$\text{GAP}'[t] = v\text{ALD} + v\text{TIM} - v\text{G3PDH} \tag{3.3.47}$$
$$\text{B1,3PG}'[t] = v\text{G3PDH} - v\text{PGK} \tag{3.3.48}$$
$$\text{PGA3}'[t] = v\text{PGK} - v\text{PGM} \tag{3.3.49}$$
$$\text{PGA2}'[t] = v\text{PGM} - v\text{ENO} \tag{3.3.50}$$
$$\text{PEP}'[t] = v\text{ENO} - v\text{PK} \tag{3.3.51}$$
$$\text{Pyr}_{internal}'[t] = v\text{PK} - v\text{LDH} - v\text{PyrTr} \tag{3.3.52}$$
$$\text{Lac}_{internal}'[t] = v\text{LDH} - v\text{LacTr} \tag{3.3.53}$$
$$\text{ADP}'[t] = v\text{HK} + v\text{PFK} - v\text{PGK} - v\text{PK} + v\text{ATPase} \tag{3.3.54}$$
$$\text{NAD}'[t] = v\text{LDH} - v\text{G3PDH} + v\text{GlrDH} \tag{3.3.55}$$
$$\text{Gly}_{external}'[t] = v\text{GlrDH} \tag{3.3.56}$$
$$\text{Pyr}_{external}'[t] = v\text{PyrTr} \tag{3.3.57}$$
$$\text{Lac}_{external}'[t] = v\text{LacTr} \tag{3.3.58}$$

The presence of new permeation pathways and increased permeability of the parasitised erythrocytes to a variety of solutes[115] led to the assumption that the concentrations of glucose, lactate, pyruvate and glycerol experienced by the intracellular parasite, would be similar to those found in the human blood plasma. On this basis, the concentrations glucose, lactate, pyruvate and glycerol in the model were fixed at concentrations found in the blood plasma of healthy and mildly infected patients (Table 3.17).

Table 3.17: External metabolite concentrations and moiety concentrations. In the model the external metabolite concentrations were fixed at concentrations similar to those found in the blood plasma of healthy to mildly infected malaria patients. The total moiety concentrations of ATP:ADP and NADH:NAD^+ were set to represent concentrations measured in scientific literature.

	Concentration (mM)		
Fixed Parameter	Model	Literature	Reference
Glucose $_{external}$	5.0	4.0 - 6.0	[1,60]
$Lactate_{external}$	2.0	2.0 - 5.0	[210,118]
$Pyruvate_{external}$	0.20	0.13 - 0.35	[118]
$Glycerol_{external}$	0.15	0.10 - 0.20	[163,78]
ATP + ADP moiety	4.0	0.90 - 4.4	[37,178,204]
NADH + NAD^+ moiety	3.0	2.9 $\pm$ 0.50	[204]

3.3.3.3 Steady state analysis

The initial concentrations of each of the variable metabolites were set to approximately their steady state concentrations (Table 3.18). These conditions could be varied (as long as total moiety concentrations remained the same), without impacting the steady state fluxes and concentrations. The model attains steady state under the conditions described above and the resulting fluxes and metabolite concentrations are given in Table 3.18.

Table 3.18: Kinetic model initial conditions and steady state predictions. The starting concentrations and the steady state metabolite concentrations and fluxes as described by the model of *P. falciparum* glycolysis are summarised below. The external metabolites were clamped at concentrations that are found in mildly malaria infected patients (Table. 3.17).

Metabolite	Concentration (mM)		Flux	Rate
	Initial	Steady State		(μmol·min^{-1} ·mg^{-1})
Glucose	3.0	2.8	J_{GlcTr}	0.0486
G6P	3.0	2.5	J_{LacTr}	0.0920
F6P	1.0	0.8	J_{GlyTr}	0.00512
F1,6BP	2.0	2.0	J_{PyrTr}	0.00512
DHAP	1.0	1.5		
GAP	0.10	0.070		
B1,3PG	0.0020	0.0010		
3PGA	1.0	0.47		
2PGA	0.040	0.041		
PEP	0.010	0.0078		
PYR	0.30	0.25		
LAC	3.0	2.7		
ATP	2.0	2.25		
ADP	1.0	0.75		
NADH	0.5	0.20		
NAD^+	2.5	2.8		

The steady state glycolytic flux is remarkably similar to that found for another human parasite, *T. brucei* (0.07 vs. 0.05 μmol·min^{-1} ·mg^{-1}protein) and the 1:1 ratio of glycerol and pyruvate flux is as expected to balance the loss of NADH reduction due to pyruvate export. The steady state metabolite concentrations look physiologically feasible, with no concentrations being abnormally high or low.

3.4 General Discussion

In this study we have followed a bottom up approach for constructing a model of *P. falciparum* glycolysis. Bakker *et al.*[7] (*T. brucei*) and Teusink *et al.* (yeast)[205] used bottom up approaches similar to the approach in this study to try to understand glycolysis on the basis of the pathway kinetics alone. The lack of kinetic parameters available in the scientific literature for *P. falciparum* prevented the method of Bakker *et al*, who utilised numerous parameters from scientific literature, and necessitated an approach similar to van Eunen *et al.*[215] and Teusink *et al.*[205] who characterised a number of enzymes.

We have presented the thorough biochemical characterisation of each *P. falciparum* glycolytic enzyme and incorporated the resulting rate equations into a detailed kinetic model. In this study, most of the kinetic data were fitted to simple reversible Michaelis-Menten (uni-uni reactions) or random order rapid equilibrium (bi-bi reactions) "convenience" equations[126,41]. It is not expected that all of the bi-bi reactions have random binding order, but the kinetic behaviour is well described by these equations. For the purposes of this work, the exact enzyme mechanism is not essential as the aim of the work was not to understand the underlying mechanism of each glycolytic enzyme, but rather to see if the combined kinetics can describe glycolysis. As such, exact enzymatic mechanisms were not determined, as long as a mechanism based rate equation (e.g. random order bi-bi) could describe the kinetic behaviour over the physiological concentrations ranges of respective substrate, product and allosteric effectors.

This discussion does raise the matter of using phenomenological *versus* mechanistic rate equations. In systems biology it is not a necessity that a reaction be described by a mechanistic equation, since a model consisting of phenomenological equations (that describe kinetic behaviour of each enzyme adequately) would have similar global predictions of flux and metabolite concentrations when compared to a mechanism based model. Mechanistic based equations have the advantage that the parameters are clearly defined (e.g. half saturation constants), which also provides a standard for the comparison of parameters. The latter point is of paramount importance when utilising parameters from databases or scientific literature. Detailed mechanism based equations (e.g.

ping pong, random order equations), however, are cumbersome as they contain numerous kinetic parameters, which require a substantial amount of experimental data for fitting the parameters[41,172]. Somewhere in between purely phenomenological and detailed mechanism based equations are so-called generalised equations such as presented by Hanekom *et al.*[172], Liebermeister *et al.*[126] and Cornish-Bowden *et al.*[41]. These generalised equations have well defined constants, incorporate thermodynamic principles, can describe a wide variety of enzymatic behaviour, but consist of fewer parameters than a detailed equation, which can thus be readily determined experimentally.

This work builds on the work of others and increases our knowledge of *P. falciparum* glycolysis at a biochemical level. At an enzyme level we found few allosteric regulators, but this work has highlighted PEP, ADP and ATP as being important for the regulation of PFK, PK and TIM activity. The regulation of TIM and PK by PEP has recently been proposed to play a role in controlling the redox metabolism in yeast[77]. The regulation of the same enzymes in *P. falciparum* by PEP may thus serve a similar purpose.

The model, as well as all of the kinetic data, is available for viewing, interrogation or download on JWS online (http://jjj.biochem.sun.ac.za). The online version has the advantage that a user can analyse and interrogate the model without specialised software or skills. The availability of the kinetic data are provided for two purposes i) a user can see the description of the kinetic data and ii) it allows a user to fit custom equations to the data, which is of particular interest to someone incorporating the data into a larger dataset and fitting the combination of the data to more detailed or simplified equation.

The compilation of the kinetic model described in this work provides a good tool for understanding glycolysis in terms of the underlying kinetics as well as for identifying potential drug targets. In the work by Bakker *et al.* and *Teusink et al.*, the fluxes and metabolites concentrations could be described by models composed of glycolytic enzyme kinetics and it appears it may do so for *P. falciparum*. The current model reaches steady state with physiologically feasible steady state metabolite concentrations and fluxes and provides the foundation for further investigating and analysis. To investigate if the

kinetics can describe glycolysis in *P. falciparum* the model predictions will be compared to metabolic fluxes and metabolite concentrations *in vivo* in the next chapter. A model validated in this manner promises to be an important heuristic tool for drug discovery in *P. falciparum* glycolysis.

3.5 Conclusion

We have described a systematic approach to modelling the glycolytic pathway of asexual *P. falciparum*. Each of the enzymes was biochemically characterised and its kinetic behaviour described by a mechanistic rate equation. The integration of all the rate equations into a kinetic model has yielded a tool to analyse the behaviour of the system as a whole. The model predicts physiologically relevant steady state fluxes as well as metabolite concentrations. The individual kinetics indicate the importance of ATP, ADP and PEP as modulators of enzyme activity and suggest that they may be important for the regulation of *P. falciparum* glycolysis. Further analysis of the model is expected to yield insight into the regulation of the system, as well as identify the enzymes that are most important in controlling *Plasmodium* glycolysis. For a detailed analysis and validation of the model I refer the reader to the next chapter.

Chapter 4

Construction of a detailed kinetic model of asexual *Plasmodium falciparum* glycolysis, Part 2: Model validation and analysis

Penkler, G.P[1], Adams, W.P.[2], Rautenbach, M., Snoep, J.L.

4.1 Introduction

Malaria infection results in the death of millions of people annually, most of who are children under the age of 5 (WHO, Annual Report 2011). Wide spread drug resistance to most frontline antimalarials has promoted initiatives to combat *Plasmodium spp.* at many levels ranging from combating the mosquito vector, to targeting various stages of the parasite life cycle within the human host. In the asexual phase, *Plasmodium spp.* derives most of its ATP from glycolysis and as such, this pathway has been investigated as a potential drug target. Phosphoglucoisomerase[202], aldolase[219], triosephosphate isomerase[216,106], phosphoglycerate kinase[148] and lactate dehydrogenase[34,73,20] have been proposed as drug targets and inhibited *in vitro*. These enzymes have been investigated in isolation, but to date, the role of these enzymes in the pathway as a whole has not been considered.

To examine a pathway as a whole, the field of systems biology provides a

[1]Is responsible for all of sample generation, and all analysis of experimental and theoretical data presented in this chapter. The data from two unlabelled-glucose flux experiments presented in my M.Sc. thesis were incorporated with experimental fluxes determined with ^{14}C labelled glucose and further unlabelled-glucose flux experiments (Section 4.3.1).

[2]Adams, W., was responsible for the HPLC analysis of the ^{14}C external metabolite samples. During the HPLC analysis, Adams also identified glycerol as a product of *P. falciparum* trophozoite glycolysis.

variety of frameworks such as Metabolic Control Analysis (MCA), Hierarchical Regulation Analysis, Elementary Mode Analysis, Metabolic Flux Analysis, Flux Balance Analysis (these methods are reviewed by Geenen *et al.*[71]) and supply-demand analysis[89].

MCA, developed independently by Kascer & Burns[107] and Heinrich & Rapoport[168,82], is a theoretical framework that defines coefficients that quantify i) the relative change in steady state systemic properties (e.g. steady state flux, J, or metabolite concentration, c) due to a small change in a reaction step (i.e. enzyme rate, v), defined as flux or concentration control coefficients ($C_v^J = \frac{d\ln J}{d\ln v}$ and $C_v^c = \frac{d\ln c}{d\ln v}$ respectively) and ii) the relative change in a local property such as an enzyme rate (v) due to a small change in an effector or substrate concentration, as elasticity coefficients ($\epsilon_s^v = \frac{\partial\ln v}{\partial\ln s}$). The systemic control coefficients can be expressed in terms of local elasticity coefficients via connectivity and summation theorems[88].

As such MCA makes it possible to quantitatively understand the systemic properties in terms of the properties of each reaction step. For more detail on MCA and its formulation, refer to reviews by Fell *et al.*[64] and Hofmeyr[87].

The summation theorem for the flux control coefficients is useful at it means that the control of flux and metabolites may be distributed across the enzymes in the pathway and moves away from the idea of a 'rate limiting' step. This has important implications for drug target identification within a metabolic network.

As previously stated, the glycolytic enzymes of *Plasmodium spp.* have been studied in isolation and proposed as drug targets without taking into consideration the pathway as a whole. Targeting an enzyme, which has a low control of the flux, would require a high degree of inhibition and this has repercussions in terms of toxicity for the host unless it is highly specific. Targeting a flux-controlling enzyme or better yet, a number of flux-controlling reactions[138] would be preferable. Targeting the enzymes of *Plasmodium spp.* glycolysis is challenging as there is often a high degree of homology between the human and parasite glycolytic enzymes (Chapter 2). Obtaining drug specificity is thus crucial. Or is it? Consider a reaction step that has a high flux control in the parasite, but the same reaction has low control in the host. Inhibition of such a step would have a much greater effect on the parasite than on the

host, even if the drug would inhibit parasite and host enzyme to the same degree. Applying such a differential control approach has been proposed as a tool for drug target identification[8,98] and has been utilised by Bakker *et al.*[8] to identify the *Trypanosoma brucei* glucose transporter as a potential drug target.

A detailed mathematical model in combination with MCA could be important tools for drug target identification. The strength of such an approach is largely dependent on the accuracy of the model. This can be assessed via model validation. A typical method of validating models is to compare model predictions to independent experimental datasets (i.e. data not used for model construction).
A more substantial form of validation would be to compare model predictions to experiments where specific perturbations are made to the system. These perturbations could include inhibiting a single step or multiple reactions, increasing an enzyme activity (i.e. by over expressing a particular enzyme), or deleting a step (i.e. knockout strain). However, these perturbations are often complex to perform experimentally and it is also difficult to ascertain if a perturbation of a certain step is not also perturbing a variety of other reactions. What then can be considered a good validation and perhaps even more importantly, a sufficient validation?
A perfect model would include the entire system and accurately describe the response of the system to a wide range of perturbations. This is perhaps the holy grail of systems biology - the silicon cell - a model that is able to describe every reaction, pathway and interaction at a macromolecular level[200]. Systems biology models are tools to further our understanding of a system, and validation should give i) a measure of confidence using the model as a tool to investigate the system and ii) support for predictions and hypotheses derived from model analysis.

Evaluating the responses of a model to parameter perturbations is another important part of validation. Such an assessment is made in a sensitivity analysis, and is a useful means of critically examining whether a parameter or set of parameters is unduly influencing the model output. A method of sensitivity analysis that is often used, is to vary each parameter value by a small degree and quantify the relative increase or decrease in a systemic property

(i.e. flux or metabolite concentrations). These effects can be quantified as *response coefficients*[108] and are useful in identifying parameters that severely influence model output. Ideally, parameters that substantially influence the model should be determined as accurately as possible. More comprehensive global sensitivity analysis methods (see Saltelli *et al.*[180] for review) simultaneously vary all parameters within a given range (compared to a small change in the case of response coefficients). These methods quantify the relative contribution of each parameter (first order) or combination of parameters (multiple order) to the variation observed in the model output. Such methods are computationally expensive and more technical to implement, but do provide a more comprehensive examination of the parameter set.

In the previous chapter (Chapter 3) we constructed and described a detailed kinetic model of asexual *P. falciparum* glycolysis during the trophozoite phase. In this chapter we examine if the model, on the basis of the enzyme kinetics alone can describe the glycolytic flux and metabolite concentrations *in vivo*. Following this validation, we analyse the model with a sensitivity analysis and MCA, and compare the results with drug targets suggested in the scientific literature. The validated model provides a useful heuristic tool for improving our current understanding of *P. falciparum* glycolysis.

4.2 Methods

For reference each of the enzyme abbreviations are defined as follows: HK, *hexokinase*; PGI, *phosphoglucoisomerase*; PFK, *phosphofructokinase*; ALD, *aldolase*; TIM, *triosephosphate isomerase*; G3PDH, *glyceraldehyde 3-phosphate dehydrogenase*; PGK, *phosphoglycerate kinase*; PGM *phosphoglycerate mutase*; ENO, *enolase*; PK, *pyruvate kinase*; LDH, *lactate dehydrogenase*; αGlyPDH, *glycerol 3-phosphate dehydrogenase*; G6PDH, *glucose 6-phosphate dehydrogenase*

Each of the metabolites used in this work are abbreviated as follows: G6P, *glucose 6-phosphate*; F6P, *fructose 6-phosphate*; F1,6BP *fructose 1,6-bisphosphate*; DHAP, *dihydroxy acetone phosphate*; GAP, *glyceraldehyde 3-phosphate*; B1,3PG, *bis 1,3-phosphoglycerate*; 3PGA, *3-phosphoglycerate*; 2PGA, *2-phosphoglycerate*;

PEP, *phosphoenolpyruvate*.
Reagents were obtained from *Sigma Aldrich*, unless otherwise stated.

4.2.1 Culturing and isolation of *P. falciparum*

P. falciparum D10 was routinely cultured in A^+ erythrocytes (obtained from the Western Province blood bank, South Africa) at 3 - 4% *v/v* haematocrit in culture medium consisting of RPMI 1640, 0.5% *m/v* Albumax II®, 22 mM glucose, 25 mM HEPES, 3 mM hypoxanthine and 50 μg/mL gentamicin sulphate, under 3% oxygen, 4% carbon dioxide and 93% nitrogen at 37 ° C as described elsewhere (36, 146). Synchronisation of the cultures was maintained by centrifuging the infected erythrocytes (750 × g, 3 min) and suspending the pellet in 5% *m/v* sorbitol[97]. Following 5 min incubation at 37 ° C and centrifugation (750 × g, 3 min), the pellet was suspended in culture media and cultured as described above. Sorbitol destroys all but the ring stage parasites[97], ensuring that they are kept in phase. Isolation of trophozoites was achieved using a saponin lysis protocol[178], which permeabilises the erythrocyte and parasitophorous vacuolar membrane by interacting with the cholesterol found in these membranes[3,4]. More than 95% of parasites isolated in this manner can maintain a transmembrane potential and exclude 0.04% *v/v* trypan blue[177]. Saponin (0.05% *m/v* and 0.005% *w/w* active component sapogenin) was added to infected erythrocytes suspended in culture medium (typically 5% *v/v* haematocrit). After mixing by inversion, the suspension was centrifuged (1800 × g, 7 min). Upon removal of the supernatant, the parasites were washed twice in culture medium or a buffer of choice.

4.2.2 Flux and Internal Metabolite Experiments

For the glycolytic flux and metabolite determination experiments, trophozoites were isolated, washed twice and suspended in incubation a modified Ringer buffer (5 or 10 mM glucose, 50 mM HEPES, 1 mM $MgCl_2$, 10 mM KCL, 120 mM NaCl, pH 7.1) similar to that described by Wünsch *et al.*[224]. In this buffer the parasites were able to exclude 0.04% *v/v* trypan blue. Immediately after suspension, two aliquots were taken for cell counting (Improved Neubauer Haemocytometer) and total protein determinations (method of Bradford *et*

al.[19]). External metabolites were determined in two ways i) enzymatically and ii) using a radiolabelled HPLC method with ^{14}C labelled glucose (1:80 ratio) as substrate. For both methods, time point samples of the incubation were centrifuged (5000 $\times$ g, 1 min) and the supernatant i) retained for enzymatic determinations or ii) added to acetonitrile (70% v/v final) for HPLC determination (see below). For the determination of internal metabolites at specific time intervals, aliquots of the cell suspension were taken and metabolism halted by the addition of 70% m/v perchloric acid (12% m/v final concentration). Following 1 min sonication and centrifugation (10 min, 20 000xg, 4 °C), the supernatant was retained for the enzymatic determination of the glycolytic metabolites. The supernatant was neutralised with 10 M KOH. Samples were stored at -80°C until analysis.

4.2.3 Enzymatic Glucose, Lactate, Pyruvate and Glycerol determinations

Extracellular D-glucose was assayed by linking it to NADP reduction via HK and G6PDH. Samples and standards were incubated at room temperature in HEPES buffer (50 mM, pH 7.5) containing HK (5 U/mL), ATP (0.2 mM), G6PDH (10 U/mL) and NADP (0.5 mM). After a 15 minute incubation period the absorbance at 340 nm was measured. Extracellular L-lactate was assayed by using an LDH and NAD^+ linked assay. After a 20 min incubation period at room temperature in HEPES buffer (50 mM, pH 7.5) containing LDH (10 U/ml), NAD^+ (0.2 mM) and hydrazine (16 μL/ml), samples and standards were measured at 340 nm. Hydrazine binds to pyruvate and thus thermodynamically drives the unfavourable LDH reaction (reverse) to completion. Glycerol was measured using the method developed by Eggstein and Kuhlmann[55]. Glycerol samples and standards were incubated in assay buffer (150 mM HEPES (150 mM), $MgSO_4$ (15 mM), pH 7.5) with glycerol kinase (8.4 U/ mL), PEP (1 mM), NADH (0. 4 mM), ATP (1 mM), pyruvate kinase (3 U/mL) and lactate dehydrogenase (3.6 U/ mL) and the oxidation of NADH after 10 min was measured at 340 nm. Pyruvate samples and standards were incubated in HEPES buffer (50 mM, pH 7.5) containing LDH (10 U/mL) and NADH (0.1 mM) and the absorbance after 10 minutes measured at 340 nm.

4.2.4 Enzymatic Determination of Metabolites

The intermediates of upper glycolysis (G6P, F6P, F1,6BP, DHAP and GAP) were all assayed within a single sample (180 μL) by linking the metabolite assays to the reduction of NADP via G6PDH or oxidation of NADH via α-glycerolPDH. G6P was determined by adding G6PDH (1U/mL final) and NADP (5mM final). Total change in absorbance at 340 nm was determined upon completion of the reaction. A spike of G6P (20 μM) was added and change in absorbance determined once the reaction was complete. To the same sample, PGI (1U/mL final) was added for assaying F6P and again the total change in absorbance determined. After completion, a 20 μM F6P spike was added to the mixture. In a similar stepwise (sample/spike) manner, DHAP, GAP and FBP were determined via NADH (0.8 mM final) and α-glycerolPDH (1U/mL final, TPI (1U/mL) and aldolase (1U/ml) respectively. Under these experimental conditions there is a linear dependency between absorbance (340 nm) and metabolite (G6P, F6P and F1,6BP) concentration (2 - 200 μM). The change in absorbance for the 20 μM intermediate spike was thus used as an internal standard to determine the concentration of each intermediate within the sample. The intermediates of lower glycolysis could not be determined due to high concentrations of lactate and pyruvate in the samples. This prevented the linked determination of PEP and the phosphoglycerates via LDH and NADH.

Trophozoite counts (Improved Neubauer Haemocytometer) and the assumption of a trophozoite cytosolic volume of 28 fL[2] were used to calculate the intracellular concentration of each metabolites.

4.2.5 Glucose, Lactate, Pyruvate and Glycerol HPLC Determinations

The method of Antonio *et al.*[5] was employed to determine the concentrations of the radiolabelled extracellular glucose, lactate, pyruvate and glycerol. Antonio *et al.*[5] did not detect glycerol as it ionises poorly in an ESI (electro-spray ionisation) source. Glucose, lactate, pyruvate and glycerol eluted at 13.4, 6.5, 10.1 and 10.4 min respectively. We confirmed that the eluent at 10.4 min was glycerol using enzyme determination assays. Briefly, separation occurred on

a ZIC®-HILIC column (150×7.5mm, 5 μm, 200 Å, SeQuant™, Merck, Darmstadt, Germany) fitted with a guard column (20×2.1mm, 5 μm, SeQuant™, Merck, Darmstadt, Germany) on a HPLC system. The system consists of a SpectraSYSTEM P4000 pump (Thermo Separation™ products, San Jose, CA, USA), a SpectraSYSTEM AS3000 autosampler (Thermo Separation™ products, San Jose, CA, USA) and a Flo-One liquid scintillation spectrophotometer (Radiomatic, Tampa, FL, USA). A flow rate of 1.0 mL/min and an injection volume of 100 μL were used. Separation occurred at room temperature (25°C). Mobile phase A consisted of acetonitrile (0.1% *m/v* formic acid) and mobile phase B of 5 mM ammonium acetate, pH 4 (0.1% *m/v* formic acid). The method was slightly modified by pumping 90% *v/v* A through the system for 1 min, prior to the initiation of the gradient elution profile. The analogue intensity (V) data were integrated and analysed with *Mathematica 8.0*®.

4.2.6 Model Simulations and Analysis

Most of the model simulations presented in this thesis were performed using *Wolfram Mathematica 8.0*®. The kinetic model of *P. falciparum* glycolysis is available on JWS Online (jjj.biochem.sun.ac.za)[201,144] for interrogation or download in various standard formats. Steady state analysis and metabolic control analysis was performed both in *Wolfram Mathematica 8.0*®, JWS Online and Copasi[96]. Parameter sensitivity analysis of the model was performed using Copasi[96].

4.3 Results

In the preceding chapter we reported the construction of a detailed kinetic model of *P. falciparum* glycolysis, which consists of mechanistic rate equations that were obtained from the biochemical characterisation of each of the glycolytic enzymes. Upon integration of the model, steady state was obtained and here we aim to validate the model by comparison of the model prediction to the steady state glycolytic data obtained with isolated trophozoite incubations. As such we test whether our knowledge of the isolated enzyme kinetics can describe the glycolytic behaviour of intact trophozoites.
For the model validation we needed to adapt the model minimally by i) setting

the ATPase rate and ii) adding kinetics to the glycerol branch. *P. falciparum* utilises the nett production of ATP during glycolysis in a variety of biosynthetic and homeostatic processes. This rate of ATP consumption, however, cannot be measured experimentally and had to be fitted. In the model , the ATPase rate determines the ATP:ADP ratio to some extent and the ATPase rate was fitted to obtain an ATP:ADP ratio of 3. This is in agreement with experimentally determined ratios, which vary between 1 (glucose starved) and 5.7[37,68,178,204].

In asexual *P. falciparum* the enzymes involved in the production of glycerol are not yet known and in the model the glycerol 3-phosphate dehydrogenase is assumed to produce glycerol.

4.3.1 External metabolite fluxes

The complete conversion of ^{14}C glucose to lactate, pyruvate and glycerol was measured over 90 min in isolated trophozoites (Figs. 4.2 & 4.2). The external metabolite concentrations were quantified with an HPLC / scintillation counter method (see methods), which successfully separated each external metabolite (Fig. 4.1). Glucose, lactate, pyruvate and glycerol eluted at 13.4, 6.5, 10.1 and 10.4 min respectively. Pyruvate and glycerol eluted in quick succession from the HPLC column. In most of the samples the two peaks could be separated and a pyruvate: glycerol ratio of 0.92 $\pm$ 0.23 (SD, n = 7) was obtained. When the two peaks could not be separated, a 1:1 ratio was assumed. To our knowledge this is the first report of the combined production of pyruvate and glycerol in *Plasmodium spp.*. Glycerol production has been observed[125], and pyruvate has been shown to be transported by a proton coupled monocarboxylate transporter[57], but has not been measured extracellularly. We show a production ratio of 1:1, which would lead to a closed redox balance, i.e. the glycerol production balances the excess NADH produced due to pyruvate excretion. This is not a unique for Apicomplexans, as *T. brucei* also transports pyruvate across the plasma membrane and utilises glycerol production to maintain redox balance[7].

Figure 4.1: HPLC chromatograms of ^{14}C labelled external metabolites produced by isolated *P. falciparum* trophozoites. Isolated *P. falciparum* trophozoites were incubated in a labelled glucose containing buffer. Samples taken over time were analysed for extracellular glucose (GLC), pyruvate (PYR), glycerol (GLR) and lactate (LAC). Shown are chromatograms of samples taken at 0, 45 and 135 min, which indicate the consumption of glucose and production of extracellular metabolites. The combined results of these labelled glucose incubation experiments are presented in Fig. 4.2.

The pathway fluxes provide an important part of the validation as they represent the combined effect of all the individual enzyme kinetics. As a means of validating the model we simulated the glucose incubation experiments. To reflect the experimental set up, three additions were made to the model, i) by including the total incubation (650 μL) and the total trophozoite cytosolic volume (6.9 $\pm$ 0.57 μL, n = 3) and ii) setting the external metabolites to those measured at 15 min (Fig. 4.2) and iii) changing the fixed external metabolite concentrations to time dependent variables. The first change was incorporated to ensure the correct internal to external volume ratio and the second change was made as it takes the cells approximately 10 min to reach a constant uptake rate. The final change was to allow the model to predict how the external metabolite concentrations change over time. The total cytosolic

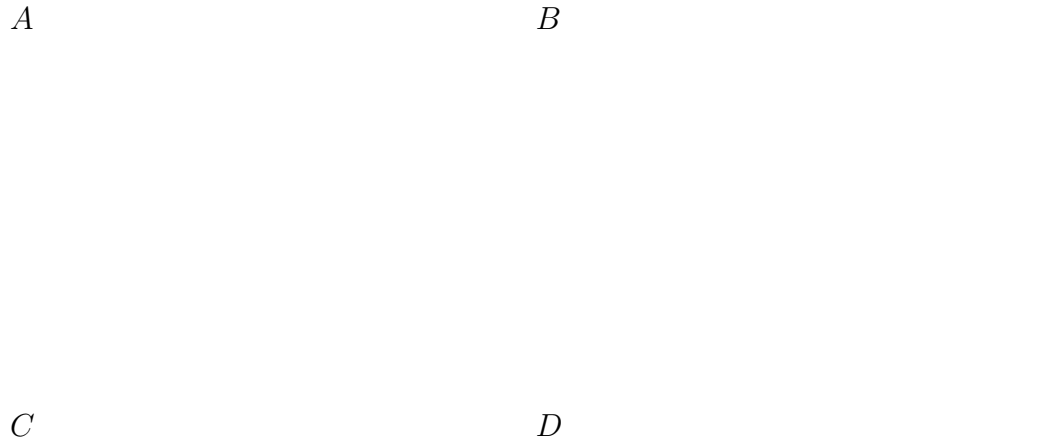

Figure 4.2: Model predictions of external fluxes compared to experimental results. Saponin derived *P. falciparum* trophozoites were incubated in ^{14}C glucose and external metabolite concentrations determined over a period of 90 minutes. Data points (■ and ●) represent two independent experiments, with the concentrations of A) glucose B) lactate, C) glycerol and D) pyruvate determined in singleton for each time point. For the predicted flux, the thickly dashed line is the model prediction with a glucose transporter V_{max} of 0.21 μmol·min^{-1}·mg^{-1}. The two closely matching finely dashed lines represent model prediction at the upper and lower boundary of the experimentally determined glucose transport V_{max} values.

volume was calculated from cell counts we assumed a cytosolic volume of 28 fL per trophozoite[2].

In Figure 4.2 we compare the experimental data with the prediction of the altered model. There is an excellent correlation between the model prediction and experimentally determined external metabolite concentrations for the period between 15 and 100 minutes. The V_{max} of the glucose transporter was previously determined to be 0.21 with a lower and upper range of 0.14 & 0.30 μmol·min^{-1}·mg^{-1}. To show that the 50% error on the parameter did not in-

fluence the model unduly we also show the flux predictions over a much larger range (0.1, 1.0 μmol·min^{-1}·mg^{-1}) of the glucose transporter maximal activity (Fig. 4.2). Even within the wide range of glucose transporter rates, the model still predicts the experimental results accurately. We assumed the system to be in steady state for the 15 to 50 minute period and the steady state flux values are given in Table 4.1.

The V_{max} of the glycerol-3-phosphate dehydrogenase activity was fitted to the measured glycerol production rate, which excludes this flux as part of the model validation. None of the other fluxes are fitted, and the good description of experimental data by the model provides a good degree of model validation.

Table 4.1: Experimentally determined glycolytic flux in *P. falciparum* trophozoites. Glycolytic fluxes for *P. falciparum* trophozoites were experimentally determined by incubating the parasites in 5 mM external glucose and measuring the change in external metabolites over time. The values represent the linear uptake or production rate over a period of at least 30 minutes. The experimental column includes both labelled and unlabelled incubations. The model prediction of steady state fluxes are given for an external glucose concentration set at 5 mM, lactate 1 mM, glycerol 0.2 mM and pyruvate 0.15 mM and V_{max} for the glucose transport set to 0.21 μmol·min^{-1}·mg^{-1}. The upper and lower limits were determined by setting the glucose transporter V_{max} to its upper and lower values and adjusting the ATPase rate to obtain an ATP:ADP ratio of 3 in each case.

Flux	Experimental flux ± SEM μmol·min^{-1}·mg^{-1}	n	Model Prediction (Lower/Upper Range) μmol·min^{-1}·mg^{-1}
$J_{glucose}$	0.060 ± 0.0068	4	0.0486 (0.043 - 0.055)
$J_{lactate}$	0.11 ± 0.0076	5	0.0920 (0.077 - 0.098)
$J_{pyruvate}$	0.0056 ± 0.0017	2	0.00512 (0.0046 - 0.0059)
$J_{glycerol}$	0.0063± 0.0013	2	0.00512 (0.0046 - 0.0059)

In addition to the labelled glucose flux experiments, additional flux experiments were performed with unlabelled glucose. In these experiments the external metabolites were determined enzymatically (see materials and methods)

and the fluxes were estimated from the change in concentration over time. These fluxes compare well to those obtained during the labelled uptake experiments and to those predicted by the model. In each of the flux experiments a constant flux was reached after approximately 10 minutes. Thereafter the respective consumption and production rates were estimated with linear regression over at least a 30 min period (Table 4.1).

4.3.2 Internal metabolite concentrations

By comparing experimentally measured internal metabolite concentrations to those predicted by the model, a second method of validation was obtained. In the scientific literature some glycolytic metabolite data are available, such as for the mouse infecting *P. berghei*[181]. However, these metabolites were determined in infected erythrocytes (parasitemia >75%) and the concentrations were compared to those found in the erythrocyte (See Table 4.2). For isolated *P. falciparum* trophozoites, as far as we are aware, the glycolytic metabolites have not previously been determined, although lactate has been measured, as well as ATP, ADP and NAD^+[204] (Table 4.2).

In this work the steady state concentrations of glucose 6-phosphate (G6P), fructose 6-phosphate (F6P) and fructose 1,6-bisphosphate (F1,6BP) were determined enzymatically (Table 4.2). The intermediate determinations were limited to upper glycolysis due to high concentrations of extracellular pyruvate and lactate which prevented the enzymatic determination of metabolites found in the lower half of glycolysis via lactate dehydrogenase. GAP and DHAP were assayed, but the concentrations were below the limit of detection (l.o.d) which was an intracellular concentration of approximately 100 μM. Due to the high volume of isolated parasites required to determine the intermediates, samples of a trophozoite incubation were taken at only two time intervals (30 and 40 min). At these intervals glucose consumption and product formation rates had reached a constant value and the system is expected to be in steady state. The concentration difference between the two points was not significant ($P < 0.05$, $n = 6$) and the average values for the time points are presented (mean $\pm$ SEM, $n = 12$) in Table 4.2.

Table 4.2: Summary of metabolite concentrations as predicted by the model and determined experimentally in this work and in scientific literature. The metabolite concentrations determined in this work are in steady state (see text for discussion), but it is not known whether this is true for those determined by Teng *et al.* and Sander *et al.*. The experimental values determined in this study are derived from three independent incubation experiments, where time points at 30 and 40 minutes were analysed in duplicate. For the predicted metabolite concentrations, model parameters (e.g. external metabolite concentrations, external and cytosolic volume) were set to match those of the metabolite experiment at 30 and 40 minutes. The predicted concentration is at a glucose transport V_{max} value of 0.21 μmol·min^{-1}·mg^{-1} as well as for the lower and upper ranges (parentheses).

	Intracellular Metabolite Concentrations (mM)				
Metabolite	Model (Lower/Upper Range)	*P. falciparum*[1] trophozoites	Mouse Erythrocytes[2]	*P. berghei*[2] Infected Erythrocytes	*P. falciparum*[3] trophozoites
Glucose	1.5 (0.86 - 2.4)	-	8.6 ± 1.0	4.9 ± 1.6	-
G6P	1.6 (1.1 - 2.2)	0.79 ± 0.058	0.12 ± 0.033	0.18 ± 0.026	-
F6P	0.50 (0.35 - 0.68)	0.15 ± 0.014	0.035 ± 0.0080	0.053 ± 0.013	-
F1,6BP	1.1 (0.60 - 1.6)	0.75 ± 0.14	0.040 ± 0.023	0.083 ± 0.034	-
DHAP	1.1 (0.90 - 1.4)	<0.1[4]	0.096 ± 0.052	0.12 ± 0.027	-
GAP	0.050 (0.040 - 0.060)	<0.1[4]	0.0046 ± 0.0021	0.0065 ± 0.0045	-
2,3BPG	-	-	15 ± 1.8	5.6 ± 1.2	-
1,3BPG	0.00076 (0.011 - 0.0010)	-	-	-	-
3PGA	0.39 (0.31 - 0.39)	-	0.08 ± 0.018	0.045 ± 0.016	-
2PGA	0.035 (0.031 - 0.041)	-	0.013 ± 0.0042	0.012 ± 0.0055	-
PEP	0.0067 (0.0056 - 0.0077)	-	0.025 ± 0.0094	0.030 ± 0.0081	-
Pyruvate	1.6 (1.6 - 1.6)	-	0.098 ± 0.021	0.19 ± 0.053	-
Lactate	13 (13 - 13)	-	3.9 ± 0.88	7.8 ± 2.7	1.1 ± 0.8
ADP	0.75	-	0.26 ± 0.030	0.25 ± 0.070	1.1 ± 0.4
ATP	2.25	-	2.8 ± 0.32	2.7 ± 0.34	2.0 ± 0.9
NAD^+	2.87 (2.88 - 2.87)	-	-	-	2.9 ± 0.5
NADH	0.13 (0.12 - 0.13)	-	-	-	-

1 This study

2 Determined for *P. berghei* infected (enriched to 75% parasitemia) mouse erythrocytes [181]

3 Determined using ^{1}H NMR in isolated *P. falciparum* trophozoites [204]

4 Below the limit of detection for intracellular metabolites (± 100 μM)

The model was adapted to reflect the isolated trophozoite experiments in which the metabolite concentrations were determined. The external metabolites concentrations of the model were fixed (2.7 mM glucose, 12 mM lactate, 1.5 mM pyruvate, 1.5 mM glycerol) at concentrations estimated to occur in the samples midway between 30 and 40 minutes. The model was allowed to reach steady state and the predicted metabolite concentrations are shown in Table 4.2 for comparison to concentrations measured *in vivo*. As with the flux predictions, the steady state metabolites were also calculated at both high (1.0) and low (0.1) glucose transporter V_{max} and these boundaries are listed in parenthesis in Table 4.2.

4.3.3 Model Analysis

4.3.3.1 Metabolic control analysis

To quantify the importance of each of the enzyme for the steady state behaviour of the glycolytic pathway, we performed metabolic control analysis on the system. The complete matrix of flux and concentration control coefficients are presented in Appendix A in Table A.1 and A.2 respectively. Subsets of the coefficients with relatively high values are shown in Table 4.3 and 4.4. *P. falciparum* does not have a single 'rate limiting' step, and the majority of the flux control is divided across five reactions, namely the glucose transporter (vGlcTr), hexokinase (vHK), phosphofructokinase (vPFK), glyceraldehyde 3-phosphate dehydrogenase (vG3PDH), and the ATP demand reaction (vATPase) (Table 4.3). The enzymes with high flux control, as well as glycerol 3-phosphate dehydrogenase (vGlrDH) and lactate dehydrogenase (vLDH) have the highest degree of concentration control (Table 4.4).

Table 4.3: Selected flux control coefficients. The coefficients were determined by JWS Online and Copasi for the model of *P. falciparum* glycolysis during the asexual trophozoite phase. The reactions with the majority of the flux control, namely the glucose transporter (vGlcTr), hexokinase (vHK), phosphofructokinase (vPFK), glyceraldehyde 3-phosphate dehydrogenase (vG3PDH), and the ATP demand reaction (vATPase) are shown. The complete set of flux control coefficients are shown in Appendix A.

	vGlcTr	vHK	vPFK	vG3PDH	vATPase
J_{GlcTr}	0.223	0.438	0.353	0.306	-0.448
J_{HK}	0.223	0.438	0.353	0.306	-0.448
J_{PGI}	0.223	0.438	0.353	0.306	-0.448
J_{PFK}	0.223	0.438	0.353	0.306	-0.448
J_{ALD}	0.223	0.438	0.353	0.306	-0.448
J_{TPI}	0.244	0.478	0.385	0.335	-0.489
J_{G3PDH}	0.233	0.457	0.368	0.320	-0.467
J_{PGK}	0.233	0.457	0.368	0.320	-0.467
J_{PGM}	0.233	0.457	0.368	0.320	-0.467
J_{ENO}	0.233	0.457	0.368	0.320	-0.467
J_{PK}	0.233	0.457	0.368	0.320	-0.467
J_{LDH}	0.244	0.478	0.385	0.335	-0.489
J_{LacTr}	0.244	0.478	0.385	0.335	-0.489
J_{ATPase}	0.244	0.478	0.385	0.335	-0.489
J_{GlrDH}	0.050	0.098	0.079	0.063	-0.100
J_{PyrTr}	0.050	0.098	0.079	0.063	-0.100

Table 4.4: Summary of selected concentration control coefficients. The coefficients were determined with JWS Online and Copasi. Similar to the flux control coefficients, the majority of the concentration control is in the glucose transporter (vGlcTr), hexokinase (vHK), phosphofructokinase (vPFK), glyceraldehyde 3-phosphate dehydrogenase (vG3PDH), and the ATP demand reaction (vATPase) as well in the glycerol producing reaction (vGlrDH). The complete set of control coefficients are shown in Appendix A.

	vGlcTr	vHK	vPFK	vG3PDH	vATPase	vGlrDH
ATP	0.244	0.478	0.385	0.335	-1.49	-0.110
DHAP	0.298	0.584	0.470	-0.648	-0.613	-0.155
GAP	0.297	0.581	0.468	-0.662	-0.616	-0.155
Pyr	0.009	0.017	0.014	0.011	-0.017	0.154
2PGA	0.237	0.465	0.374	0.325	-0.415	-0.052
NAD	-0.004	-0.008	-0.007	-0.006	0.009	0.010
Glucose	0.511	-0.288	-0.232	-0.202	0.295	0.003
F6P	0.452	0.887	-0.390	-0.338	-0.445	-0.093
LAC	0.006	0.012	0.010	0.009	-0.013	-0.004
3PGA	0.276	0.541	0.435	0.378	-0.519	-0.062
G6P	0.464	0.909	-0.366	-0.317	-0.470	-0.093
PEP	-0.055	-0.108	-0.087	-0.076	1.31	0.076
B1,3PG	1.168	2.29	1.85	1.60	-5.85	-0.457
F1,6BP	0.668	1.31	1.06	-1.07	-1.38	-0.291
NADH	0.072	0.141	0.114	0.100	-0.144	-0.168
ADP	-0.740	-1.45	-1.17	-1.02	4.52	0.333

4.3.3.2 Parameter Sensitivity Analysis

We used parameter sensitivity analysis in the study as a tool to test if any parameters were unduly influencing the model. A general parameter sensitivity analysis was performed using Copasi, yielding flux response coefficients (Appendix A, Tables A.3 & A.4) that describe the relative change in steady state flux or metabolite concentrations due to a small change in parameter value. An overall consideration of the flux response coefficients indicates that no single parameter has an unusually high coefficient and in this model, the

parameters with higher flux response coefficients are also from reactions with high flux control (HK, PFK, G3PDH and the glucose transport). The enzyme that has the most parameters with high response coefficients is PFK, which is described by a MWC equation. In this equation, the parameters in particular which have high response coefficients are the c_γ and L parameters, which alter the equilibrium ratio of the R and the T-state. These higher response coefficients are thus not considered to be unusual.
Two Michaelis constants for aldolase were obtained from the scientific literature and the response coefficients for these constants, K_{DHAP} and K_{GAP}, are both below 0.045, which indicates that these parameters do not have a large effect on steady state model behaviour.

Pyruvate and lactate are transported by the same monocarboxylate transporter and this transporter is well characterised[44,57]. We used the kinetic parameters from scientific literature, but the maximal specific activity was measured at 4°C. We increased the experimental rate by assuming a Q_{10} of 2. The response coefficients in themselves do not indicate if this assumption has an influence on model output, as it looks at only a small change in parameter. We showed (Appendix A Fig. A.4) that varying the V_{max} between the original V_{max} value determined at 4°C and the 8-fold extrapolation induces almost no change in steady state flux and only influences the concentration of lactate and to lesser extent, pyruvate.

The V_{max} of the glycerol producing enzyme was fitted to obtain the correct glycerol flux. Increasing the rate 2-fold almost doubles the glycerol and pyruvate flux, has no influence on the glucose flux and little influence (5%) on the lactate flux (Fig. A.5). G6P also decreases by 50%. These results indicate that fitting the glycerol flux does not detract from the good model prediction of glucose and lactate flux.
The ATP:ADP ratio was varied (by altering the ATPase activity) between and upper and lower boundaries (6 and 1) as measured in scientific literature to determine its effect on steady state model behaviour. At the upper boundary the glycolytic flux increases approximately 10% and apart from increasing the F1,6BP (+ 50%) and 1,3BPG (2-fold increase) concentrations, there was minimal effect on the other metabolite concentrations (Appendix A, Figs. A.1,

A.2 & A.3).

4.4 Discussion

In Chapter 3, we presented the construction of a detailed kinetic model of *P. falciparum* glycolysis. The model was composed of rate equations derived from a thorough biochemical characterisation of each enzyme in isolation. Can our understanding of the individual kinetics describe glycolysis *in vivo*? To answer this question we measured the steady state fluxes and metabolite concentrations in isolated trophozoites and compared them to the model prediction.

The glucose and lactate fluxes of several experiments (Table 4.1) compare well to the model. The model not only predicts the linear region of uptake and production, but also the decreasing rate of glucose uptake, as external glucose concentration drops to below the K_m value (1.8 mM) for external glucose (Fig. 4.2). It should be highlighted that this good prediction of steady state flux and glucose run-out conditions is an important validation for the mathematical model. It should be emphasized that apart from the glycerol branch none of the model parameters were fitted to the flux data set. The model parameters were determined in independent experiments on the isolated enzymes. Considering that each of the kinetic parameters contains experimental error and that this model has over 100 parameters, it raises the question of how the model can predict the glycolytic flux to within 15% of the experimentally determined values. Even during early stages of model construction, the flux prediction was comparable to measured fluxes and the glycolytic flux has been highly reproducible experimentally. What is the reason for this flux robustness? MCA theory shows that control of the flux can be divided across all of the reactions within the system. Thus if one step had almost all of the flux control, the accuracy of the parameters within this step would be greatly reflected in the accuracy of the flux predictions. In this model, glycolytic flux control is divided predominantly between five reactions (Table A.1), namely the glucose transporter (0.223), hexokinase (0.438), phosphofructokinase (0.353), glyceraldehyde 3-phosphate dehydrogenase (0.306) and ATPase (-0.448). The remaining enzymatic steps have minor control over the flux (<0.1),which would mean that experimental error in the parameters of these reactions, would only

have a small effect on flux prediction at that particular steady state. This is confirmed when one considers the PSA results, which indicate that only the parameter values of the flux controlling enzymes have high response coefficients (Table A.3) and that parameters of the enzymes with no flux control have almost no effect on steady state flux. In the extreme case where a single enzyme or reaction has almost all of the flux control, a 10% error in its rate would be reflected in a 10% error in the flux. In this model, however, even though the flux prediction is more sensitive to error in the controlling enzymes, there are four enzyme reactions that divide most of the flux control. As such, error in these reactions, has less of an impact on the steady state flux. (e.g. an error of 10%, in say the V_{max} of HK, would only equate to a 4.2% error in flux prediction). By assuming random unbiased error (e.g. 20% over and under-predictions) across the four enzymes (excluding the ATPase reaction, which cannot be experimentally determined), one would expect that the total error in flux prediction would be less than 20% and may explain why the flux predictions compare well to those measured *in vivo*. This concept of robustness has been mathematically formalised in a dissertation by Quinton-Tulloch *et al.*[164] and concludes among others, that a wide distribution of the flux control increases the robustness in flux.

It has been noted that the use of irreversible rate equations, such as used for PK and PFK in this model, may skew or artificially alter the flux control distribution no matter how high the equilibrium constant[42]. However, Cornish-Bowden and Cardenas[42] showed that provided there is a feedback loop that allows communication around an irreversible step, the model behaves in an almost identical fashion. Although PK and PFK are modelled with irreversible MWC equations, they do have product inhibition terms. This ensures that the irreversible reaction does not isolate one part of the pathway and does not influence model prediction.

The metabolite concentrations predicted by the model for F1,6BP compare well (1.1 vs. 0.74 mM), but for G6P and F6P there is a 2-3 fold over prediction of what was measured (Table 4.2). Predicted DHAP concentrations are considerably higher than measured and this accumulation of DHAP in the model may be due to the way in which the glycerol branch was modelled. Since

the enzymes for the production of glycerol in asexual *P. falciparum* are as yet unknown, the glycerol branch was grouped into a single equation and the V_{max} was fitted to obtain the correct flux. If an additional enzyme step is incorporated into the glycerol pathway, the predicted concentration of DHAP may well be lower. Predicted GAP concentrations (0.050 mM) are in agreement with the inability to quantify the concentration experimentally as it is below the limit of detection in our assays. The predicted internal lactate concentration is fairly high at 13 mM, but in *P. berghei* infected erythrocytes it has been measured at approximately 8 mM (Table 4.2). The 1.1 mM intracellular lactate concentration measured by Teng *et al.* (Table. 4.2) is not in disagreement with the model, where internal lactate concentrations are strongly dependent on the extracellular lactate concentrations. If extracellular lactate concentration were low (e.g. 1 mM) during the determination by *Teng et al* (compared to 12 mM in this work), the model would predict a very similar internal lactate concentration.
Overall the model gives a good description of metabolic flux and the steady state metabolite concentrations are comparable to those found *in vivo*. Bakker *et al.*[7] (*T. brucei*) and Teusink *et al.*[205] (yeast) could also, on the basis of the underlying kinetics, largely describe glycolysis. It would appear that at least for small networks for which good enzyme assays are available, such as glycolysis, the kinetics of the individual enzymes are sufficient in describing systemic properties such as flux and metabolite concentrations.

The asexual stage of *Plasmodium spp.* derives most of its ATP from glycolysis and as such, this pathway has been investigated as a potential drug target. Phosphoglucoisomerase[202], aldolase[219], triosephosphate isomerase[216,106], phosphoglycerate kinase[148] and lactate dehydrogenase[34,73,20]) have been proposed as drug targets and inhibited *in vitro*. The validated model provides a unique tool to investigate each of these proposals on the basis of their metabolic control. MCA of the model highlights four steps (glucose transporter, HK, PFK and G3PDH) as having most of the flux and concentration control (Tables A.1, A.2). Of these, only the glucose transporter has been proposed as a drug target. The remaining proposed drug targets, PGI, ALD, PGK and LDH, have low control of the glycolytic flux and in each of these a high degree of inhibition would be required before having an effect on glycolytic flux. The glucose

transporter, PfHT1, has been proposed and investigated quite extensively as a potential drug target[155], without taking into account the metabolic control structure of *P. falciparum* glycolysis. A further step would be to use differential control analysis and also take into account the metabolic control structure of the host. MCA of the Holzhutter *et al.* model of erythrocyte glycolysis[94] indicates that glucose transporter has negligible control of the flux and when compared the high control of the *P. falciparum* transporter, MCA highlights this step as a potential drug target. We would expect that interfering with glycolysis, the parasite's main ATP producing pathway will strongly inhibit its growth rate.

An interesting question that arises from the MCA results is the high concentration control (>1) over PEP by the GlcTr, HK, PFK, G3PDH and PK (-1.0). The finding that PEP inhibits TPI strongly, and inhibits PK in *P. falciparum* (Chapter 3) and activates PFK in *P. berghei*[22] identifies PEP as a key regulatory molecule in *Plasmodium spp.* and suggests that it may regulate glycerol metabolism. Hypothetically, on the basis of the control coefficients, the reduction in PK expression would result in an increased PEP concentration. This in turn would activate PFK (*P. berghei)* and would further increase the PEP concentration, ultimately inhibiting TPI strongly. The almost complete inhibition of TPI, would be expected to increase the glycerol flux. Grüning *et al.*[77] reported a similar feedback loop in yeast, where low PK activity results in the accumulation of PEP resulting in the inhibition of TPI and consequent activation of the pentose phosphate pathway. The current model describes the glycerol branch with a single rate limiting (flux control coefficient 0.78) reaction and is thus not suitable for testing the above hypothesis that PEP regulates the glycerol flux in *P. falciparum.* However, the model does highlight the importance of PEP and upon further elucidation of the glycerol pathway the model may improve our understanding of the regulation of the glycerol flux.

Lian *et al.*[125] showed that asexual *P. falciparum* produces glycerol and our finding of an experimental ratio of approximately 1:1 for the glycerol and pyruvate flux indicates that the glycerol branch is essential for maintaining redox balance by oxidising excess NADH produced due to pyruvate excretion. The role of glycerol during the asexual phase is unclear. It may be that since the

monocarboxylate transporter cannot differentiate between lactate and pyruvate, the production of glycerol is required for redox balance. Alternatively, glycerol itself may play a physiological role as it does in yeast, where it has been shown to be important for osmotic regulation[110,91].
P. falciparum does have a gene for glycerol kinase[186], but it has been shown that it is not expressed during the asexual stage and enzyme activity could also not be detected (this study and[186]). A gene or putative gene sequence for glycerol-3-phosphate phosphatase is also not present in the genome[125]. PGM2, an isozyme of phosphoglycerate mutase, has been reported to have phosphatase activity towards a number of substrates[85] and it is possible that it can use glycerol 3-phosphate as a substrate. These findings do raise the question of how glycerol is produced in asexual *P. falciparum* and why the parasite does not express glycerol kinase during the asexual phase.

4.5 Conclusion

We have constructed and validated a kinetic model for asexual *P. falciparum* glycolysis. We have shown that the model describes the steady fluxes well and in addition gives similar metabolites concentrations. However, these are overestimated compared to those measured experimentally. Furthermore, assumptions made during model construction have been shown to not greatly influence the model output. Having constructed and validated the model, the model was analysed as a whole using MCA and PSA to investigate potential drug targets and improve our understanding of its regulation.

Several enzymes within the *P. falciparum* glycolysis have been proposed as potential drug targets. In order to evaluate these proposals a kinetic model was constructed (Chapter 3) and validated as a tool for the analysis of the system as a whole. Independently of fitting, the model, purely as a function of the independently determined enzyme kinetics, describes the steady state glycolytic fluxes in isolated trophozoites and predicts the metabolite concentrations in upper glycolysis within a factor of two. Model analysis showed that the assumptions used during model construction do not have a large influence on the system behaviour and that the validated model gives a good representation

of *P. falciparum* glycolysis during the asexual phase. The validated model indicates that PEP may play a role in the regulation of the glycerol flux. Model analysis highlighted the glucose transporter, HK, PFK and G3PDH as the enzymes with the highest flux and metabolite control, indicating that these enzymes should be preferentially targeted over those with minimal control. Furthermore, this work adds further support for research aimed at targeting the glucose transporter, PfHT1 in the quest for novel antimalarials.

Chapter 5

Differential control analysis as a tool for drug target identification in *Plasmodium falciparum*

Penkler, G.P., Rautenbach, M., Snoep, J.L.

5.1 Introduction

P. falciparum, with its dual host life cycle and numerous physiologically different forms and stages, presents a vast array of potential drug targets. Finding an effective drug target has proven difficult, however, and the challenges are amplified by the parasites' extraordinary ability to become resistant to most antimalarials within a decade or two. Asexual *Plasmodium spp.* relies almost entirely on glycolysis for ATP. As such, several glycolytic enzymes have been proposed as potential drug targets[155,219,169,20].
Previously, we biochemically characterised each of the glycolytic enzymes and from the data constructed and validated a detailed kinetic model of asexual *P. falciparum* glycolysis (Chapters 3 & 4). Metabolic control analysis of the model indicated that the *P. falciparum* glycolytic pathway does not have a single 'rate-limiting' step, but that the hexose transporter (PfHT1), hexokinase (HK), phosphofructokinase (PFK) and glyceraldehyde 3-phosphate dehydrogenase (G3PDH) are the enzymes most important for controlling the flux.

Metabolic control analysis (MCA) is a method that can be used to determine the degree of flux control exerted by an enzyme and was developed independently by Kascer & Burns[107] and Heinrich & Rapoport[168,82] and further developed by others (see[64,87]for review). MCA is a theoretical framework that

defines: i) flux (J) and concentration (c) control coefficients (C_v^J & C_v^c), which quantify the relative change of steady state systemic behaviour, (e.g. J and c), due to a small change in a local reaction rate, v (Eq. 5.1.1).

$$C_v^J = \frac{d\ln J}{d\ln v} \quad \& \quad C_v^c = \frac{d\ln c}{d\ln v} \tag{5.1.1}$$

ii) elasticity coefficients (ϵ_p^v) which quantify the relative change in the local reaction rate, v, due to a small change in an effector, p, (e.g. substrate or inhibitor concentration) (Eq. 5.1.2).

$$\epsilon_p^v = \frac{\partial\ln v}{\partial\ln p} \tag{5.1.2}$$

iii) response coefficients (R_p^J & R_p^c), which describe the relative change in a systemic property such as flux or metabolite concentration due to a change in a local parameter, p. These response coefficients can be further described as the product of their respective elasticity and control coefficient (Eq. 5.1.3). For more detail on MCA and its formulation, refer to[64,87].

$$R_p^J = \frac{d\ln J}{d\ln p} = C_{v_i}^J \cdot \epsilon_p^{v_i} \quad \& \quad R_p^c = \frac{\partial\ln c}{\partial\ln p} = C_{v_i}^c \cdot \epsilon_p^{v_i} \tag{5.1.3}$$

MCA, which has been used as a tool to amongst others i) improve our understanding of certain diseases (see[33] for review), ii) suggest novel strategies to treat cancer[138] and iii) identify drug targets in African sleeping sickness[8] and cancer[147]. For drug target identification, the approach has generally been to identify an enzyme, or group of enzymes[138] with a high flux or concentration control. Inhibition of these reactions is expected to require lower concentrations of inhibitor, compared to reactions with low flux control. In addition to considering the enzymes which have high control in the pathogen, one should also consider the host metabolic control structure[8,98]. Subsequently one can identify enzyme(s) with a high flux control in the parasite, whereas the equivalent reaction in the host has a low flux control. Due to this *differential control*, inhibition of this enzyme to the same degree in both the parasite and host would have a greater effect on the parasite and would reduce the side effects of drugs that are not completely selective. This differential control approach has been proposed as a tool for drug target identification[8,98], but has yet to be demonstrated *in vivo*. A measure of the degree of differential control defined by Hornberg *et al.*[98] is given by the ratio of the host and pathogen flux

response coefficients for a drug.

In our previous work, model analysis indicated that the PfHT1 has a relatively high control of the glycolytic flux and that the glucose transporter in the host erythrocyte has almost no control (Chapter 4). This provided the ideal opportunity to test the concept of *differential control analysis* as a tool for drug target identification *in vivo* (i.e. on whole trophozoites and erythrocytes) and is the focus of this article. If the model predictions were correct, specific inhibition of the glucose transporter in *P. falciparum* would lead to a far greater decrease in flux in the parasite than in the host's erythrocytes even with a comparable inhibition of both glucose transporters. A compound that has been widely utilised for inhibiting glucose transport is cytochalasin B. Cytochalasins are fungal metabolites with similar structural and biological activity characteristics. Cytochalasin B is perhaps best known as an inhibitor of actin microfilament dynamics[129], which would explain a number of observed cellular effects (motility[31], morphology[183], adhesion[56] and division changes[31]). Of interest in this study, is the observation that cytochalasin B is a potent inhibitor of glucose transport in erythrocytes[10,14,50,76] as well as in *Plasmodium spp.*[116,119,222,223]. In erythrocytes, most studies have reported the inhibition of glucose efflux[10,14,50,76], but it has also been shown to inhibit glucose uptake into pink erythrocyte ghosts strongly[120]. Bloch[14] reported that glucose efflux is nearly completely inhibited by 100 μM cytochalasin B in human erythrocytes. Glucose uptake via GLUT1 and PfHT1, which have been expressed in frog oocytes is inhibited by cytochalasin B, with approximately 75% inhibition for PfHT1 with 50 μM[223]. Cytochalasin B is also reported to inhibit the uptake of 2-DOG into infected erythrocytes[116].
The mechanism by which cytochalasin B inhibits glucose transport is unclear, but for erythrocytes it has been shown to bind asymmetrically to the transporter in a noncompetitive manner[10,14], although others have reported competitive binding kinetics[50]. Although the mechanism is uncertain, it is clear from the erythrocyte ghost and frog oocyte experiments that although cytochalasin B induces a number of cellular changes, it does inhibit the glucose transporters of human erythrocytes and *P. falciparum*. Despite the low specificity of cytochalasin B, it appears that in the central carbon metabolism the only mode of action is on the glucose transporter.

Our previous findings indicated that PfHT1 has a relatively high control over glycolytic flux and that the erythrocyte glucose transporter has almost no flux control. In this Chapter we investigate the model prediction of differential control of the flux by the glucose transporter in *Plasmodium spp.* and human erythrocytes. We present experimental evidence of differential control by showing that inhibition of the glucose transporter with cytochalasin B in intact *P. falciparum* trophozoites and erythrocytes decreases the glycolytic flux in the parasite, but not in the erythrocyte.

5.2 Methods

5.2.1 Culturing and isolation of *P. falciparum*

P. falciparum D10 was routinely cultured in A^+ erythrocytes (kindly donated by the Western Province blood bank) at 3 - 4% *v/v* haematocrit in culture medium consisting of RPMI 1640, 0.5% *m/v* Albumax II® , 22 mM glucose, 25 mM HEPES, 3 mM hypoxanthine and 50 μg/mL gentamicin sulphate, under 3% oxygen, 4% carbon dioxide and 93% nitrogen at 37 ° C as described elsewhere (36, 146). Synchronisation of the cultures was ensured by centrifuging the infected erythrocytes (750 × g, 3 min) and suspending the pellet in 5% *m/v* sorbitol[97]. Following 5 min incubation at 37 ° C and centrifugation (750 × g, 3 min), the pellet was suspended in culture media and cultured as described above. Sorbitol destroys all but the ring stage parasites[97], ensuring that they are kept in phase.

Isolation of trophozoites from infected erythrocytes was achieved using a saponin lysis protocol[178], which permeabilises the erythrocyte and parasitophorous vacuolar membrane by interacting with the cholesterol found in these membranes[3,4]. Greater than 95% of parasites isolated in this manner can maintain a transmembrane potential and exclude 0.04% *v/v* trypan blue[177]. Saponin (0.05% *m/v* and 0.005% *w/w* active component sapogenin) was added to infected erythrocytes suspended in culture medium (typically 5% *v/v* haematocrit). After mixing by inversion, the suspension was centrifuged (1800 × g, 7 min). Upon removal of the supernatant, the parasites were washed twice in

culture medium or a buffer of choice.

5.2.2 Inhibition of glycolytic flux

For the flux experiment, trophozoites were isolated, washed twice and then suspended in modified Ringer incubation buffer (5 mM glucose, 50 mM HEPES, 1 mM $MgCl_2$, 10 mM KCL, 120 mM NaCl, pH 7.1) similar to that described by Wünsch *et al.*[224], containing between 0 and 100 μM cytochalasin B made up in DMSO (final concentration <0.5% *m/v*). In this buffer the parasites were able to exclude 0.04% *v/v* trypan blue. Two aliquots were taken for cell counting (Improved Neubauer haemocytometer). Aliquots of the incubation suspension were taken over 60 min and following centrifugation (10 000 × g, 5 min, 4°C) the supernatant was retained for the determination of extracellular lactate. The control contained no cytochalasin B, but an equivalent concentration of DMSO.

Extracellular L-lactate was assayed by using a lactate dehydrogenase (LDH) and NAD^+ linked assay. After samples and standards were incubated for 20 min at room temperature in HEPES buffer (20 mM) containing LDH (10 U/ml), NAD^+ (0.2 mM) and hydrazine (16 μL/ml), absorbance was determined at 340 nm on a spectrophotometer (VarioSkan microplate reader, Thermo Electron Corporation). Hydrazine binds to pyruvate and thus thermodynamically drives the unfavourable LDH reaction (reverse) to completion.

5.2.3 Inhibition of ^{14}C Glucose Uptake

Isolated parasites were washed twice and then suspended in glucose free modified Ringer buffer (50 mM HEPES, 1 mM $MgCl_2$, 10 mM KCL, 120 mM NaCl, pH 7.1) similar to that described by Wünsch *et al.*[224]. In this buffer the parasites were able to exclude 0.04% *v/v* trypan blue. Between 30 and 90 μL of trophozoites (1×10^9 trophozoites/mL final concentration) were mixed with an equal volume of glucose (10 mM final concentration, 1:100 label to unlabelled ^{14}C glucose) and cytochalasin B (0 - 200 μM final concentration) made up in DMSO (final concentration <0.5% *m/v*). The experiment was performed at 37°C and the reaction was quenched after 500 ms with 5 mL incubation buffer containing 100 mM unlabelled glucose kept at −5°C on a salt-ice mixture. The

rapid quenching was performed using a quench-flow device describe previously (Appendix B B). The quenched trophozoites were immediately transferred to a filter (covered with a thin layer of filter aid Celite 545, Sigma-Aldrich to prevent clogging) and washed with a further 10 mL ice cold incubation buffer. After washing, the filter was added to a scintillation vial containing 5 mL scintillant, incubated overnight and then counted on a scintillation counter. As a control, trophozoites were quenched prior to the addition of labelled glucose, and subsequently following the same sample preparation procedure.

5.2.4 Effect of Cytochalasin B on glycolytic enzyme activity

The specific activity of each glycolytic enzyme in the presence of 100 μM cytochalasin B was determined in NAD^+/NADP linked kinetics assays as described previously (Chapter 3). As a control the enzymes were also assayed without cytochalasin B, but the assay mixture included the same concentration of DMSO (solvent for Cytochalasin B).

5.2.5 Model Simulations and Analysis

Most of the model simulations presented in this chapter were performed using *Wolfram Mathematica 8.0*®. The kinetic model of *P. falciparum* glycolysis is available on JWS Online (jjj.biochem.sun.ac.za)[201,144] for interrogation or download in various standard formats. Steady state analysis and metabolic control analysis was performed both in *Wolfram Mathematica 8.0*®, JWS Online and Copasi[96].

5.3 Results

In previous work we constructed a detailed kinetic model of *P. falciparum* glycolysis, using kinetic parameters determined *in vitro* (Chapter 3). The model was validated by comparing model predictions (purely based on the measured isolated enzyme kinetics) to steady state system behaviour, i.e. flux and metabolite concentrations in intact *P. falciparum* trophozoites. Previous metabolic control analysis of the *P. falciparum* kinetic model and a model of erythrocyte glycolysis[95] (Chapter 4), revealed that the glucose transporter

had high control in the parasite and low control in the host, indicative of an effective drug target. To identify all potential drug targets in the network, we extend this analysis to include each of the glycolytic enzymes and quantify the effectivity (see Introduction, Eq. 5.3.1) of each reaction. Furthermore, to demonstrate this predicted differential control of the glucose transporter in the host and parasite we investigate i) the inhibition of ^{14}C glucose transport (zero trans uptake) in *P. falciparum* trophozoites by cytochalasin B and ii) the inhibition of lactate flux by cytochalasin B in intact isolated trophozoites and uninfected erythrocytes. The inhibition of glucose transport in erythrocytes by cytochalasin B was not investigated as this has been well characterised in the scientific literature. If model simulations are correct, it is expected that the glucose flux would be inhibited to a far greater degree in the parasite than the flux in the erythrocyte, even if both glucose transporters are inhibited to the same degree.

5.3.1 Metabolic Control Analysis

Metabolic control analysis was performed on the *P. falciparum* model as well as the model of erythrocyte glycolysis compiled by Holzhutter *et al.*[95] using JWS Online[201,144]. For both models, the flux control coefficients of each enzyme on the glycolytic flux are summarised in Table 5.1. For two other models of erythrocyte glycolysis, the control distribution is similar to the Holzhutter *et al.*[95] model with the ATPase and 2,3 bisphosphoglycerate shunt having most of the flux control[53]. The Holzhutter *et al.* model was used in this work as it includes the glucose transporter as an explicit reaction step.

As defined before, effectivity (Eq. 5.3.1) can be quantified as the ratio of the drug response coefficients and this can be further expressed in terms of the elasticity and flux control coefficients (Eq. 5.3.1). This ratio was termed *selectivity*, but it is ambiguous as it does not differentiate between drug selectivity (i.e. degree of selective drug binding and inhibition of the parasite and host enzyme) and the subsequent selective inhibition of the flux. To disambiguate, we define the degree to which a drug inhibits the pathogen flux compared to the host flux as *effectivity*. We maintain the definition of drug selectivity as the degree to which the drug inhibits the pathogen enzyme compared to the inhibition observed for the host enzyme.

In the instance of a non-selective drug that inhibits both pathogen and host enzymes to the same degree, the elasticities would be equal ($\epsilon_{\text{drug}}^{v(\text{pathogen})} = \epsilon_{\text{drug}}^{v(\text{host})}$) and the effectivity can be described as the ratio of the flux control coefficients.

$$\text{effectivity} = \frac{R_{\text{drug}}^{J(\text{pathogen})}}{R_{\text{drug}}^{J(\text{host})}} = \frac{C_{v_i}^{J(\text{pathogen})} \cdot \epsilon_{\text{drug}}^{v_i(\text{pathogen})}}{C_{v_i}^{J(\text{host})} \cdot \epsilon_{i}^{v_i(\text{host})}} \tag{5.3.1}$$

To determine the effectivities of each enzyme in parasite and erythrocyte glycolysis, we assumed that a drug would inhibit both enzymes to the same degree (i.e. elasticity coefficients are equal) and thus the effectivity is the ratio of the flux control coefficients. For each enzyme the effectivity is listed in Table 5.1, with the pyruvate transporter (PyrTr) having the highest unscaled effectivity. However, despite its high effectivity, the PyrTr is not the best target as it only has a low control in the parasite. Ideally an effectivity index should also highlight potential drug targets and as such, favour a reaction with a high control in the parasite and low control in the host. Consider two reactions, one reaction with a high flux control coefficient (e.g. 0.9) and the other having a low flux control coefficient (e.g. 0.01), each with an effectivity of 10 (i.e. where control of the equivalent reactions in the host are a factor 10 less). Both of these steps have the same effectivity, but intuitively it would be preferable to target the reaction with higher control in the parasite. We propose a logarithmicly scaled effectivity (Eq. 5.3.2), which scales the coefficients and favours reactions with high control in the parasite. In the example above where both reactions have an effectivity of 10, the reaction with high flux control has a scaled effectivity of 5.5 compared to 1.5 for the reaction with low flux control. A higher scaled effectivity would theoretically provide a better drug target.

$$\text{scaled effectivity} = \frac{\text{Log}\left(\left|R_{\text{drug}}^{J(\text{host})}\right|\right)}{\text{Log}\left(\left|R_{\text{drug}}^{J(\text{pathogen})}\right|\right)} = \frac{\text{Log}\left(\left|C_{v_i}^{J(\text{host})} \cdot \epsilon_{\text{drug}}^{v_i(\text{host})}\right|\right)}{\text{Log}\left(\left|C_{v_i}^{J(\text{pathogen})} \cdot \epsilon_{\text{drug}}^{v_i(\text{pathogen})}\right|\right)} \tag{5.3.2}$$

Both the standard and scaled (logarithmic) effectivity methods were applied to the *P. falciparum* and the erythrocyte flux control distributions (Table 5.1) and the enzymes are ranked in terms of their scaled effectivity.

Table 5.1: Summary of glucose flux control coefficients in *P. falciparum* and human erythrocytes. The glucose flux control coefficients for each glycolytic enzyme were obtained by metabolic control analysis of *P. falciparum* and erythrocyte glycolysis models. The effectivity of each enzyme in both the standard ratio form (Eq. 5.3.1) and logarithmic scaled form (Eq. 5.3.2) is listed. The enzymes are ranked in terms of the highest scaled effectivity.

	$C^{J_{Glucose}}_{v_{enzyme}}$		Standard	Scaled
Enzyme	*P. falciparum*	Erythrocytes	Effectivity	Effectivity
G3PDH	0.306	-0.000500	608	6.41
GlcTr	0.223	0.000140	1652	5.94
PFK	0.353	0.0229	15.4	3.63
PyrTr	-0.0240	-0.00000413	5811	3.32
HK	0.438	0.0681	6.43	3.25
ALD	0.0780	-0.00323	24.1	2.25
LacTr	0.00300	-0.00000747	402	2.03
LDH (NADH)	0.0500	-0.00359	13.9	1.88
TPI	0.00300	-0.0000313	95.8	1.79
PGI	0.0200	0.00452	4.42	1.38
PGM	0.00100	0.00238	0.420	0.874
ENO	0.00100	0.00439	0.228	0.786
PK	0.00100	0.0134	0.0746	0.624
ATPase	-0.448	0.703	0.637	0.439
PGK	0	0.00545	0	-
GlrTr	-0.00500	-	-	-
LDH (NADPH)	-	0.0101	-	-
B1,3PG shunt	-	0.208	-	-

The top five effectivities determined by both methods indicate glyceraldehyde 3-phosphate dehydrogenase (G3PDH), the glucose transporter (GlcTr), and phosphofructokinase (PFK) as potential drug targets. The logarithmic scaled method, however, provides a better ranking of the reactions as potential drug targets as it ascribes a higher value to reactions with high control in the parasite, even if there is a large percentage difference in the parasite and host flux

control. These scaled effectivity rankings indicate G3PDH, GlcTr and PFK to be the best potential drug targets in *P. falciparum* glycolysis.

5.3.2 Inhibiting the *P. falciparum* glucose transporter

The scaled effectivities (Table 5.1) indicated that G3PDH and the glucose transporter are good potential drug targets, based on their significant control of glycolytic flux in the parasite and low flux control in the erythrocyte. In order to test this hypothesis, the glucose transporter was chosen for inhibition experiments as i) it has been well characterised for the human erythrocyte and *P. falciparum* and ii) cytochalasin B is a known inhibitor of the glucose transporter in both organisms.

In erythrocytes, the inhibition of glucose transporter by cytochalasin B has been well characterised (see Introduction) with more than 95% inhibition of efflux achieved at 100 μM cytochalasin B[14]. To characterise the inhibition of the *P. falciparum* glucose transport by cytochalasin B, we used a simple quench flow device (Appendix B B) to measure the zero-trans uptake rate of ^{14}C glucose at different inhibitor concentrations. The rapid quench time (0.5 s) ensured that we measured zero-trans influx and were not measuring metabolism (Chapter 3). To kinetically characterise the inhibition we assumed no inhibition of glucose transport by internal glucose (i.e. zero-trans influx) as described by Eq. 5.3.3.

The uptake rate of labelled ^{14}C glucose into isolated trophozoites was reduced by cytochalasin B with almost complete reduction (93%) obtained at 100 μM (Fig 5.1). The uptake rates are presented as a percentage of the uninhibited rate (0.18 μmol·min^{-1}·mg^{-1}). These results are in good agreement with Woodrow *et al.*[223] who reported 75% inhibition at 50 μM cytochalasin B, compared to approximately 70% determined in this work. To obtain an inhibition constant for cytochalasin B, we assumed i) zero-influx kinetics (i.e. no internal glucose) and ii) cytochalasin B acts as a noncompetitive inhibitor. The data were fitted (Fig. 5.1) in *Wolfram Mathematica 8.0* to a Michaelis-Menten equation with cytochalasin B acting as a noncompetitive inhibitor (Eq. 5.3.3), where V_{GlcTr} is the maximal enzyme rate, K_{Glc} is the Michaelis constant for glucose, $K_{i_{cytB}}$ is the inhibition constant for cytochalasin B, and glucose and

cytB refer to the concentrations of glucose and cytochalasin B respectively. The V_{GlcTr} was determined previously as 0.207 μmol·min^{-1}·mg^{-1} and K_{Glc} determined as 1.8 ± 0.9 mM (Chapter 3) and the concentration of glucose in the assay was 5 mM. The fitted $K_{i_{cytB}}$ was 11 ± 3.7 μM, which is substantially higher than $K_{i_{cytB}}$, 0.17 ± 0.018 μM (zero-trans entry)[120] and 0.50 μM (efflux)[14], determined for glucose transport in erythrocytes.

$$v\mathrm{GlcTr} = \frac{V_{\mathrm{GlcTr}} \cdot \frac{\mathrm{glucose}}{K_{\mathrm{Glc}}}}{1 + \frac{\mathrm{cytB}}{K_{i_{\mathrm{cytB}}}} + \frac{\mathrm{glucose}}{K_{\mathrm{Glc}}} + \frac{\mathrm{cytB \cdot glucose}}{\mathrm{Ki_{cytB}} \cdot K_{\mathrm{Glc}}}} \tag{5.3.3}$$

Figure 5.1: Inhibition of ^{14}C labelled glucose transport into isolated trophozoites by cytochalasin B. The rate of ^{14}C glucose uptake was determined using a simple quench flow device at a sampling time of 500 ms. The rate is expressed as a percentage of the uninhibited rate (0.18 μmol·min^{-1}·mg^{-1}). The data were fitted to Eq. 5.3.3 and an inhibition constant of 11 ± 3.7 μM was obtained for cytochalasin B. The data are from four biological repeats with n ≥ 2 technical repeats. Error bars represent SEM.

5.3.3 Inhibition of lactate flux

5.3.3.1 Experimental

To investigate the response of the glycolytic flux (i.e. lactate flux) to the inhibition of the transporter by cytochalasin B, we measured the production of extracellular lactate by intact erythrocytes and isolated trophozoites incubated in 5 mM glucose and varying concentrations of the inhibitor (Fig. 5.2). Inhibition of glycolytic flux was not observed in erythrocytes whereas almost complete inhibition was obtained at 100 μM cytochalasin B in trophozoites (Fig. 5.2). A dose response curve of cytochalasin B with respect to lactate flux in isolated trophozoites (Fig. 5.2) gives an IC_{50} value of 15 ± 1.1 μM and a Hill coefficient of -1.8 ± 0.33. The IC_{50} is defined as the concentration of cytochalasin B required to obtained 50% inhibition of flux.

5.3.3.2 Model Simulations

With the detailed kinetic models for *P. falciparum* glycolysis (Chapter 3 & 4) and erythrocyte glycolysis[95] we can simulate the effect of inhibition of the glucose transport activity on the steady state glycolytic flux.
In the Holzhutter model the glucose transporter needed to be decreased to a very large extent before any inhibition of the glycolytic flux was observed. To obtain a significant decrease in glycolytic flux (i.e. >5%) the transporter needed to be inhibited by more than 90%. In the cytochalasin B inhibition experiment we used very high cytochalasin B concentrations of up to 200 μM. We are not sure of the exact percentage inhibition of glucose transport activity in the erythrocyte at these cytochalasin B concentrations, but we expect higher than 90% inhibition[14]. As such we would have expected to see a small decrease in the glycolytic flux in the erythrocytes at the higher cytochalasin B concentrations.

Figure 5.2: Inhibition of glycolytic flux in *P. falciparum* trophozoites and uninfected erythrocytes by cytochalasin B compared to the model prediction of flux inhibition. The rate of lactate production in erythrocytes and isolated *P. falciparum* was determined over a 30 min period when incubated in 5 mM glucose and varying concentrations of cytochalasin B. The flux is expressed as a percentage of the uninhibited flux. For *P. falciparum* trophozoites the inhibition data were fitted to a dose response equation yielding an IC_{50} value of 15 ± 1.1 μM and a Hill coefficient of -1.8 ± 0.31 (see Insert). There is no observable inhibition in the erythrocyte glycolytic flux. The data are the combination of two independent biological repeats with technical repeats in triplicate. The bold dashed line represents model simulations of lactate flux as a function of cytochalasin B concentration. The finely dashed lines represent the same simulation, but reflect the experimental error of the fitted inhibition constant for cytochalasin B. Error bars are SEM, n = 6

For the trophozoites we have measured the cytochalasin B inhibition of glucose transport and it is therefore easy to simulate the inhibition in the detailed kinetic model. Such a simulation can address the question; can the inhibition of the flux be ascribed to the inhibition of the glucose transporter alone? To simulate the inhibition of the lactate flux in *P. falciparum* we modified the

model by including a new equation (Eq. 5.3.4) for glucose transport, which included noncompetitive inhibition by cytochalasin B. For the equation, we i) assumed symmetrical noncompetitive binding of cytochalasin B and ii) used the inhibition constant ($K_{i_{cytB}}$, 11 ± 3.7 μM) determined in this study (Fig. 5.1) and iii) assumed internal and external concentrations of cytochalasin B were equal. The V_{GlcTr} was determined previously as 0.21 μmol·min^{-1}·mg^{-1} and K_{Glc} determined as 1.8 ± 0.9 mM (Chapter 3). The subscripts *ext* and *int* refer to external and internal concentrations respectively.

$$v\mathrm{GlcTr} = \frac{V_{\mathrm{GlcTr}} \cdot \frac{\mathrm{glucose_{ext}}}{K_{\mathrm{Glc}}} \cdot \left(1 - \frac{\mathrm{glucose_{int}}}{\mathrm{glucose_{ext}} \cdot K_{\mathrm{eq}}}\right)}{\left(1 + \frac{\mathrm{glucose_{ext}}}{K_{\mathrm{Glc}}} + \frac{\mathrm{glucose_{int}}}{K_{\mathrm{Glc}}} + \frac{\mathrm{glucose_{ext}} \cdot \mathrm{cytB_{ext}}}{K_{\mathrm{Glc}} \cdot K_{i_{\mathrm{cytB}}}} + \frac{\mathrm{glucose_{int}} \cdot \mathrm{cytB_{int}}}{K_{\mathrm{Glc}} \cdot K_{i_{\mathrm{cytB}}}} + \frac{\mathrm{cytB_{ext}}}{K_{i_{\mathrm{cytB}}}} + \frac{\mathrm{cytB_{int}}}{K_{i_{\mathrm{cytB}}}}\right)} \quad (5.3.4)$$

The modified model provided a tool to investigate how the cytochalasin B inhibition of the transporter influences glycolytic flux (i.e. lactate flux). The inhibition experiment was simulated in the model by determining the steady state lactate flux over a range of cytochalasin B concentrations (0 - 100 μM), and expressing it as a percentage of the uninhibited flux (Fig. 5.2). This was also simulated with the $K_{i_{cytB}}$ set to its upper and lower ranges within the experimental error (11 ± 3.7 μM) and indicated in Figure 5.2 as finely dashed lines. The experimental inhibition of flux is slightly underestimated by the model, at high cytochalasin concentrations, but it describes the overall inhibition experiment quite well (Fig. 5.2).

5.3.4 Inhibition of glycolytic enzymes

As previously mentioned, cytochalasin B inhibits the glucose transporter in both *Plasmodium spp.* and erythrocytes and also influences a number of cellular processes. We assume the inhibition of the flux is due to the inhibition of the glucose transporter since none of the known effects of cytochalasin B interfere with the central carbon metabolism. In addition, the following observations are in agreement with this assumption: i) in erythrocytes, cytochalasin B does not influence the production rate of lactate and as such it is not expected to inhibit glycolysis at an enzyme level, and ii) glucose transport is inhibited by cytochalasin B in pink erythrocytes, and iii) glucose uptake via PfHT1, which was expressed in frog oocytes is inhibited by cytochalasin B. As a further control to ensure that the inhibition of lactate flux is not due to

the inhibition of the glycolytic enzymes, we measured the specific activity of each glycolytic enzyme in isolated *P. falciparum* lysates under near saturating substrate concentrations in the presence or absence of 100 μM cytochalasin B (Fig. 5.3).

No significant ($P < 0.05$ $n = 6$) inhibition at 100 μM cytochalasin B was observed for any of the enzymes. If anything, a mild activation of the enzyme rate (PGI, ENO, and LDH) is observed, although the reason for this is unclear. These results, in addition to the previously mentioned reasons, provide further evidence that the inhibition of the flux during the short time period of the incubation experiments, is directly due to the inhibition of the glucose transporter.

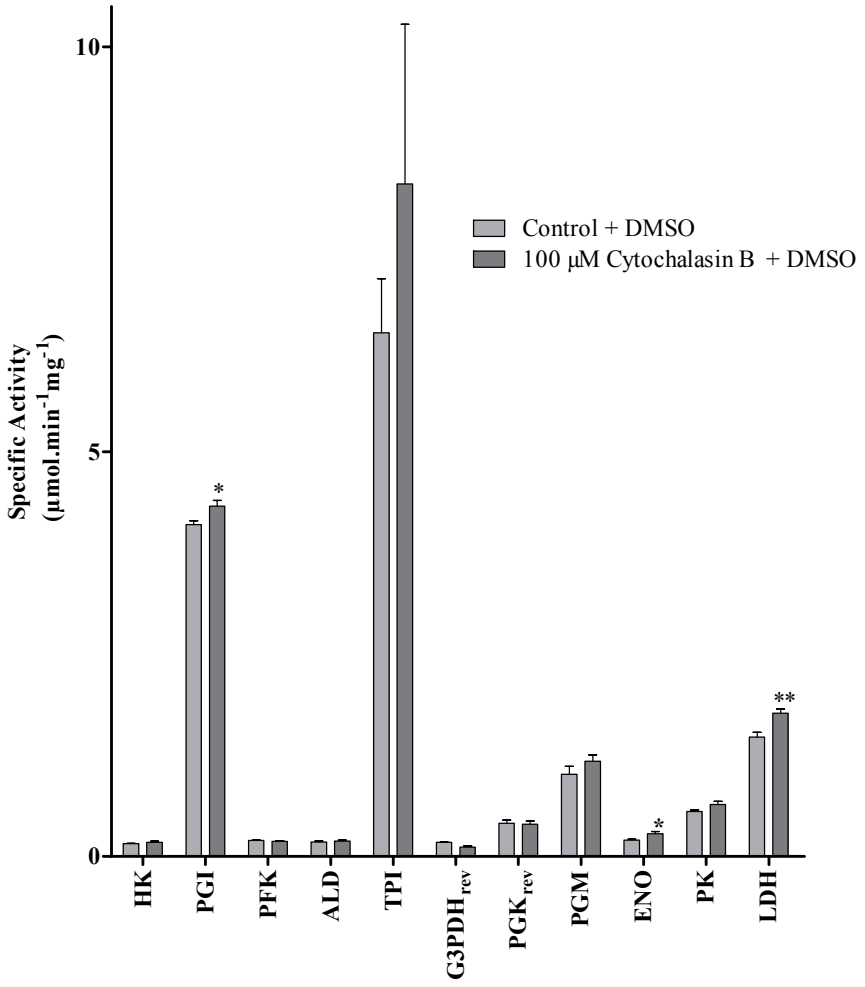

Figure 5.3: Specific activities for the glycolytic enzymes of *P. falciparum* in the presence or absence of cytochalasin B. The specific activity of each glycolytic enzyme was determined at near saturating substrate concentrations, in the presence or absence of 100 μM cytochalasin B prepared in DMSO. The control excluded cytochalasin, but included an equivalent concentration of DMSO. No inhibition of enzyme activity by cytochalasin B is observed, although small, but significant increases in activity are observed for PGI and ENO (Paired T-test, $P < 0.05$) and LDH (Paired T-test, $P < 0.01$). The data are from a single biological experiment, but the enzyme activities were determined from two independent trophozoite isolations. In each isolation the enzyme activity was determined in triplicate. Error bars represent SEM, n = 6, except in the case of PFK where n = 3. HK (hexokinase), PGI (phosphoglucoisomerase), PFK (phosphofructokinase), ALD (aldolase), TPI (triosephosphate isomerase), G3PDH$_{rev}$ (glyceraldehyde 3-phosphate dehydrogenase in the reverse direction), PGK$_{rev}$ (Phosphoglycerate kinase assayed in reverse direction), PGM (phosphoglycerate mutase), ENO (enolase), PK (pyruvate kinase), LDH (lactate dehydrogenase)

5.3.5 Control coefficient of PfHT1

In this study we show that cytochalasin B directly inhibits the glucose transporter (a local property) and that this inhibition of the transporter results in a decrease in the glycolytic flux (systemic property). These local and systemic properties can be described by elasticity and response coefficients (see introduction) respectively. The elasticity of PfHT1 quantifies the degree of change in the rate of the transporter due to a small change in the concentration of the inhibitor (cytB) and can be mathematically described as:

$$\epsilon_{\mathrm{cytB}}^{v\mathrm{GlcTr}} = \frac{\partial \ln v\mathrm{GlcTr}}{\partial \ln \mathrm{cytB}}$$

The relative change in the steady state lactate flux (J_{Lac}) due to a small change in the inhibitor concentration (cytB) can be defined mathematically as a response coefficient:

$$R_{\mathrm{cytB}}^{J_{Lac}} = \frac{d \ln J_{Lac}}{d \ln cytB} = C_{v\mathrm{GlcTr}}^{J_{Lac}} \cdot \epsilon_{cytB}^{v\mathrm{GlcTr}}$$

The response coefficient can be further described as the product of the flux control coefficient (i.e. $C_{v\mathrm{GlcTr}}^{J_{Lac}}$) and the elasticity. The control coefficient can thus be determined by the ratio of the response coefficient and the elasticity:

$$C_{v\mathrm{GlcTr}}^{J_{Lac}} = \frac{R_{\mathrm{cytB}}^{J_{Lac}}}{\epsilon_{cytB}^{v\mathrm{GlcTr}}} = \frac{\frac{d \ln J_{Lac}}{d \ln cytB}}{\frac{\partial \ln v\mathrm{GlcTr}}{\partial \ln \mathrm{cytB}}} = \frac{d \ln J_{\mathrm{Lac}}}{\partial \ln v_{\mathrm{GlcTr}}}$$

Thus a plot of the percentage change of the lactate flux as a function of the percentage glucose transporter activity can be used to determine the flux control coefficient (Fig. 5.4). The slope of resulting curves at 100% transport activity would reflect the relative change in the lactate flux (i.e. the flux control coefficient). To determine the flux control coefficient we plotted the percentage of lactate flux as a function of percentage glucose transporter activity for i) experimentally measured values, ii) the equations used to describe the experimental data (i.e. Hill equation, Insert - Fig. 5.2 and Eq. 5.3.3, a Michaelis-Menten equation with a noncompetitive inhibitor, Fig. 5.1) and iii) model simulations (as described for the prediction of lactate flux, Fig. 5.2) where the $K_{i_{cytB}}$ was set to its upper and lower ranges within the experimental error (11 ± 3.7 μM)

.

Figure 5.4: Determination of the control coefficient for *P. falciparum* PFHT1. Percentage of lactate flux is plotted as function of the percentage of the glucose transport activity in *P. falciparum*. Uninhibited transporter activity (100%) equates to 100% lactate flux. As the transporter activity is decreased, the lactate flux decreases accordingly. The slope of the curves near 100% glucose transporter activity is equal to the flux control coefficient for the glucose transporter (see text for discussion). The experimental data for *P. falciparum* shown here is the ratio of the percentage *flux* (Fig. 5.2) and percentage transporter *rate* at identical cytochalasin B inhibitor concentrations. The fitted curve describes the decrease in flux and glucose transporter rate predicted by the equations that were used to fit the experimental flux inhibition (Hill equation, see Insert Fig. 5.2) and glucose transporter inhibition (Eq. 5.3.3, Fig. 5.1). The model simulation (bold dashed line) describes the predicted decrease in lactate production as a function of the transporter activity. The simulation was also determined at the upper and lower ranges (finely dashed lines) of the experimentally determined $K_{i_{cytB}}$ (11 ± 3.7 μM). The control coefficients obtained from the slopes near 100% transporter activity are listed in Table 5.2.

The slope of the experimental data were taken between approximately 75% and 100% (smallest experimental perturbation) of the glucose transporter ac-

tivity and yielded a flux control coefficient of 0.315. For the equations the slope was taken at 100% transporter activity. The flux control coefficient for the model simulations was determined using two methods, i) the elasticity matrix inversion method described by[87] and implemented on JWS Online and ii) a perturbation method (Fig. 5.4 where cytochalasin B concentration was increased (i.e. transporter activity and flux decrease). For the latter method, the error on the cytochalasin inhibition constant $K_{i_{cytB}}$, could also be incorporated by repeating the calculation at higher and lower values (11 $\pm$ 3.7 μM). The glucose transporter flux control coefficients are listed in Table 5.2.

Table 5.2: Flux control coefficients for the *P. falciparum* glucose transporter. Flux control coefficients were determined from the slopes of experimental and model simulation data shown in Fig. 5.4. For the experimental data, the slope was taken between approximately 75% and 100%. For model simulation, the control coefficient was determined using a standard matrix inversion method as well as by the perturbation method. For the latter, model simulation was determined at $K_{i_{cytB}}$ set to its upper and lower ranges within the experimental error (11 $\pm$ 3.7 μM). The resulting lower and upper flux control coefficients are indicated in parentheses.

Source	$C^{J_{Lac}}_{vGlcTr}$
Experimental	0.315
Experimental Fitted Curve	0.0100
Model Simulation: Matrix Method	0.223
Model Simulation: Perturbation Method	0.228 (0.172 - 0.340)

5.4 Discussion

Differential control analysis is a powerful tool to identify enzymes in the pathogen with high flux control where the equivalent reaction has a low flux control in the host. A reaction with high differential control presents a favourable drug target as inhibition of the host and parasite enzyme to the same degree is expected to affect the parasite to a larger degree than the host.

This work has three aims. Firstly to identify potential drug targets in *P. falciparum* using differential control analysis, secondly to demonstrate via inhibition experiments that a differential effect in host and parasite can be obtained and thirdly, to experimentally determine the flux control coefficient ($C^J_{v_{GlcTr}}$) of the glucose transporter in *P. falciparum* as a form of validating the kinetic model.

Metabolic control analysis of an erythrocyte model of glycolysis[95] and the *P. falciparum* kinetic model (Chapter 3 & 4) indicates (Table 5.1) that the glucose transporter, HK, PFK and G3PDH as well as the ATPase share most of the flux control in asexual *P. falciparum*. For the erythrocyte the ATPase and the 2,3 -bisphosphoglycerate shunt have the highest control of the glycolytic flux[53] and the glucose transporter in the erythrocyte has no flux control.

The hexose transporter, PfHT1[155], aldolase[219], triosephosphate isomerase[169] and lactate dehydrogenase[20] have been proposed as potential drug targets in glycolysis of *P. falciparum*. The low flux control coefficients of aldolase, LDH and TPI would indicate that in order to use these as drug targets, the step would need to be inhibited to a large extent to inhibit parasite glycolysis. When one considers the scaled effectivities (Table 5.1), Glucose transport, HK, and G3PDH are ranked the highest and are possibly the best potential drug targets in *P. falciparum* glycolysis. *P. falciparum* PFK is also highly ranked, which would indicate an attractive target, but its control in the erythrocyte is only a factor 15 less. As such, this target would require a greater degree of drug specificity, so as to not inhibit the host.

In contrast to the erythrocyte GLUT1, MCA of a detailed model of *P. falciparum* glycolysis shows that the parasite transporter, PfHT1, has significant control ($C^J_{vPfHT1} = 0.221$) of the glycolytic flux. Inhibition of the transporter should result in a significant inhibition of the flux. To demonstrate differential control *in vivo* we set out to show that the inhibition of the glucose transporter in erythrocytes (shown by others) and *P. falciparum* leads to an inhibition of glycolytic flux in *P. falciparum*, but not in erythrocytes.

In *P. falciparum* the glycolytic flux is strongly inhibited by cytochalasin B (Fig. 5.2). The inhibition of the lactate flux is ascribed to the inhibition of PfHT1, which was almost completely inhibited at 100 uM (Fig. 5.1) *in vivo*. In stark contrast, the flux of the erythrocyte was not visibly inhibited by 200 μM cytochalasin B (Fig. 5.2), even though at half this concentration, the transporter has been shown to be inhibited by more than >95%[14]. Furthermore, analysis of the Holzhutter model indicated 5% inhibition of flux at 90% inhibition of glucose transporter. Thus although the transporter in erythrocytes needs to be inhibited to a much larger extent than the transporter in the parasite, we would have expected to see a small decrease in erythrocyte flux at the highest cytochalasin B concentrations. It has recently been shown that unless the rate of glucose uptake rate in erythrocytes is measured in under 30 ms, the maximal uptake rate is underestimated and does not reflect zero-trans influx kinetics[15]. Thus, if the V_{max} of glucose transport in the Holzhutter model is underestimated, it may explain why no inhibition of the flux is observed. It has been reported that, due to the high over-capacity of the glucose transporter (10^3 fold greater than glucose utilisation), more than 99% inhibition of the transporter would be required to observe inhibition of the glycolytic flux[14]. This may explain our finding that 200 μM cytochalasin B does not inhibit glycolytic flux in erythrocytes.

By including a rate equation that captured the kinetics of the noncompetitive inhibition of the glucose transporter by cytochalasin B into the model, we could give a good description of the inhibition of lactate flux in *P. falciparum* trophozoites by cytochalasin B *in vivo*. This finding provides further evidence that inhibition of the glucose transporter by cytochalasin B alone is sufficient to describe the inhibition of the flux.

These findings successfully demonstrate the differential control *in vivo* predicted by the model and also show that by inhibiting both transporters to a similar degree ($> 97\%$), only the parasite flux is influenced. This demonstration highlights the glucose transporter as a potential target as well as the strength of differential control analysis. Although this study highlights the glucose transporter as a potential drug target within malaria glycolysis, only the parasite and erythrocyte glucose transporter control coefficients have been compared. In reality, the human body has a number of different glucose transporters within a variety of different tissues (e.g. brain, muscle, liver). In these cases, the glucose transporter may have a high control of the glycolytic flux, and consequently a lower effectivity and less attractive drug target. Inhibition of these targets could also, in many cases, be highly toxic to the host. It would therefore be necessary to also evaluate the metabolic flux control of the glucose transporter in other tissues before trying to develop glucose transport inhibitors. Another factor to consider when developing inhibitors of glucose transport is the fact that the glucose concentration is expected to vary between tissues. In tissues with glucose concentrations lower than found in the blood stream, competitive inhibitors of glucose transport would potentially exacerbate toxicity in the host by inhibiting glucose uptake to a large degree. As such, glucose transport inhibitors should preferably be uncompetitive to ensure efficacy regardless of the glucose concentration.

Does high scaled effectivity always present a good potential drug target? This would not always be the case, especially in complex nonlinear systems. The reason for this is that control coefficients typically represent a change in flux or metabolite concentration over a small (typically 1%) change in enzyme rate. For larger changes, as would be expected during a drug inhibition, the change in flux or metabolite concentrations may not be linear. As the enzyme is inhibited, the control would be expected to increase. If the pathogen and host control coefficients changed in a similar manner, then the pathogen would always be inhibited to a greater extent. However, one could foresee a scenario where an enzyme with low control may reach a threshold point and suddenly gain a great deal of control in a network, whereas in the pathogen the change in control could be linear and result in a greater degree of inhibition in the

host. In selecting a drug target based on model analysis, it may thus be valuable to consider more than just the control coefficients and also examine the effect of large changes to enzyme rate. Furthermore, alternative pathways or isozymes should also be considered, as inhibiting a reaction may not influence the pathogen if it is able to utilise an alternative pathway.

For determining the effectivities, we assumed a similar degree of inhibition to both host and pathogen enzymes, which is useful when analysing a network for potential drug targets if drug selectivity ($\epsilon_{drug}^{v_{pathogen}} / \epsilon_{drug}^{v_{host}}$) is unknown. The half maximal inhibition constants for cytochalasin B, are 10 fold lower for the erythrocyte transporter than for the parasite transporter and as such the erythrocyte transporter it is inhibited to a greater extent at a similar concentration of cytochalasin B. The strength of the effectivity definition is that it can take both selectivity of inhibition and the differential control into account. Thus whereas the selectivity of the cytochalasin B is poor, its effectivity for inhibiting flux in the parasite is high due to the large percentage difference in control coefficients.

We were able to determine a flux control coefficient (0.32) for the glucose transporter from experimental data, which was approximately 1.5 times greater than calculated by MCA (0.22). However, the experimental control is expected to be a slight overestimation as it was determined over a large (20%) change in transporter activity, whereas control coefficients typically are determined for very small changes. Model simulation over the large change yielded a flux control coefficient range (0.17 - 0.34), which is in good agreement with the experimentally determined value. The large discrepancy between the control coefficients determined from the experimental data (0.32) and that determined from the fitted curve (0.01) is due to the type of equation that was used to fit the data points. The sigmoidal nature of a Hill equation results in a low gradient (i.e. control coefficient) at the origin (i.e. 100% PfHT1 activity, Fig. 5.4). The small number of data points biases the curve towards a more sigmoidal shape (especially the % PfHT1 activity at 50 μM cytochalasin B, Fig. 5.4), and inevitably results in a more sigmoidal fit and reduced control coefficient. This does, however, not detract from the good comparison between the experimentally determined control coefficient and that determined by model

simulation.
This good comparison of experimental data and model prediction provides, in conjunction with previous work (Chapter 4), a further validation for the kinetic model. Not only can the model give a good prediction for the reference criteria for which it was constructed, but it also gives a fair prediction of a perturbation of this reference condition (i.e. inhibition titration). It thus provides a greater degree of confidence in using the kinetic model as a tool for drug target identification and for understanding the systemic behaviour of the network.

The other potential drug target that was highlighted in this study is G3PDH, which has a high differential control ratio, and has a glycolytic flux control coefficient of 0.306 in the parasite. Poolman *et al.*[160] demonstrated that iodoacetate inhibits G3PDH in *Streptococcus spp.* and used the compound to determine the flux control strength of the enzyme. Iodoacetate could be used to investigate the flux control of G3PDH in the erythrocyte and *P. falciparum* trophozoites, in a similar manner to which cytochalasin B was used in this study.

This study has identified drug targets based on differential control analysis and we have demonstrated the concept *in vivo*. Differential control analysis highlighted the glucose transporter and G3PDH as potential drug targets in *P. falciparum*. We were able to demonstrate the differential control inhibition *in vivo* by showing that although cytochalasin B specifically inhibits both the erythrocyte and *P. falciparum* glucose transporter, only the flux of the parasite is inhibited with negligible effect on the host erythrocyte. These findings highlight the importance of detailed kinetic models and differential control analysis as tools for drug target identification.

Chapter 6

General Discussion, Conclusions and Future Work

The aim of the research reported in this thesis was threefold: Firstly, to create a detailed kinetic model of *P. falciparum* glycolysis and secondly use this model as a tool for drug target identification in the pathway. Lastly, we aimed to demonstrate experimentally that the predicted drug target was effective in intact *P. falciparum* trophozoites. During the project we also addressed questions such as i) is the bottom up approach used in this study to construct and validate a kinetic model applicable to other pathways and organisms and ii) whether a model constructed in this manner gives a sufficient description of the network to use as a tool for drug target identification and iii) whether differential control analysis of networks is a suitable approach for drug target identification in general.

We have shown that a model of *P. falciparum* glycolysis constructed from the individual enzyme kinetics measured experimentally *in vitro* can predict the metabolic fluxes, metabolites concentrations in intact *P. falciparum* trophozoites. In addition, our model was able to predict an enzyme inhibitor titration of the glucose transporter for which a flux control coefficient could be determined. This description was achieved without fitting and raises the question of whether any network can be well described on the basis of enzyme kinetics. Kinetic models of yeast[205,215] and *T. brucei* glycolysis[7] have also, from the enzyme kinetics, been able to give a good description of systemic properties. It thus appears that, at least for smaller networks, this bottom up approach can sufficiently describe a system and can be used for applications such as drug target identification. Experimentally, the enzymes of glycolysis are relatively

simple to characterise biochemically, with the result that the kinetic data is fairly accurate. It would be expected that kinetic data would be more error prone and less complete for pathways (e.g. pentose phosphate pathway, tricarboxylic acid cycle, purine nucleotide biosynthesis) in which the enzymes are more difficult to characterise biochemically. However, in this study we used some kinetic parameters from the scientific literature (e.g. V_{max} for pyruvate and lactate transport, K_{DHAP} and K_{GAP}) and had a range of uncertainty in other parameters, such as the ATP:ADP ratio. These were shown to not influence the model prediction unduly. Furthermore, PSA of the model indicated that less than a third of the parameters had high response coefficients. These findings indicate that having accurate kinetic data, although preferable, is not a prerequisite for an accurate systemic description. For complex networks it may thus be possible to still adequately describe systemic behaviour with error prone or incomplete kinetic data. Furthermore, by iteratively identifying parameters that have a high influence on model behaviour or prediction with MCA and PSA, it is possible to prioritise time and resources to experimentally improving the accuracy of important parameters. Such an approach may provide kinetic models at less cost in terms of time and resources and still be sufficient as a tool for drug target identification

Differential control analysis of the host and parasite kinetic models indicated that of the suggested *P. falciparum* glycolytic drug targets, glyceraldehyde 3-phosphate dehydrogenase and the glucose transporter were the most attractive due to their high effectivity. The finding that the glucose transporter has high effectivity, provides further support to research currently directed at selectively inhibiting this transporter[103,101,198].

Until now, differential control analysis has only been suggested as a tool for drug target identification and has not been demonstrated *in vivo*. Having presented experimental evidence of the differential flux control of the erythrocyte and *P. falciparum* glucose transporter, we demonstrated that this knowledge can be used to effectively inhibit the parasite glycolytic flux. This difference in inhibition is achieved despite the fact that the erythrocyte transporter is inhibited to an even greater degree than the parasite transporter. This finding highlights differential control analysis as a tool for drug target identification; Even though a drug may inhibit the host enzyme to a greater extent than the

pathogen, if the effectivity of the reaction is high enough, the host would be influenced to a lesser degree than the pathogen.
Since humans have a number of tissues, each with distinct requirements in terms of metabolism and consequently different pathway regulation, enzyme expression and possibly network topology, the metabolic control profile of a network would be tissue specific. As such the effectivity of a drug compared to the pathogen could differ in different tissues. Therefore, the glucose transporter might not necessarily have such a low flux control in other human tissues (compared to the erythrocyte). It would therefore be expedient to perform differential control analysis on a number of different tissue specific pathways or consider enzymes whose function or metabolic control is expected to be conserved between tissues.

The kinetic model has already enhanced our understanding of *P. falciparum* glycolysis by indicating the flux controlling enzymes and by showing that glycerol production is required to maintain trophozoite redox balance. Another aspect that could be investigated is the role of the kinetic regulation of PFK and PK in *P. falciparum* glycolysis. In particular PK, which exhibits cooperativity with regards to ATP and inhibition by both of its substrates raises the question of the role of this kinetic behaviour in the glycolytic pathway. Does the regulation improve network robustness, have a role in the glycerol metabolism by regulating the PEP concentration or possibly have a role in the PEPC branch?

The importance of the PPP in the detoxification of reactive oxygen species and free ferriprotoporphyrin IX (FP) warrants that the current model be extended to include this pathway. Such a combined model would improve the understanding of its link to glycolysis and whether GluPho, the first enzyme in this pathway, which has been highlighted as a potential drug target plays an important role in controlling the PPP flux.

This study has considered the isolated trophozoite and uninfected erythrocytes. The logical progression of the kinetic model presented in this work, would be to integrate it into a model of erythrocyte glycolysis. This is currently being investigated in our research group. Such a model would be particularly useful for understanding host-pathogen relationships such as the change

in intra-erythrocyte 2,3-bisphosphoglycerate (2,3BPG) concentrations, which regulates oxygen homoeostasis within the erythrocyte. In theory, if parasite metabolism increased the intracellular concentration of 2,3 BPG significantly, it would promote oxygen release from the haemoglobin. This release of oxygen may have important implications for the oxidative stress experienced by the parasite.

6.1 Conclusion

This study has merged the disciplines of biochemistry and systems biology to investigate and identify potential drug targets in the glucose catabolism of *P. falciparum*. In the study, each of the glycolytic enzymes of asexual *P. falciparum* glycolysis were biochemically characterised and described by a mechanistic rate equation. Without the need for fitting, the kinetic ODE model constructed with these rate equations gave a fair description of the steady state flux, flux control coefficient of the glucose transporter and some of the metabolic intermediate concentrations. This validated model provides a measure of confidence in the drug targets that were identified in *P. falciparum* glycolysis with differential control analysis. Furthermore, we were able to experimentally demonstrate differential control of the glucose transport in the parasite and host erythrocyte. This shows that even though a drug may inhibit the host *enzyme* to a greater extent than in the pathogen, the pathogen's *flux* is still inhibited to a greater degree provided the effectivity is high enough. This finding highlights the strength of kinetic models and differential control analysis as tools for drug target identification. The detailed kinetic model constructed in this study provides a strong foundation for future extension, which will aim to improve our understanding of the central carbon metabolism as well as host-pathogen metabolic interactions.

Appendices

Appendix A

Supplementary Material for Chapter 4: Model Validation and Analysis

A.1 Metabolic Control Analysis

JWS Online and Copasi were used to perform MCA on the model and determine the flux and concentration control coefficient matrices (Table A.1 & A.2).

Table A.1: Complete set of flux control coefficients for the model of *P. falciparum* glycolysis during the asexual trophozoite phase. The majority of the flux control is divided across the glucose transporter (GlcTr), hexokinase (HK), phosphofructokinase (PFK), glyceraldehyde 3-phosphate dehydrogenase (G3PDH), and the ATP demand reaction (ATPase), which are highlighted in bold. The coefficients were determined by Copasi

	vGlcTr	vHK	vPGI	vPFK	vALD	vTPI	vG3PDH	vPGK	vPGM	vENO	vPK	vLDH	vLacTr	vATPase	vGlrDH	vPyrTr
J_{GlcTr}	**0.223**	**0.438**	0.020	**0.353**	0.078	0.003	**0.306**	0.000	0.001	0.001	0.001	0.050	0.003	**-0.448**	-0.005	-0.024
J_{HK}	**0.223**	**0.438**	0.020	**0.353**	0.078	0.003	**0.306**	0.000	0.001	0.001	0.001	0.050	0.003	**-0.448**	-0.005	-0.024
J_{PGI}	**0.223**	**0.438**	0.020	**0.353**	0.078	0.003	**0.306**	0.000	0.001	0.001	0.001	0.050	0.003	**-0.448**	-0.005	-0.024
J_{PFK}	**0.223**	**0.438**	0.020	**0.353**	0.078	0.003	**0.306**	0.000	0.001	0.001	0.001	0.050	0.003	**-0.448**	-0.005	-0.024
J_{ALD}	**0.223**	**0.438**	0.020	**0.353**	0.078	0.003	**0.306**	0.000	0.001	0.001	0.001	0.050	0.003	**-0.448**	-0.005	-0.024
J_{TPI}	**0.244**	**0.478**	0.021	**0.385**	0.085	0.003	**0.335**	0.000	0.001	0.001	0.001	0.076	0.005	**-0.489**	**-0.110**	-0.037
J_{G3PDH}	**0.233**	**0.457**	0.020	**0.368**	0.081	0.003	**0.320**	0.000	0.001	0.001	0.001	0.062	0.004	**-0.467**	-0.054	-0.030
J_{PGK}	**0.233**	**0.457**	0.020	**0.368**	0.081	0.003	**0.320**	0.000	0.001	0.001	0.001	0.062	0.004	**-0.467**	-0.054	-0.030
J_{PGM}	**0.233**	**0.457**	0.020	**0.368**	0.081	0.003	**0.320**	0.000	0.001	0.001	0.001	0.062	0.004	**-0.467**	-0.054	-0.030
J_{ENO}	**0.233**	**0.457**	0.020	**0.368**	0.081	0.003	**0.320**	0.000	0.001	0.001	0.001	0.062	0.004	**-0.467**	-0.054	-0.030
J_{PK}	**0.233**	**0.457**	0.020	**0.368**	0.081	0.003	**0.320**	0.000	0.001	0.001	0.001	0.062	0.004	**-0.467**	-0.054	-0.030
J_{LDH}	**0.244**	**0.478**	0.021	**0.385**	0.085	0.003	**0.335**	0.000	0.001	0.001	0.001	0.076	0.005	**-0.489**	**-0.110**	-0.037
J_{LacTr}	**0.244**	**0.478**	0.021	**0.385**	0.085	0.003	**0.335**	0.000	0.001	0.001	0.001	0.076	0.005	**-0.489**	**-0.110**	-0.037
J_{ATPase}	**0.244**	**0.478**	0.021	**0.385**	0.085	0.003	**0.335**	0.000	0.001	0.001	0.001	0.076	0.005	**-0.489**	**-0.110**	-0.037
J_{GlrDH}	**0.050**	**0.098**	0.004	**0.079**	0.017	0.001	**0.063**	0.000	0.000	0.000	0.000	-0.171	-0.012	**-0.100**	**0.887**	**0.084**
J_{PyrTr}	**0.050**	**0.098**	0.004	**0.079**	0.017	0.001	**0.063**	0.000	0.000	0.000	0.000	-0.171	-0.012	**-0.100**	**0.887**	**0.084**

Table A.2: Complete set of concentration control coefficients as determined for the model of *P. falciparum* glycolysis during the asexual trophozoite phase. Concentration control coefficients with a value above 0.3 are highlighted in bold. The coefficients were determined by Copasi

	vGlcTr	vHK	vPGI	vPFK	vALD	vTPI	vG3PDH	vPGK	vPGM	vENO	vPK	vLDH	vLacTr	vATPase	vGlrDH	vPyrTr
ATP	**0.244**	**0.478**	0.021	**0.385**	0.085	0.003	**0.335**	0.000	0.001	0.001	0.001	0.076	0.005	**-1.49**	**-0.110**	-0.037
DHAP	**0.298**	**0.584**	0.026	**0.470**	0.104	-0.016	**-0.648**	-0.001	-0.002	-0.002	-0.003	-0.072	-0.005	**-0.613**	**-0.155**	0.035
GAP	**0.297**	**0.581**	0.026	**0.468**	0.103	0.004	**-0.662**	-0.001	-0.002	-0.002	0.001	-0.074	-0.005	**-0.616**	**-0.155**	0.036
Pyr	0.009	0.017	0.001	0.014	0.003	0.000	0.011	0.000	0.000	0.000	0.000	-0.030	-0.002	**-0.017**	**0.154**	**-0.160**
2PGA	**0.237**	**0.465**	0.021	**0.374**	0.083	0.003	**0.325**	0.000	0.001	**-1.03**	**-0.051**	**0.062**	0.004	**-0.415**	**-0.052**	-0.031
NAD	-0.004	-0.008	0.000	-0.007	-0.001	0.000	-0.006	0.000	0.000	0.000	0.000	0.015	0.001	0.009	0.010	-0.007
Glucose	**0.511**	**-0.288**	-0.013	**-0.232**	-0.051	-0.002	**-0.202**	0.000	-0.001	-0.001	0.000	-0.033	-0.002	**0.295**	0.003	0.016
F6P	**0.452**	**0.887**	0.040	**-0.390**	-0.086	-0.003	**-0.338**	0.000	-0.001	-0.001	-0.001	-0.035	-0.002	**-0.445**	**-0.093**	0.017
Lac	0.006	0.012	0.001	0.010	0.002	0.000	0.009	0.000	0.000	0.000	0.000	0.002	-0.026	-0.013	-0.004	0.000
3PGA	**0.276**	**0.541**	0.024	**0.435**	**0.096**	0.004	**0.378**	0.000	**-0.606**	**-0.582**	**-0.028**	**0.073**	0.005	**-0.519**	**-0.062**	-0.036
G6P	**0.464**	**0.909**	-0.020	**-0.366**	-0.081	-0.003	**-0.317**	0.000	-0.001	-0.001	-0.001	-0.032	-0.002	**-0.470**	**-0.093**	0.015
PEP	-0.055	**-0.108**	-0.005	-0.087	-0.019	-0.001	-0.076	0.000	0.000	0.000	**-1.02**	**-0.028**	-0.002	**1.31**	**0.076**	**0.014**
B1,3PG	**1.17**	**2.29**	0.102	**1.85**	**0.407**	0.016	**1.60**	**-0.215**	**-0.555**	**-0.533**	-0.023	**0.349**	0.024	**-5.85**	**-0.457**	**-0.171**
F1,6BP	**0.668**	**1.31**	0.059	**1.06**	**-0.272**	-0.010	**-1.07**	-0.001	-0.003	-0.003	-0.002	-0.111	-0.008	**-1.38**	**-0.291**	0.054
NADH	0.072	**0.141**	0.006	0.114	0.025	0.001	**0.100**	0.000	0.000	0.000	0.000	**-0.255**	-0.017	**-0.144**	**-0.168**	**0.125**
ADP	**-0.740**	**-1.45**	-0.065	**-1.17**	-0.258	-0.010	**-1.02**	-0.001	-0.003	-0.003	-0.002	**-0.230**	-0.016	**4.52**	**0.333**	**0.112**

A.2 Parameter Sensitivity Analysis

A.2.1 Response Coefficients

Copasi was used to determine the flux response coefficients (Table A.3).

A.2.2 ATP:ADP ratio

Figure A.1: Model predictions of steady state flux for glucose uptake and lactate, pyruvate and glycerol production as a function of the ATP:ADP ratio. The ratio was obtained by fitting the ATPase reaction, where higher rates lead to a lower ratio.

Figure A.2: Model predictions of steady state metabolite concentrations in upper glycolysis. The concentrations for metabolites in upper glycolysis (G6P, F6P, F1,6BP, DHAP and GAP) and the first metabolite in lower glycolysis 1,3-BPG are shown across a range of ATP:ADP ratios. The ratio was obtained by fitting the ATPase reaction

Figure A.3: Model predictions of steady state metabolite concentrations in lower glycolysis. The concentrations for the metabolites found in lower glycolysis (3-PG, 2-PG, PEP, Pyruvate, Lactate and NAD) of *P. falciparum* are shown across a range of ATP:ADP ratios. In each instance the desired ratio was obtained by fitting the ATPase reaction.

A.2.3 Pyruvate and Lactate Transport Rate

$A1$ $A2$

$B1$ $B2$

Figure A.4: Broad range parameter sensitivity analysis of the monocarboxylate transporter. Lactate and pyruvate are transported out of the parasite via a monocarboxylate transporter that has been characterised in *P. falciparum* at 4°C. The rate of transport at 37°C is expected to be up to 8 fold greater, based on the assumption of a Q10 of 2. The response of the model to A) Lactate transporter V_{max} and (B) Pyruvate transporter V_{max} was investigated over a range covering the indicated published value and hypothesised rate at 37°C. The effects on both flux (A1 & B1) as well as steady state metabolite concentrations of all metabolites (A2 & B2) are shown. For simplicity, all metabolites are shown together as for the lactate transporter rate (A2) only lactate vary and for the pyruvate transporter (B2), pyruvate is not visibly affected. Overall, the MCT transporter rate has minimal effect on the overall model prediction and the assumption of an 8 fold increase in reaction rate, plausible or not, only impacts model output to a small degree.

A.2.4 Glycerol Transport Rate

A *B*

Figure A.5: Effect of the glyceraldehyde 3-phosphate dehydrogenase on model prediction. The V_{max} for the glyceraldehyde 3-phosphate dehydrogenase was fitted to obtain an experimentally determined glycerol flux. The influence on this behaviour is shown for all the external fluxes (A) and on the steady state metabolite concentrations (B) is indicated. For B, the largest change is the G6P concentration, while others are largely unaffected.

A.3 Response Coefficients

Table A.3: Summary of selected flux response coefficients Part 1. Response coefficients for all the model kinetic parameters were calculated in Copasi, and coefficients with a value of greater than 0.1 are presented here. The parameters of the flux controlling glucose transporter (GlcTr), hexokinase (HK), phosphofructokinase (PFK) and glyceraldehyde 3-phosphate dehydrogenase (G3PDH) and lactate dehydrogenase (LDH) have the highest response coefficients.

Enzyme	GlcTr	HK			PFK								
Parameter	K_{Glc}	K_{ATP}	K_{G6P}	K_{Glc}	c1	$c\gamma1$	$c\gamma2$	$c\gamma3$	gr	K_{ADP}	K_{F6P}	$K_{F1,6BP}$	K_{iATP}	L
J_{GlcTr}	-0.107	-0.166	0.321	-0.339	-0.291	-0.302	-0.177	-0.176	0.325	0.118	-0.319	0.154	0.223	-0.317
J_{HK}	-0.107	-0.166	0.321	-0.339	-0.291	-0.302	-0.177	-0.176	0.325	0.118	-0.319	0.154	0.223	-0.317
J_{PGI}	-0.107	-0.166	0.321	-0.339	-0.291	-0.302	-0.177	-0.176	0.325	0.118	-0.319	0.154	0.223	-0.317
J_{PFK}	-0.107	-0.166	0.321	-0.339	-0.291	-0.302	-0.177	-0.176	0.325	0.118	-0.319	0.154	0.223	-0.317
J_{ALD}	-0.107	-0.166	0.321	-0.339	-0.291	-0.302	-0.177	-0.176	0.325	0.118	-0.319	0.154	0.223	-0.317
J_{TPI}	-0.116	-0.181	0.350	-0.370	-0.318	-0.329	-0.194	-0.192	0.355	0.131	-0.348	0.168	0.243	-0.346
J_{G3PDH}	-0.111	-0.173	0.335	-0.354	-0.304	-0.315	-0.185	-0.184	0.339	0.124	-0.333	0.161	0.233	-0.331
J_{PGK}	-0.111	-0.173	0.335	-0.354	-0.304	-0.315	-0.185	-0.184	0.339	0.124	-0.333	0.161	0.233	-0.331
J_{PGM}	-0.111	-0.173	0.335	-0.354	-0.304	-0.315	-0.185	-0.184	0.339	0.124	-0.333	0.161	0.233	-0.331
J_{ENO}	-0.111	-0.173	0.335	-0.354	-0.304	-0.315	-0.185	-0.184	0.339	0.124	-0.333	0.161	0.233	-0.331
J_{PK}	-0.111	-0.173	0.335	-0.354	-0.304	-0.315	-0.185	-0.184	0.339	0.124	-0.333	0.161	0.233	-0.331
J_{LDH}	-0.116	-0.181	0.350	-0.370	-0.318	-0.329	-0.194	-0.192	0.355	0.131	-0.348	0.168	0.243	-0.346
J_{LacTr}	-0.116	-0.181	0.350	-0.370	-0.318	-0.329	-0.194	-0.192	0.355	0.131	-0.348	0.168	0.243	-0.346
J_{ATPase}	-0.116	-0.181	0.350	-0.370	-0.318	-0.329	-0.194	-0.192	0.355	0.131	-0.348	0.168	0.243	-0.346
J_{GlrDH}	-0.024	-0.037	0.072	-0.076	-0.065	-0.067	-0.040	-0.039	0.073	0.055	-0.071	0.034	0.050	-0.071
J_{PyrTr}	-0.024	-0.037	0.072	-0.076	-0.065	-0.067	-0.040	-0.039	0.073	0.055	-0.071	0.034	0.050	-0.071

Table A.4: Summary of selected flux response coefficients Part 2. Response coefficients for all the model kinetic parameters were calculated in Copasi, and coefficients with a value of greater than 0.1 are presented here. The parameters of the flux controlling glucose transporter (GlcTr), hexokinase (HK), phosphofructokinase (PFK) and glyceraldehyde 3-phosphate dehydrogenase (G3PDH) and lactate dehydrogenase (LDH) have the highest response coefficients.

Enzyme	G3PDH			LDH			
Parameter	K_{GAP}	K_{NAD}	K_{NADH}	K_{LAC}	K_{NAD}	K_{NADH}	K_{PYR}
J_{GlcTr}	-0.286	-0.175	0.149	0.125	0.151	-0.154	-0.139
J_{HK}	-0.286	-0.175	0.149	0.125	0.151	-0.154	-0.139
J_{PGI}	-0.286	-0.175	0.149	0.125	0.151	-0.154	-0.139
J_{PFK}	-0.286	-0.175	0.149	0.125	0.151	-0.154	-0.139
J_{ALD}	-0.286	-0.175	0.149	0.125	0.151	-0.154	-0.139
J_{TPI}	-0.313	-0.191	0.163	0.190	0.230	-0.234	-0.211
J_{G3PDH}	-0.299	-0.183	0.156	0.156	0.188	-0.192	-0.173
J_{PGK}	-0.299	-0.183	0.156	0.156	0.188	-0.192	-0.173
J_{PGM}	-0.299	-0.183	0.156	0.156	0.188	-0.192	-0.173
J_{ENO}	-0.299	-0.183	0.156	0.156	0.188	-0.192	-0.173
J_{PK}	-0.299	-0.183	0.156	0.156	0.188	-0.192	-0.173
J_{LDH}	-0.313	-0.191	0.163	0.190	0.230	-0.234	-0.211
J_{LacTr}	-0.313	-0.191	0.163	0.190	0.230	-0.234	-0.211
J_{ATPase}	-0.313	-0.191	0.163	0.190	0.230	-0.234	-0.211
J_{GlrDH}	-0.059	-0.036	0.031	-0.429	-0.517	0.528	-0.429 -0.517 0.528 0.476

Appendix B

Development of a Simple Quench Flow Device

B.1 Introduction

Glucose uptake in *P. falciparum* trophozoites has been shown to be rapid. Manual uptake assays, which are limited in speed and accuracy were not sufficient to capture zero-trans uptake rates. Commercial quench-flow devices have the advantage that they are extremely rapid with sampling times less than 10 ms, but they are expensive and require large volumes of sample. The latter point in particular is relevant, as obtaining large volumes of isolated *P. falciparum* trophozoites is difficult due to the culture volume required. The availability of programmable logic boards prompted the idea of creating a solenoid valve based quench-flow device. The main criteria for the device were low sample volume ($<$50 μL), minimal wastage and a quench time of approximately 100 ms.

B.2 Materials

The Arduino Uno Logic Board with an ATmega328 microcontroller was purchased from *RS Components* (South Africa). A standard 24V relay board to open the solenoid valves (8 mm 2/3 way Universal X-Valve, 24 VDC, 100 PSI, *Parker Hannifin Corporation*, USA) when triggered by a 5 VDC signal from the Arduino logic board was bought on *Ebay.com*. An LCD and keypad model for the Arduino Logic board was bought from *Ebay.com*. Standard 12

VDC and 24 VDC power sources were obtained from *RS Components* (South Africa). PTFE (Teflon) tubing (2 mm) was used throughout. Samples were mixed through a 4 way HPLC mixer. One way valves (Fourmost Auto Plug-one way valve) were obtained from *Phil's Hobby Shop* (Illinois, USA).

B.3 Machine Design

B.3.1 Design Overview

A quench-flow reaction device typically involves mixing two or more reagents and halting the reaction with a quench buffer after a short pre-set time. The quench-flow device presented here (Fig. B.1), has two sample ports and a quench buffer injection port. Samples are manually pipetted into the sample ports and closed. The samples are mixed through the mixing chamber, when then high pressure (200 kPa) sample lines are opened by the solenoid S1. S1 is kept open and after a set time (programmable quench time), the S2 valve is opened and this drives quench buffer from the buffer reservoir through the mixing chamber and onto the sample held in the collection vial. This effectively quenches the reaction and the contents of the collection vial can be further analysed (e.g. spectrophotometer). Two non-return valves were incorporated into the design to ensure correct sample and quench buffer directionality and also ensure that the solenoid valves could not be flooded.

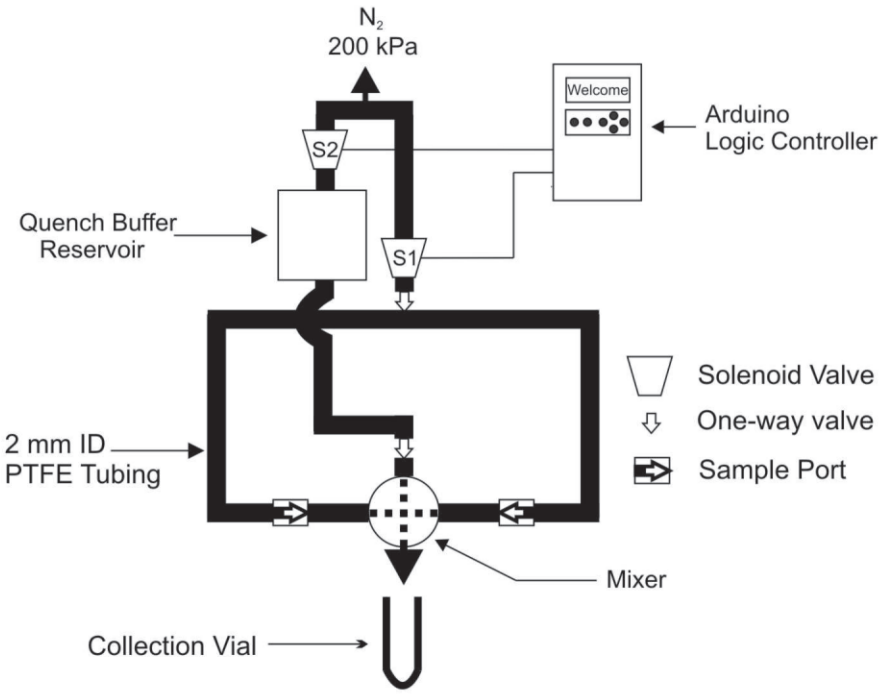

Figure B.1: Schematic description of the quench-flow device. Samples (e.g. cells and glucose, or substrate and enzymes) are manually inserted into the sample ports 1 and 2 respectively, which are subsequently closed. Initiating the quench-flow device from the controller opens solenoid valve S1, which opens the pressure line and injects the samples through the mixing chamber into the collection vial. After the set quench time (e.g. 500 ms), solenoid valve S2 is triggered, and the pressure line drives quench buffer through the mixing device and into the collection chamber, quenching the reaction. Although not indicated on the diagram, each of the sample and quench-flow lines are temperature regulated and the quench buffer reservoir is kept in an salt ice bath (see text for description).

B.3.1.1 Sample Ports

Most quench-flow devices that are commercially available require a fairly large volume of sample, as a lot of sample remains in the tubing. Obtaining high volumes (up to 1 mL) of isolated *P. falciparum* trophozoites is expensive and very labour intensive. To minimise wastage, two in-line sample ports were inserted near the mixing chamber. To insert the sample, these ports are opened and the required sample volume (30 - 200 μL) is manually pipetted into the

port. This method has the advantage that the accuracy of the sample volume is determined by the pipette rather than the quench device. Furthermore, the close proximity of the sample to the mixing chamber reduces the dead time, and minimises the loss of sample that remains in the tubing.

B.3.1.2 Quenching

The quench buffer reservoir was typically a 500 mL shot bottle kept in a salt-ice bath at -20 °C. Opening of the S2 solenoid valve would increase the pressure in the reservoir and drive buffer through the quench line and through the mixing chamber. The advantage of quenching through the mixing chamber is that any residual mixed sample in the chamber and line is flushed into the collection vial, thus minimising sample loss. This is particularly relevant when using cells (i.e. yeast or *P. falciparum* trophozoites), that are fairly viscous and do not entirely flush through during the mixing cycle.

B.3.1.3 Mixing

A simple 4-channel HPLC mixer was incorporated into the device. In simple T-mixers, it has been shown that the distance that the mixed sample travels after the T-section greatly determined the extent of mixing[30]. In this device, the distance was approximately 7 cm, and the sample was injected into a collection vial providing additional mixing. For the quench times (>150 ms) required for our assays this mixing was deemed sufficient. Specialised mixing micro-volume devices are commercial available and could easily be incorporated into the device if more complete mixing were required.

B.3.1.4 Controller

Two solenoid valves (closed by default) were controlled by a self-programmed Arduino Uno logic board. The logic board is linked to an LCD screen and keypad. When triggered by the user a 24 VDC relay was activated, which in turn opened the solenoid valves. The time between opening the first (S1, Fig. B.1) and second (S2, Fig. B.1) solenoid valve determined the quench time of the reaction. From the menu, a user can set with the keypad i) the *Quench Time*, which is defined as the time between mixing samples and quenching, ii) the *Mix Delay* which is the time the quench valve is open (i.e. the longer the

mix time, the greater the volume of quench buffer is injected) and iii) The air flush time, which after manual flushing of the system is used to dry the area before another sample run.

B.3.1.5 Temperature Regulation

We required an assay temperature of 37 °C. To regulate this temperature 1.5 mm silicon piping was coiled over the sample ports and mixing chamber. This pipe was connected to a water bath and warm water circulated through the heating coil using a peristaltic pump. Temperature of the mixing chamber was checked with a thermometer. A separate piping coil was placed on the quench line and a peristaltic pump circulated a salt-water mixture at 0 °C.

B.3.1.6 Flushing

After each assay run, sample ports and mixing chamber were flushed by manually injecting assay buffer through the sample ports with a 100 mL syringe. After sufficient rinsing (>20 mL), an *Air Flush* option on the controller was activated which was used to remove residual buffer and dry the chambers.

B.3.1.7 Pressure

The pressure line was linked to a nitrogen gas canister (*Afrox*, South Africa). Pressure was regulated to 200 kPa.

B.4 Calibration

Calibration of the quench-flow device is required to determine the dead-time. When the first solenoid valve opens at T_0, it takes time before the samples are mixed. Furthermore, when the quench solenoid valve is opened it takes time for the reaction to be completely quenched.

The rapid oxidation of NADH by 70% *m/v* perchloric acid (PCA) was used for device calibration. 100 μL of 20 mM NADH was mixed with 100 μL 70% *m/v* PCA and the reaction was quenched with approximately 1.5 mL 1 N NaOH between 0.1 and 5 s (Fig. B.2). After quenching, to account for small variations in quench volume, the volume of all the quenched samples was adjusted

to 2 mL. Aliquots of each sample were diluted between 10 and 50 time and to quantify the remaining NADH, the absorbance at 340 nm was measured on a spectrophotometer (Biotek PowerWave™ 340). As a control (A_0), the NADH was added to the quench buffer prior to the addition of PCA.

From these data, the dead time can be calculated from Eq. B.4.1[157], where A_t describes the absorbance measured at a specific time, A_0 refers to the control absorbance with no reaction occurring, k refers to the first order rate constant, t refers to time and t_d refers to the dead time. The data were fitted to this equation in *Wolfram Mathematica 8.0*, which yielded a dead time of 151 ± 62.0 ms.

$$A_t = A_0 e^{-k(t+t_d)} \tag{B.4.1}$$

Figure B.2: Determination of the quench-flow device dead time. The dead time of the quench-flow device was determined by measuring the rapid oxidation of NADH by 70% *m/v* PCA. To obtain the dead time, t_d, the data between 0 and 500 ms were fitted to Eq. B.4.1. A dead time of 151 ± 62.0 ms was calculated. The data is the combination of two independent experiments and error bars are SEM, n = 4.

B.5 Discussion

We required a simple and cost effective quench-flow device that could operate with very low sample volumes (30 μL) with minimal wastage at quench speeds of approximately 100 ms.

The air pressured system presented here meets these requirements fairly well. In particular it is able to utilise very low sample volumes with minimal wastage. The dead time is a bit higher than initially wanted, but still suitable for our assay requirement. This dead time could be improved by increasing the pressure of the gas line, but would require different solenoid valves. Another option would be to pressurise the buffer reservoir, but this raises safety concerns and would require a specialised reservoir for the pressure. This method would also require the buffer to move through the solenoid valve and thus the solenoid specification should cater for required quench buffers (e.g. corrosive quench buffers)

Further development of the device is possible, but at present it is suitable for our requirements and promises to be an important tool for investigating the glucose uptake in *P. falciparum* trophozoites.

List of References

1. Agbenyega, T., Angus, B. J., Bedu-Addo, G., Baffoe-Bonnie, B., Guyton, T., Stacpoole, P. W., and Krishna, S. (2000). Glucose and lactate kinetics in children with severe malaria. *J. Clin. Endocrinol. Metab.*, 85(4):1569–1576.

2. Allen, R. and Kirk, K. (2004). Cell volume control in the *Plasmodium*-infected erythrocyte. *Trends Parasitol.*., 20(1):7–10.

3. Ansorge, I., Benting, J., Bhakdi, S., and Lingelbach, K. (1996). Protein sorting in *Plasmodium falciparum*-infected red blood cells permeabilized with the pore-forming protein streptolysin O. *Biochem. J.*, 315:307–314.

4. Ansorge, I., Paprotka, K., Bhakdi, S., and Lingelbach, K. (1997). Permeabilization of the erythrocyte membrane with streptolysin O allows access to the vacuolar membrane of *Plasmodium falciparum* and a molecular analysis of membrane topology. *Mol. Biochem. Parasitol.*, 84(2):259–261.

5. Antonio, C., Larson, T., Gilday, A., Graham, I., Bergström, E., and Thomas-Oates, J. (2008). Hydrophilic interaction chromatography/electrospray mass spectrometry analysis of carbohydrate-related metabolites from *Arabidopsis thaliana* leaf tissue. *Rapid Commun. Mass Spectrom.*, 22(9):1399 –1407.

6. Atamna, H., Pescarmona, G., and Ginsburg, H. (1994). Hexose-monophosphate shunt activity in intact *Plasmodium falciparum* infected erythrocytes and in free parasites. *Mol. Biochem. Parasitol.*, 67:79–89.

7. Bakker, B. M., Michels, P. A., Opperdoes, F. R., and Westerhoff, H. V. (1997). Glycolysis in bloodstream form *Trypanosoma brucei* can be understood in terms of the kinetics of the glycolytic enzymes. *J. Biol. Chem.*, 272(6):3207–3215.

8. Bakker, B. M., Westerhoff, H. V., Opperdoes, F. R., and Michels, P. A. (2000). Metabolic control analysis of glycolysis in trypanosomes as an approach to improve selectivity and effectiveness of drugs. *Mol. Biochem. Parasitol.*, 106(1):1–10.

9. Barrett, M. P. (1997). The pentose phosphate pathway and parasitic protozoa. *Parasitol. Today*, 13(1):11–16.

10. Basketter, D. A. and Widdas, W. F. (1978). Asymmetry of the hexose transfer system in human erythrocytes. comparison of the effects of cytochalasin B, phloretin and maltose as competitive inhibitors. *J. Physiol.*, 278:389–401.

11. Becker, K., Tilley, L., Vennerstrom, J. L., Roberts, D., Rogerson, S., and Ginsburg, H. (2004). Oxidative stress in malaria parasite-infected erythrocytes: host-parasite interactions. *Int. J. Parasitol.*, 34(2):163–189.

12. Bisson, L. F. and Fraenkel, D. G. (1983). Involvement of kinases in glucose and fructose uptake by *Saccharomyces cerevisiae*. *Proc. Natl. Acad. Sci. U. S. A.*, 80(6):1730 –1734.

13. Blacklow, S. C., Raines, R. T., Lim, W. A., Zamore, P. D., and Knowles, J. R. (1988). Triosephosphate isomerase catalysis is diffusion controlled. appendix: Analysis of triose phosphate equilibria in aqueous solution by ^{31}P NMR. *Biochemistry*, 27(4):1158–1167.

14. Bloch, R. (1973). Inhibition of glucose transport in the human erythrocyte by cytochalasin B. *Biochemistry*, 12(23):4799–4801.

15. Blodgett, D. M. and Carruthers, A. (2004). Conventional transport assays underestimate sugar transport rates in human red cells. *Blood Cells Mol. Dis.*, 32(3):401–407.

16. Bosia, A., Ghigo, D., Turrini, F., Nissani, E., Pescarmona, G. P., and Ginsburg, H. (1993). Kinetic characterization of Na^+/H^+ antiport of *Plasmodium falciparum* membrane. *J. Cell. Physiol.*, 154(3):527–534.

17. Boyer, P. D. and Robbins, E. A. (1957). Determination of the equilibrium of the hexokinase reaction and the free energy of hydrolysis of adenosine triphosphate. *J.Biol. Chem.*, 224(1):121–135.

18. Bozdech, Z. and Ginsburg, H. (2005). Data mining of the transcriptome of *Plasmodium falciparum*: the pentose phosphate pathway and ancillary processes. *Malar. J.*, 4(1):17–29.

19. Bradford, M. (1976). A rapid and sensitive method for the quantitation of microgram quantities of protein utilizing the principle of protein-dye binding. *Anal. Biochem.*, 72:248–254.

20. Brady, R. L. and Cameron, A. (2004). Structure-based approaches to the development of novel anti-malarials. *Curr. Drug Targets*, 5(2):137–149.

21. Brown, W. M., Yowell, C. A., Hoard, A., Vander Jagt, T. A., Hunsaker, L. A., Deck, L. M., Royer, R. E., Piper, R. C., Dame, J. B., Makler, M. T., and Vander Jagt, D. L. (2004). Comparative structural analysis and kinetic properties of lactate dehydrogenases from the four species of human malarial parasites. *Biochem.*, 43(20):6219–6229.

22. Buckwitz, D., Jacobasch, G., and Gerth, C. (1990a). Phosphofructokinase from *Plasmodium berghei*: a kinetic model of allosteric regulation. *Mol. Biochem. Parasitol.*, 40(2):225–232.

23. Buckwitz, D., Jacobasch, G., and Gerth, C. (1990b). Phosphofructokinase from *Plasmodium berghei*. influence of Mg^{2+}, ATP and Mg^{2+}-complexed ATP. *Biochem. J.*, 267(2):353–357.

24. Buckwitz, D., Jacobasch, G., Gerth, C., Holzhutter, H. G., and Thamm, R. (1988). A kinetic model of phosphofructokinase from *Plasmodium berghei*. influence of ATP and fructose-6-phosphate. *Mol. Biochem. Parasitol.*, 27(2-3):225–232.

25. Buckwitz, D., Jacobasch, G., Kuckelkorn, U., Plonka, A., and Gerth, C. (1990c). Glucose-6-phosphate dehydrogenase from *Plasmodium berghei*: kinetic and electrophoretic characterization. *Exp. Parasitol.*, 70(3):264–275.

26. Buehner, M., Ford, G. C., Moras, D., Olsen, K. W., and Rossman, M. G. (1973). D-glyceraldehyde-3-phosphate dehydrogenase: three-dimensional structure and evolutionary significance. *Proc. Natl. Acad. Sci. U.S.A.*, 70(11):3052–3054.

27. Byrant, C., Voller, A., and Smith, M. (1964). The incorporation of radioactivity from (14c) glucose into soluble metabolic intermediates of malarial parasites. *Am. J. Trop. Med. Hyg.*, 13:515–519.

28. Bzik, D. J., Fox, B. A., and Gonyer, K. (1993). Expression of *Plasmodium falciparum* lactate dehydrogenase in *Escherichia coli*. *Mol. Biochem. Parasitol.*, 59(1):155–166.

29. Campanale, N., Nickel, C., Daubenberger, C., Wehlan, D., Gorman, J., Klonis, N., Becker, K., and Tilley, L. (2003). Identification and characterization of heme-interacting proteins in the malaria parasite, *Plasmodium falciparum*. *J. Biol. Chem.*, 278(30):27354–27361.

30. Capretto, L., Cheng, W., Hill, M., and Zhang, X. (2011). Micromixing within microfluidic devices. *Top. Curr. Chem.*, 304:27–68.

31. Carter, S. B. (1967). Effects of cytochalasins on mammalian cells. *Nature*, 213(5073):261–264.

32. Caruthers, J., Bosch, J., Buckner, F., Van Voorhis, W., Myler, P., Worthey, E., Mehlin, C., Boni, E., DeTitta, G., Luft, J., Lauricella, A., Kalyuzhniy, O., Anderson, L., Zucker, F., Soltis, M., and Hol, W. G. (2006). Structure of a ribulose 5-phosphate 3-epimerase from *Plasmodium falciparum*. *Proteins*, 62(2):338–342.

33. Cascante, M., Boros, L. G., Comin-Anduix, B., de Atauri, P., Centelles, J. J., and Lee, P. W.-N. (2002). Metabolic control analysis in drug discovery and disease. *Nat Biotechnol*, 20(3):243–249.

34. Chaikuad, A., Fairweather, V., Conners, R., Joseph-Horne, T., Turgut-Balik, D., and Brady, R. L. (2005). Structure of lactate dehydrogenase from *Plasmodium vivax*: complexes with NADH and APADH. *Biochem.*, 44(49):16221–16228.

35. Chan, M. and Sim, T. (2005). Functional analysis, overexpression and kinetic characterisation of pyruvate kinase from *Plasmodium falciparum*. *Biochem. Biophys. Res. Comm.*, 326:188–196.

36. Chan, M., Tan, D. H., and Sim, T. S. (2007). *Plasmodium falciparum* pyruvate kinase as a novel target for antimalarial drug-screening. *Travel Med. Infect. Dis.*, 5(2):125–131.

37. Choi, I. and Mikkelsen, R. (1990). *Plasmodium falciparum*: ATP/ADP transport across the parasitophorous vacuolar and plasma membranes. *Exp. Parasitol.*, 71(4):452–462.

38. Clarke, J. L., Scopes, D. A., Sodeinde, O., and Mason, P. J. (2001). Glucose-6-phosphate dehydrogenase-6-phosphogluconolactonase. a novel bifunctional enzyme in malaria parasites. *Eur. J. Biochem.*, 268(7):2013–2019.

39. Cloonan, N., Fischer, K., Cheng, Q., and Saul, A. (2001). Aldolase genes of *Plasmodium* species. *Mol. Biochem. Parasitol.*, 113(2):327–330.

40. Collard, F., Collet, J. F., Gerin, I., Veiga-da Cunha, M., and Van Schaftingen, E. (1999). Identification of the cDNA encoding human 6-phosphogluconolactonase, the enzyme catalyzing the second step of the pentose phosphate pathway. *FEBS Lett.*, 459(2):223–226.

41. Cornish-Bowden, A. and J.H.S., H. (2005). Kinetic characterization of enzymes for systems biology. *The Biochemist*, 27:11–14.

42. Cornish-Bowden, A. and L., C. M. (2000). *Animating the Cellular Map*, chapter 10. Irreversible Reactions in Metabolic Simulations: how reversible is irreversible?, pages 65 – 71. Stellenbosch University Press.

43. Cox-Singh, J., Davis, T., Lee, K.-S., Shamsul, S., Matusop, A., Ratnam, S., Rahman, H., Conway, D., and Singh, B. (2008). *Plasmodium knowlesi* malaria in humans is widely distributed and potentially life threatening. *Clin. Infect. Dis.*, 46(2):165–171.

44. Cranmer, S., Conant, A. R., Gutteridge, W. E., and Halestrap, A. P. (1995). Characterization of the enhanced transport of L- and D-lactate into human red blood cells infected with *Plasmodium falciparum* suggests the presence of a novel saturable lactate proton cotransporter. *J. Biol. Chem.*, 270(25):15045–15052.

45. Cranmer, S., Magowan, C., Liang, J., Coppel, R., and Cooke, B. (1997). An alternative to serum for cultivation of *Plasmodium falciparum in vitro*. *Trans. R. Soc. Trop. Med. Hyg.*, 91(3):363–365.

46. Crooke, A., Diez, A., Mason, P., and Bautista, J. (2006). Transient silencing of *Plasmodium falciparum* bifunctional glucose-6-phosphate dehydrogenase-6-phosphogluconolactonase. *FEBS J.*, 273(7):1537–1546.

47. Daubenberger, C. A., Poltl-Frank, F., Jiang, G., Lipp, J., Certa, U., and Pluschke, G. (2000). Identification and recombinant expression of glyceraldehyde-3-phosphate dehydrogenase of *Plasmodium falciparum*. *Gene*, 246(1-2):255–264.

48. Dawkins, P. and Dickens, F. (1965). The oxidation of d- and l-glycerate by rat liver. *Biochem. J.*, 94:353–367.

49. Desai, S. A., Krogstad, D. J., and McCleskey, E. W. (1993). A nutrient-permeable channel on the intraerythrocytic malaria parasite. *Nature*, 362(6421):643–646.

50. Devés, R. and Krupka, R. M. (1978). Cytochalasin B and the kinetics of inhibition of biological transport: a case of asymmetric binding to the glucose carrier. *Biochim. Biophys. Acta.*, 510(2):339–348.

51. Döbeli, H., Trzeciak, A., Gillessen, D., Matile, H., Srivastava, I. K., Perrin, L. H., Jakob, P. E., and Certa, U. (1990a). Expression, purification, biochemical

characterization and inhibition of recombinant *Plasmodium falciparum* aldolase. *Mol. Biochem. Parasitol.*, 41(2):259–268.

52. Döbeli, H., Trzeciak, A., Gillessen, D., Matile, H., Srivastava, I. K., Perrin, L. H., Jakob, P. E., and Certa, U. (1990b). Expression, purification, biochemical characterization and inhibition of recombinant *Plasmodium falciparum* aldolase. *Mol. Biochem. Parasitol.*, 41(2):259–268.

53. du Preez, F., Conradie, R., Penkler, G., Holm, K., van Dooren, F., and Snoep, J. (2007). A comparative analysis of kinetic models of erythrocyte glycolysis. *J. Theor. Biol.*

54. Dunn, C. R., Banfield, M. J., Barker, J. J., Higham, C. W., Moreton, K. M., Turgut-Balik, D., Brady, R. L., and Holbrook, J. J. (1996). The structure of lactate dehydrogenase from *Plasmodium falciparum* reveals a new target for anti-malarial design. *Nat. Struct. Biol.*, 3:912–915.

55. Eggstein, M. and Kuhlmann, E. (1974). *Methods of Enzyme Analysis*. Academic Press Inc., 2nd edition.

56. El-Kady, I. and Mostafa, M. (1995). Production of cytochalasins C, D & E from dematiaceous hyphomycetes. *Folia Microbiologica*, 40:301–303. 10.1007/BF02814213.

57. Elliott, J. L., Saliba, K. J., and Kirk, K. (2001). Transport of lactate and pyruvate in the intraerythrocytic malaria parasite, *Plasmodium falciparum*. *Biochem. J.*, 355:733–739.

58. Ernest, I., Callens, M., Opperdoes, F., and Michels, P. (1994). Pyruvate kinase of *Leishmania mexicana*. cloning and analysis of the gene, overexpression in *Escherichia coli* and characterization of the enzyme. *Mol. Biochem. Parasitol.*, pages 43–54.

59. Ernest, I., Callens, M., Uttaro, A., Chevalier, N., Opperdoes, F., Muirhead, H., and Michels, P. (1998). Pyruvate kinase of *Trypanosoma brucei*: overexpression, purification, and functional characterization of wild-type and mutated enzyme. *Protein Expr. Purif.*, 13:373–382.

60. Evans, M. L., Matyka, K., Lomas, J., Pernet, A., Cranston, I. C., Macdonald, I., and Amiel, S. A. (1998). Reduced counterregulation during hypoglycemia with raised circulating nonglucose lipid substrates: evidence for regional differences in

metabolic capacity in the human brain? *J. Clin. Endocrinol. Metab.*, 83(8):2952–2959.

61. Eyschen, J., Vitoux, B., Marraud, M., Cung, M. T., and Branlant, G. (1999). Engineered glycolytic glyceraldehyde-3-phosphate dehydrogenase binds the anti conformation of NAD^+ nicotinamide but does not experience A-specific hydride transfer. *Arch. Biochem. Biophys.*, 364(2):219–227.

62. Faller, L., Baroudy, B., Jonson, A., and Ewall, R. (1977). Magnesium ion requirements for yeast enolase activity. *Biochem.*, 16:3864–3869.

63. Famin, O. and Ginsburg, H. (2003). The treatment of *Plasmodium falciparum*-infected erythrocytes with chloroquine leads to accumulation of ferriprotoporphyrin ix bound to particular parasite proteins and to the inhibition of the parasite's 6-phosphogluconate dehydrogenase. *Parasite*, 10(1):39–50.

64. Fell, D. A. (1992). Metabolic control analysis: a survey of its theoretical and experimental development. *Biochem. J.*, 286 (Pt 2):313–330.

65. Fjeld, C. C., Birdsong, W. T., and Goodman, R. H. (2003). Differential binding of NAD^+ and NADH allows the transcriptional corepressor carboxyl-terminal binding protein to serve as a metabolic sensor. *Proc. Natl. Acad. Sci. U. S. A.*, 100(16):9202–9207.

66. Fletcher, K., Canning, M., and Theakston, R. (1977). Electrophoresis of glucose-6-phosphate and 6-phosphogluconate dehydrogenases in erythrocytes from malaria-infected animals. *Ann. Trop. Med. Parasitol.*, 71:125–130.

67. Foth, B. J., Stimmler, L. M., Handman, E., Crabb, B. S., Hodder, A. N., and McFadden, G. I. (2005). The malaria parasite *Plasmodium falciparum* has only one pyruvate dehydrogenase complex, which is located in the apicoplast. *Mol. Microbiol.*, 55(1):39–53.

68. Fry, M., Webb, E., and Pudney, M. (1990). Effect of mitochondrial inhibitors on adenosinetriphosphate levels in *Plasmodium falciparum*. *Comp. Biochem. Physiol. B*, 96(4):775–782.

69. Gardner, M. J., Hall, N., Fung, E., White, O., Berriman, M., Hyman, R. W., Carlton, J. M., Pain, A., Nelson, K. E., Bowman, S., Paulsen, I. T., James, K., Eisen, J. A., Rutherford, K., Salzberg, S. L., Craig, A., Kyes, S., Chan, M. S., Nene, V., Shallom, S. J., Suh, B., Peterson, J., Angiuoli, S., Pertea, M., Allen, J., Selengut, J., Haft, D., Mather, M. W., Vaidya, A. B., Martin, D. M., Fairlamb,

A. H., Fraunholz, M. J., Roos, D. S., Ralph, S. A., McFadden, G. I., Cummings, L. M., Subramanian, G. M., Mungall, C., Venter, J. C., Carucci, D. J., Hoffman, S. L., Newbold, C., Davis, R. W., Fraser, C. M., and Barrell, B. (2002). Genome sequence of the human malaria parasite *Plasmodium falciparum*. *Nature*, 419(6906):498–511.

70. Gayathri, P., Banerjee, M., Vijayalakshmi, A., Balaram, H., Balaram, P., and Murthy, M. R. N. (2009). Biochemical and structural characterization of residue 96 mutants of *Plasmodium falciparum* triosephosphate isomerase: active-site loop conformation, hydration and identification of a dimer-interface ligand-binding site. *Acta Crystallogr. D Biol. Crystallogr.*, 65(Pt 8):847–857.

71. Geenen, S., Taylor, P., Snoep, J., Wilson, I., Kenna, J., and Westerhoff, H. (2012). Systems biology tools for toxicology. *Arch. Toxicol.*, 86(8):1251–1271.

72. Goldberg, R., Tewari, Y., and Bhat, T. (2004). Thermodynamics of enzyme-catalyzed reactions-a database for quantitative biochemistry. *Bioinformatics*, 20(16):2874–2877.

73. Gomez, M. S., Piper, R. C., Hunsaker, L. A., Royer, R. E., Deck, L. M., Makler, M. T., and Vander Jagt, D. L. (1997). Substrate and cofactor specificity and selective inhibition of lactate dehydrogenase from the malarial parasite *P. falciparum*. *Mol. Biochem. Parasitol.*, 90(1):235–246.

74. Goodyer, I. D., Hayes, D. J., and Eisenthal, R. (1997). Efflux of 6-deoxy-D-glucose from *Plasmodium falciparum*-infected erythrocytes via two saturable carriers. *Mol. Biochem. Parasitol.*, 84(2):229–239.

75. Grall, M., Srivastava, I., Schmidt, M., Garcia, A.-M., Mauel, J., and Perrin, L. (1992). *Plasmodium falciparum*: Identification and purification of the phosphoglycerate kinase of the malaria parasite. *Exp. Parasitol.*, 75(1):10–18.

76. Griffin, J. F., Rampal, A. L., and Jung, C. Y. (1982). Inhibition of glucose transport in human erythrocytes by cytochalasins: A model based on diffraction studies. *Proc. Natl. Acad. Sci. U. S. A.*, 79(12):3759–3763.

77. Grüning, N.-M., Rinnerthaler, M., Bluemlein, K., Mülleder, M., Wamelink, M. M. C., Lehrach, H., Jakobs, C., Breitenbach, M., and Ralser, M. (2011). Pyruvate kinase triggers a metabolic feedback loop that controls redox metabolism in respiring cells. *Cell Metab.*, 14(3):415–427.

78. Hansen, M., Kun, J., Schultz, J., and Beitz, E. (2002). A single, bi-functional aquaglyceroporin in blood-stage *Plasmodium falciparum* malaria parasites. *J. Biol. Chem.*, 277(7):4874–4882.

79. Hanson, R. L., Rudolph, F. B., and Lardy, H. A. (1973). Rabbit muscle phosphofructokinase. the kinetic mechanism of action and the equilibrium constant. *J. Biol. Chem.*, 248(22):7852–7859.

80. Hayashi, M., Yamada, H., Mitamura, T., Horii, T., Yamamoto, A., and Moriyama, Y. (2000). Vacuolar H(+)-ATPase localized in plasma membranes of malaria parasite cells, *Plasmodium falciparum*, is involved in regional acidification of parasitized erythrocytes. *J. Biol. Chem.*, 275(44):34353–34358.

81. Hayward, R. (2000). *Plasmodium falciparum* phosphoenolpyruvate carboxykinase is developmentally regulated in gametocytes. *Mol. Biochem. Parasitol.*, 107(2):227–240.

82. Heinrich, R. and Rapoport, T. (1974). A linear steady-state treatment of enzymatic chains. general properties, control and effector strength. *Eur. J. Biochem.*, 42(1):89–95.

83. Helfert, S., Estevez, A., Bakker, B., Michels, P., and Clayton, C. (2001). Roles of triosephosphate isomerase and aerobic metabolism in *Trypanosoma brucei*. *Biochem J.*, 357(Pt 1):117–125.

84. Hess, B. and Plesser, T. (1979). Temporal and spatial order in biochemical systems. *Ann. N. Y. Acad. Sci.*, 316:203–213.

85. Hills, T., Srivastava, A., Ayi, K., Wernimont, A., Kain, K., Waters, A., Hui, R., and Pizarro, J. (2011). Characterization of a new phosphatase from plasmodium. *Mol. Biochem. Parasitol.*, 179(2):69–79.

86. Hoefnagel, M., Starrenburg, M., Martens, D., Hugenholtz, J., Kleerebezem, M., van Swam, I., Bongers, R., Westerhoff, H., and Snoep, J. (2002). Metabolic engineering of lactic acid bacteria, the combined approach: kinetic modelling, metabolic control and experimental analysis. *Microbiology*, 148(Pt 4):1003–1013.

87. Hofmeyr, J. (2000). Metabolic control analysis in a nutshell. *Proc. ICSB, Pasadena, California,*, pages 291–300.

88. Hofmeyr, J. and Cornish-Bowden, A. (1991). Quantitative assessment of regulation in metabolic systems. *Eur. J. Biochem.*, 200(1):223–236.

89. Hofmeyr, J. and Cornish-Bowden, A. (2000). Regulating the cellular economy of supply and demand. *FEBS Lett.*, 476(1-2):47–51.

90. Hofmeyr, J. H. S. and Cornish-Bowden, A. (1997). The reversible hill equation: how to incorporate cooperative enzymes into metabolic models. *Comput. Appl. Biosci.*, 13(4):377–385.

91. Hohmann, S. (2002). Osmotic stress signaling and osmoadaptation in yeasts. *Microbiol.Mol. Biol. Rev.*, 66(2):300–372.

92. Holmes, M. A., Buckner, F. S., Van Voorhis, W. C., Verlinde, C. L., Mehlin, C., Boni, E., DeTitta, G., Luft, J., Lauricella, A., Anderson, L., Kalyuzhniy, O., Zucker, F., Schoenfeld, L. W., Earnest, T. N., Hol, W. G., and Merritt, E. A. (2006). Structure of ribose 5-phosphate isomerase from *Plasmodium falciparum*. *Acta Crystallograph. Sect. F Struct. Biol. Cryst. Commun.*, 62(5):427–431.

93. Holzhutter, H. (2004). The principle of flux minimization and its application to estimate stationary fluxes in metabolic networks. *Eur. J. Biochem.*, 271(14):2905–2922.

94. Holzhutter, H., Jacobasch, G., and Bisdorff, A. (1985a). Mathematical modelling of metabolic pathways affected by an enzyme deficiency. a mathematical model of glycolysis in normal and pyruvate-kinase-deficient red blood cells. *Eur. J. Biochem.*, 149(1):101–111.

95. Holzhutter, H. G., Jacobasch, G., and Bisdorff, A. (1985b). Mathematical modelling of metabolic pathways affected by an enzyme deficiency. a mathematical model of glycolysis in normal and pyruvate-kinase-deficient red blood cells. *Eur. J. Biochem.*, 149(1):101–111.

96. Hoops, S., Sahle, S., Gauges, R., Lee, C., Pahle, J., Simus, N., Singhal, M., Xu, L., Mendes, P., and Kummer, U. (2006). COPASI- COmplex PAthway SImulator. *Bioinformatics*, 22(24):3067–3074.

97. Hoppe, H., Verschoor, J., and Louw, A. (1991). *Plasmodium falciparum*: a comparison of synchronisation methods for *in vitro* cultures. *Exp. Parasitol.*, 72(4):464–467.

98. Hornberg, J., Bruggeman, F., Bakker, B., and Westerhoff, H. (2007). Metabolic control analysis to identify optimal drug targets. *Prog. Drug. Res.*, 64:171, 173–89.

99. Itin, C., Burki, Y., Certa, U., and Döbeli, H. (1993). Selective inhibition of *Plasmodium falciparum* aldolase by a tubulin derived peptide and identification of the binding site. *Mol. Biochem. Parasitol.*, 58(1):135–143.

100. Joët, T., Chotivanich, K., Silamut, K., Patel, A., Morin, C., and Krishna, S. (2004). Analysis of *Plasmodium vivax* hexose transporters and effects of a parasitocidal inhibitor. *Biochem. J.*, 381(3):905–909.

101. Joët, T., Eckstein-Ludwig, U., Morin, C., and Krishna, S. (2003). Validation of the hexose transporter of *Plasmodium falciparum* as a novel drug target. *Proc. Natl. Acad. Sci. U. S. A.*, 100(13):7476–7479.

102. Joët, T., Holterman, L., Stedman, T. T., Kocken, C. H., Van Der Wel, A., Thomas, A. W., and Krishna, S. (2002). Comparative characterization of hexose transporters of *Plasmodium knowlesi, Plasmodium yoelii* and *Toxoplasma gondii* highlights functional differences within the apicomplexan family. *Biochem. J.*, 368:923–929.

103. Joët, T. and Krishna, S. (2004). The hexose transporter of *Plasmodium falciparum* is a worthy drug target. *Acta Trop.*, 89(3):371–374.

104. Jortzik, E., Mailu, B., Preuss, J., Fischer, M., Bode, L., Rahlfs, S., and Becker, K. (2011). Glucose-6-phosphate dehydrogenase-6-phosphogluconolactonase: a unique bifunctional enzyme from *Plasmodium falciparum*. *Biochem. J.*, 436(3):641–650.

105. Joshi, S., Singh, A., Kumar, A., Misra, P., Siddiqi, M., and Saxena, J. (2008). Molecular cloning and characterization of *Plasmodium falciparum* transketolase. *Mol. Biochem. Parasitol.*, 160(1):32–41.

106. Joubert, F., Neitz, A. W., and Louw, A. I. (2001). Structure-based inhibitor screening: a family of sulfonated dye inhibitors for malaria parasite triosephosphate isomerase. *Proteins*, 45(2):136–143.

107. Kacser, H. and Burns, J. A. (1973a). The control of flux. *Symp. Soc. Exp. Biol.*, 27:65–104.

108. Kacser, H. and Burns, J. A. (1973b). The control of flux. *Symp. Soc. Exp. Biol.*, 27:65–104.

109. Kanaani, J. and Ginsburg, H. (1991). Transport of lactate in *Plasmodium falciparum*-infected human erythrocytes. *J. Cell. Physiol.*, 149(3):469–476.

110. Karlgren, S., Pettersson, N., Nordlander, B., Mathai, J., Brodsky, J. L., Zeidel, M., Bill, R., and Hohmann, S. (2005). Conditional osmotic stress in yeast: a system to study transport through aquaglyceroporins and osmostress signaling. *J. Biol. Chem.*, 280(8):7186–7193.

111. Kaslow, D. and Hill, S. (1990). Cloning metabolic pathways by complementation in *Escherichia coli*. *J. Biol. Chem.*, 265:12337–12341.

112. Khan, S. and Waters, A. (2004). Malaria parasite transmission stages: an update. *Trends Parasitol.*., 20(12):575–580.

113. Kim, H., Certa, U., Döbeli, H., Jakob, P., and Hol, W. G. (1998). Crystal structure of fructose-1,6-bisphosphate aldolase from the human malaria parasite *Plasmodium falciparum*. *Biochem.*, 37(13):4388–9436.

114. Kim, J.-Y., Kim, H.-H., Shin, H.-L., Sohn, Y., Kim, H., Lee, S.-W., Lee, W.-J., and Lee, H.-W. (2012). Genetic variation of aldolase from korean isolates of *Plasmodium vivax* and its usefulness in serodiagnosis. *Malar. J.*, 11:159.

115. Kirk, K. (2001). Membrane transport in the malaria-infected erythrocyte. *Physiol. Rev.*, 81(2):495–537.

116. Kirk, K., Horner, H., and Kirk, J. (1996). Glucose uptake in *Plasmodium falciparum*-infected erythrocytes is an equilibrative not an active process. *Mol. Biochem. Parasitol.*, 82(2):195–205.

117. Knapp, B., Hundt, E., and Küpper, H. A. (1990). *Plasmodium falciparum* aldolase: gene structure and localization. *Mol. Biochem. Parasitol.*, 40(1):1–12.

118. Krishna, S., Waller, D. W., ter Kuile, F., Kwiatkowski, D., Crawley, J., Craddock, C. F., Nosten, F., Chapman, D., Brewster, D., and Holloway, P. A. (1994). Lactic acidosis and hypoglycaemia in children with severe malaria: pathophysiological and prognostic significance. *Trans. R. Soc. Trop. Med. Hyg.*, 88(1):67–73.

119. Krishna, S., Woodrow, C. J., Burchmore, R. J. S., Saliba, K. J., and Kirk, K. (2000). Hexose transport in asexual stages of *Plasmodium falciparum* and *Kinetoplastidae*. *Parasitol. Today*, 16(12):516–521.

120. Krupka, R. M. (1985). Asymmetrical binding of phloretin to the glucose transport system of human erythrocytes. *J. Membr. Biol.*, 83(1-2):71–80.

121. Kumar, S. and Banyal, H. S. (1997). Purification and characterisation of the hexokinase of *Plasmodium berghei*, a murine malaria parasite. *Acta Vet. Hung.*, 45(2):119–126.

122. Kurdi-Heidar, B. and Luzzato, L. (1990). Expression and characterization of glucose-6-phosphate dehydrogenase of *Plasmodium falciparum*. *Mol. Biochem. Parasitol.*, 41:83–92.

123. Lang-Unnasch, N. and Murphy, A. D. (1998). Metabolic changes of the malaria parasite during the transition from the human to the mosquito host. *Annu. Rev. Microbiol.*, 52:561–590.

124. Leskovac, V. (2004). *Comprehensive Enzyme Kinetics*. Kluwer academic publishers.

125. Lian, L.-Y., Al-Helal, M., Roslaini, A., Fisher, N., Bray, P., Ward, S., and Biagini, G. (2009). Glycerol: an unexpected major metabolite of energy metabolism by the human malaria parasite. *Malar. J.*, 8:38.

126. Liebermeister, W. and Klipp, E. (2006). Bringing metabolic networks to life: convenience rate law and thermodynamic constraints. *Theor. Biol. Med. Model.*, 3:41.

127. Ling, I. and Wilson, R. (1988). Glucose-6-phosphate dehydrogenase activity of the malaria parasite *Plasmodium falciparum*. *Mol. Biochem. Parasitol.*, 31:47–56.

128. Lowry, O. and Passonneau, J. (1964). The relationship between substrates and enzymes of glycolysis in brain. *J. Biol. Chem.*, 239:31–42.

129. MacLean-Fletcher, S. and Pollard, T. D. (1980). Mechanism of action of cytochalasin b on actin. *Cell*, 20(2):329–341.

130. Maeda, T., Saito, T., Harb, O., Roos, D., Takeo, S., Suzuki, H., Tsuboi, T., Takeuchi, T., and Asai, T. (2009). Pyruvate kinase type-ii isozyme in *Plasmodium falciparum* localizes to the apicoplast. *Parasitol. Int.*, 58(1):101–105.

131. Maeda, T., Saito, T., Oguchi, Y., Nakazawa, M., Takeuchi, T., and Asai, T. (2003). Expression and characterization of recombinant pyruvate kinase from *Toxoplasma gondii* tachyzoites. *Parasitol. Res.*, 89(4):259–265.

132. Maithal, K., Ravindra, G., Nagaraj, G., Singh, S., Balaram, H., and Balaram, P. (2002). Subunit interface mutation disrupting an aromatic cluster in *Plasmodium falciparum* triosephosphate isomerase: effect on dimer stability. *Protein Eng.*, 15(7):575–584.

133. Manning, S., Woodrow, C., Zuniga, F., Iserovich, P., Fischbarg, J., Louw, A., and Krishna, S. (2002). Mutational analysis of the hexose transporter of *Plasmodium falciparum* and development of a three-dimensional model. *J. Biol. Chem.*, 277(34):30942–30949.

134. McDaniel, H. and Siu, P. (1972). Purification and characterization of phosphoenolpyruvate carboxylase from *Plasmodium berghei*. *J. Bacteriol.*, 109:385–390.

135. Mehlin, C. (2005). Structure-based drug discovery for *Plasmodium falciparum*. *Comb. Chem. High Throughput Screen.*, 8(1):5–14.

136. Meier, B., Döbeli, H., and Certa, U. (1992). Stage specific expression of aldolase isozymes in the rodent malaria parasite *P. berghei*. *Mol. Biochem. Parasitol.*, 52:15–28.

137. Mony, B., Mehta, M., Jarori, G., and Sharma, S. (2009). Plant-like phosphofructokinase from *Plasmodium falciparum* belongs to a novel class of atp-dependent enzymes. *Int. J. Parasitol.*, 39(13):1441–1453.

138. Moreno-Sánchez, R., Saavedra, E., Rodríguez-Enríquez, S., Gallardo-Pérez, J., Quezada, H., and Westerhoff, H. (2010). Metabolic control analysis indicates a change of strategy in the treatment of cancer. *Mitochondrion*, 10(6):626–639.

139. Nagarajan, K. (1968). Metabolism of *Plasmodium berghei*. 3. carbon dioxide fixation and role of pyruvate and dicarboxylic acids. *Exp. Parasitol.*, 22(1):33–42.

140. O' Brian, E., Kurdi-Haidar, B., Wanachiwanawin, W., Carvajal, J., Vulliamy, T., Cappadoro, V., Mason, P., and Luzzatto, L. (1994). Cloning of the glucose-6-phosphate dehydrogenase from *Plasmodium falciparum*. *Mol. Biochem. Parasitol.*, 64:313–326.

141. O'Donnell, R. and Blackman, M. (2005). The role of malaria merozoite proteases in red blood cell invasion. *Curr.Opin. Microbiol.*, 8(4):422–427.

142. Olafsson, P. and Certa, U. (1994). Expression and cellular localisation of hexokinase during the bloodstage development of *Plasmodium falciparum*. *Mol. Biochem. Parasitol.*, 63(1):171–174.

143. Olafsson, P., Matile, H., and Certa, U. (1992). Molecular analysis of *Plasmodium falciparum* hexokinase. *Mol. Biochem. Parasitol.*, 56(1):89–101.

144. Olivier, B. and Snoep, J. (2004). Web-based kinetic modelling using JWS Online. *Bioinformatics*, 20(13):2143–2144.

145. Olszewski, K., Mather, M., Morrisey, J., Garcia, B., Vaidya, A., Rabinowitz, J., and Llinás, M. (2010). Branched tricarboxylic acid metabolism in *Plasmodium falciparum*. *Nature*, 466(7307):774–778.

146. Olszewski, K. L. and Llinás, M. (2011). Central carbon metabolism of *Plasmodium* parasites. *Mol. Biochem. Parasitol.*, 175(2):95–103.

147. Ozbayraktar, F. and Ulgen, K. (2010). Drug target identification in sphingolipid metabolism by computational systems biology tools: metabolic control analysis and metabolic pathway analysis. *J. Biomed. Inform.*, 43(4):537–549.

148. Pal, B., Pybus, B., Muccio, D. D., and Chattopadhyay, D. (2004). Biochemical characterization and crystallization of recombinant 3-phosphoglycerate kinase of *Plasmodium falciparum*. *Biochim. Biophys. Acta*, 1699(1-2):277–280.

149. Pal-Bhowmick, I., Krishnan, S., and Jarori, G. (2007a). Differential susceptibility of *Plasmodium falciparum* versus yeast and mammalian enolases to dissociation into active monomers. *FEBS J.*, 274(8):1932–1945.

150. Pal-Bhowmick, I., Mehta, M., Coppens, I., Sharma, S., and Jarori, G. (2007b). Protective properties and surface localization of *Plasmodium falciparum* enolase. *Infect. Immun.*, 75(11):5500–5508.

151. Pal-Bhowmick, I., Sadagopan, K., Vora, H., Sehgal, A., Sharma, S., and Jarori, G. (2004). Cloning, over-expression, purification and characterization of *Plasmodium falciparum* enolase. *Eur. J. Biochem.*, 271:4845–4854.

152. Pal-Bhowmick, I., Vora, H., and Jarori, G. (2007c). Sub-cellular localization and post-translational modifications of the *Plasmodium yoelii* enolase suggest moonlighting functions. *Malar. J.*, 6:45.

153. Pancholi, V. (2001). Multifunctional alpha-enolase: its role in diseases. *Cell. Mol. Life Sci.*, 58(7):902–920.

154. Parthasarathy, S., Eaazhisai, K., Balaram, H., Balaram, P., and Murthy, M. (2003). Structure of *Plasmodium falciparum* triose-phosphate isomerase-2-phosphoglycerate complex at 1.1 å resolution. *J. Biol. Chem.*, 278(52):52461–70.

155. Patel, A., Staines, H., and Krishna, S. (2008). New antimalarial targets: the example of glucose transport. *Travel Med. Infect. Dis.*, 6(1-2):58–66.

156. Pattanaik, P., Raman, J., and Balaram, H. (2002). Perspectives in drug design against malaria. *Curr. Top. Med. Chem.*, 2(5):483–505.

157. Peintler, G., Nagy, A., Horvath, A., Kortvelyesi, T., and Nagypal, I. (2000). Improved calibration and use of stopped-flow instruments. *Phys. Chem. Chem. Phys.*, 2:2575–2586.

158. Penkler, G. (2009). Construction and validation of a detailed kinetic model for *Plasmodium falciparum* during the asexual phase: A feasibility study. Master's thesis, University of Stellenbosch.

159. Penna-Coutinho, J., Cortopassi, W., Oliveira, A., Franca, T., and Krettli, A. (2011). Antimalarial activity of potential inhibitors of *Plasmodium falciparum* lactate dehydrogenase enzyme selected by docking studies. *PLoS One*, 6(7):e21237.

160. Poolman, B., Bosman, B., Kiers, J., and Konings, W. N. (1987). Control of glycolysis by glyceraldehyde-3-phosphate dehydrogenase in *Streptococcus cremoris* and *Streptococcus lactis*. *J. Bacteriol.*, 169(12):5887–5890.

161. Preuss, J., Hedrick, M., Sergienko, E., Pinkerton, A., Mangravita-Novo, A., Smith, L., Marx, C., Fischer, E., Jortzik, E., Rahlfs, S., Becker, K., and Bode, L. (2012a). High-throughput screening for small-molecule inhibitors of *plasmodium falciparum* glucose-6-phosphate dehydrogenase 6-phosphogluconolactonase. *J. Biomol. Screen.*, 17(6):738–751.

162. Preuss, J.and Maloney, P. P. S., Hedrick, M., Hershberger, P., Gosalia, P., Milewski, M.and Li, Y., Sugarman, E., Hood, B.and Suyama, E., Nguyen, K.and Vasile, S., Sergienko, E., Mangravita-Novo, A., Vicchiarelli, M., McAnally, D., Smith, L., Roth, G., Diwan, J., Chung, T., Jortzik, E., Rahlfs, S., Becker, K., Pinkerton, A., and Bode, L. (2012b). Discovery of a *Plasmodium falciparum* glucose-6-phosphate dehydrogenase 6-phosphogluconolactonase inhibitor (r,z)-n-((1-ethylpyrrolidin-2-yl)methyl)-2-(2-fluorobenzylidene)-3-oxo-3,4-dihydro-2h-benzo[b][1,4]thiazine-6-carboxamide (ml276) that reduces parasite growth *in vitro*. *J. Med. Chem.*

163. Pukrittayakamee, S., White, N. J., Davis, T. M., Supanaranond, W., Crawley, J., Nagachinta, B., and Williamson, D. H. (1994). Glycerol metabolism in severe *falciparum* malaria. *Metabolism*, 43(7):887–892.

164. Quinton-Tulloch, M. (2011). *Fragile robustness: Principles and practice*. PhD thesis, University of Manchester.

165. Racker, E. (1950). Crystalline alcohol dehydrogenase from baker's yeast. *J. Biol. Chem.*, 184(1):313–319.

166. Rahlfs, S. and Becker, K. (2006). Interference with redox-active enzymes as a basis for the design of antimalarial drugs. *Mini Rev. Med.Chem.*, 6(2):163–176.

167. Ranie, J., Kumar, V. P., and Balaram, H. (1993). Cloning of the triosephosphate isomerase gene of *Plasmodium falciparum* and expression in *Escherichia coli*. *Mol. Biochem. Parasitol.*, 61(2):159–169.

168. Rapoport, T., Heinrich, R., Jacobasch, G., and Rapoport, S. (1974). A linear steady-state treatment of enzymatic chains. a mathematical model of glycolysis of human erythrocytes. *Eur. J. Biochem.*, 42(1):107–120.

169. Ravindra, G. and Balaram, P. (2005). *Plasmodium falciparum* triosephosphate isomerase: New insights into an old enzyme. *Pure Appl. Chem.*, 77(1):281–289.

170. Read, M., Hicks, K. E., Sims, P. F., and Hyde, J. E. (1994). Molecular characterisation of the enolase gene from the human malaria parasite *Plasmodium falciparum*. evidence for ancestry within a photosynthetic lineage. *Eur. J. Biochem.*, 220(2):513–520.

171. Robien, M., Bosch, J., Buckner, F., van Voorhis, W., Worthey, E., Myler, P., Mehlin, C., Boni, E., Kalyuzhniy, O., Anderson, L., Lauricella, A., Gulde, S., Luft, J., DeTitta, G., Caruthers, J., Hodgson, K., Soltis, M., Zucker, F., Verlinde, C. M. J., Merritt, E., Schoenfeld, L., and Hol, W. (2006). Crystal structure of glyceraldehyde-3-phosphate dehydrogenase from *Plasmodium falciparum* at 2.25 å resolution reveals intriguing extra electron density in the active site. *Proteins*, 62(3):570–577.

172. Rohwer, J., Hanekom, A., Crous, C., Snoep, J., and Hofmeyr, J. (2006). Evaluation of a simplified generic bi-substrate rate equation for computational systems biology. *Syst. Biol. (Stevenage)*, 153(5):338–341.

173. Roth, E., Calvin, M., Max-Audit, J., Rosa, J., and Rosa, R. (1988a). The enzymes of the glycolytic pathway in erythrocytes infected with *Plasmodium falciparum* malaria parasites. *Blood*, 72:1922–1925.

174. Roth, E., Joulin, V., Miwa, S., Yoshida, A., Akatsuka, J., Cohen-Solal, M., and Rosa, R. (1988b). The use of enzymopathic human red cells in the study of malarial parasite glucose metabolism. *Blood*, 71(5):1408–1413.

175. Roth, E. F. and Jr. (1987). Malarial parasite hexokinase and hexokinase-dependent glutathione reduction in the *Plasmodium falciparum*-infected human erythrocyte. *J. Biol. Chem.*, 262(32):15678–15682.

176. Royer, R., Deck, L., Campos, N. M., Hunsaker, L. A., and Vander Jagt, D. L. (1986). Biologically active derivatives of gossypol: synthesis and antimalarial activities of periacylated gossylic nitriles. *J. Med. Chem.*, 29:1799–1801.

177. Saliba, K., Horner, H., and Kirk, K. (1998). Transport and metabolism of the essential vitamin pantothenic acid in human erythrocytes infected with the malaria parasite *Plasmodium falciparum*. *J. Biol. Chem.*, 273(17):10190–10195.

178. Saliba, K. and Kirk, K. (1999). pH regulation in the intracellular malaria parasite, *Plasmodium falciparum*. H^+ extrusion via a v-type H^+-ATPase. *J. Biol. Chem.*, 274(47):33213–33219.

179. Saliba, K., Krishna, S., and Kirk, K. (2004). Inhibition of hexose transport and abrogation of pH homeostasis in the intraerythrocytic malaria parasite by an O-3-hexose derivative. *FEBS Lett.*, 570(1-3):93–96.

180. Saltelli, A., Ratto, M., Tarantola, S., and Campolongo, F. (2005). Sensitivity analysis for chemical models. *Chem. Rev.*, 105(7):2811–2828.

181. Sander, B. J. and Kruckeberg, W. C. (1981). *Plasmodium berghei*: glycolytic intermediate concentrations of the infected mouse erythrocyte. *Exp. Parasitol.*, 52(1):1–8.

182. Sander, B. J., Lowery, M. S., and Kruckeberg, W. C. (1982). *Plasmodium berghei*: acid-insensitive phosphofructokinase in infected mouse erythrocytes. *Exp. Parasitol.*, 53(1):11–16.

183. Sanger, J. W. and Holtzer, H. (1972). Cytochalasin B: effects on cell morphology, cell adhesion, and mucopolysaccharide synthesis (cultured cells-contractile microfilaments-glycoproteins-embryonic cells-sorting-out). *Proc. Natl. Acad. Sci. U.S.A.*, 69(1):253–257.

184. Satchell, J., Malby, R., Luo, C., Adisa, A., Alpyurek, A., Klonis, N., Smith, B., Tilley, L., and Colman, P. (2005). Structure of glyceraldehyde-3-phosphate dehydrogenase from *Plasmodium falciparum*. *Acta Crystallogr. D Biol. Crystallogr.*, 61(Pt 9):1213–1221.

185. Scheer, M., Grote, A., Chang, A., Schomburg, I., Munaretto, C., Rother, M., Söhngen, C., Stelzer, M., Thiele, J., and Schomburg, D. (2011). BRENDA, the enzyme information system in 2011. *Nucleic Acids Res.*, 39(Database issue):D670–D676.

186. Schnick, C., Polley, S., Fivelman, Q., Ranford-Cartwright, L., Wilkinson, S., Brannigan, J., Wilkinson, A., and Baker, D. (2009). Structure and non-essential function of glycerol kinase in *Plasmodium falciparum* blood stages. *Mol. Microbiol.*, 71(2):533–545.

187. Scopes, D., Bautista, J., Vulliamy, T., and Mason, P. (1997). *Plasmodium falciparum* Glc6PD ± the N-terminal portion is homologous to a predicted protein encoded near to Glc6PD in *Haemophilus Influenzae*. *Mol. Microbiol.*, 23:847–848.

188. Sein, K. K. and Aikawa, M. (1998). The pivotal role of carbonic anhydrase in malaria infection. *Med. Hypotheses*, 50(1):19–23.

189. Shahabuddin, M., Rawlings, D., and Kaslow, D. (1994). A novel glucose-6-phosphate dehydrogenase in *Plasmodium falciparum*: cDNA and primary protein structure. *Biochim. Biophys. Acta.*, 1219:191–194.

190. Sherman, I. (1998). Carbohydrate metabolism of asexual stages. In Sherman, I., editor, *Malaria: Parasite biology, pathogenesis and protection*, pages 135–143. ASM Press, Washington, D.C.

191. Sherman, I. and I.P., T. (1966). Carbon dioxide fixation in malaria (*Plasmodium lopurae*). *Nature*, 24:639–642.

192. Sherman, I. and I.P., T. (1968). Carbon dioxide fixation in malaria-ii. *Plasmodium knowlesi* (monkey malaria). *Comp. Biochem. Physiol.*, 24:639–642.

193. Sherman, I. W. (1979). Biochemistry of *Plasmodium* (malarial parasites). *Microbiol. Rev.*, 43(4):453–495.

194. Shoemark, D., Cliff, M., Sessions, R., and Clarke, A. (2007). Enzymatic properties of the lactate dehydrogenase enzyme from *Plasmodium falciparum*. *FEBS J.*, 274(11):2738–2748.

195. Singh, A., Joshi, S., Arya, R., Kayastha, A., Srivastava, K., Tripathi, L., and Saxena, J. (2008). Molecular cloning and characterization of *Brugia malayi* hexokinase. *Parasitol. Int.*, 57(3):354–361.

196. Singh, S. K., Maithal, K., Balaram, H., and Balaram, P. (2001). Synthetic peptides as inactivators of multimeric enzymes: inhibition of *Plasmodium falciparum* triosephosphate isomerase by interface peptides. *FEBS Lett.*, 501(1):19–23.

197. Siu, P. (1967). Carbon dioxide fixation in plasmodia and the effect of some antimalarials on the enzyme. *Comp. Biochem. Physiol.*, 23:785–795.

198. Slavic, K., Delves, M., Prudencio, M., Talman, A., Straschil, U., Derbyshire, E., Xu, Z., Sinden, R., Mota, M., Morin, C., Tewari, R., Krishna, S., and Staines, H. (2011). Use of a selective inhibitor to define the chemotherapeutic potential of the plasmodial hexose transporter in different stages of the parasite's life cycle. *Antimicrob. Agents Chemother.*, 55(6):2824–2830.

199. Smith, C., Chattopadhyay, D., and Pal, B. (2011). Crystal structure of *Plasmodium falciparum* phosphoglycerate kinase: evidence for anion binding in the basic patch. *Biochem. Biophys. Res. Commun.*, 412(2):203–206.

200. Snoep, J., Bruggeman, F., Olivier, B., and Westerhoff, H. (2006). Towards building the silicon cell: a modular approach. *Biosystems*, 83(2-3):207–216.

201. Snoep, J. L. and Olivier, B. G. (2003). JWS Online cellular systems modelling and microbiology. *Microbiol.*, 149(Pt 11):3045 –3047.

202. Srivastava, I. K., Schmidt, M., Grall, M., Certa, U., Garcia, A. M., and Perrin, L. H. (1992). Identification and purification of glucose phosphate isomerase of *Plasmodium falciparum*. *Mol. Biochem. Parasitol.*, 54(2):153–64.

203. Staples, J. and Suarez, R. (1997). Honeybee flight muscle phosphoglucose isomerase: matching enzyme capacities to flux requirements at a near-equilibrium reaction. *J. Exp. Biol.*, 200(Pt 8):1247–1254.

204. Teng, R., Junankar, P., Bubb, W., Rae, C., Mercier, P., and Kirk, K. (2008). Metabolite profiling of the intraerythrocytic malaria parasite *Plasmodium falciparum* by ^{1}H NMR spectroscopy. *NMR Biomed.*

205. Teusink, B., Passarge, J., Reijenga, C., Esgalhado, E., van der Weijden, C., Schepper, M., Walsh, M., Bakker, B., van Dam, K., Westerhoff, H., and Snoep, J. (2000). Can yeast glycolysis be understood in terms of *in vitro* kinetics of the constituent enzymes? testing biochemistry. *Eur. J. Biochem.*, 267(17):5313–5329.

206. Theakston, R. and Fletcher, K. (1973). An electron cytochemical study of 6-phosphogluconate dehydrogenase activity in infected erythrocytes during malaria. *Life Sci.*, pages 405–410.

207. Thevelein, J. and Hohmann, S. (1995). Trehalose synthase: guard to the gate of glycolysis in yeast? *Trends Biochem. Sci.*, 20(1):3–10.

208. Ting, I. and Sherman, I. (1966). Carbon dioxide fixation in malaria-i. kinetic studies in *Plasmodium lophurae*. *Comp. Biochem. Physiol.*, 19:855–869.

209. Trager, W. and Jensen, J. (1976). Human malaria parasits in continuous culture. *Science*, 193:673–675.

210. Travis, S., Morrison, A., Clements, R. J., Winegrad, A., and Oski, F. (1971). Metabolic alterations in the human erythrocyte produced by increases in glucose concentration. the role of the polyol pathway. *J. Clin. Invest.*, 50(10):2104–2112.

211. Uyeda, K. (1979). Phosphofructokinases. *Adv. Enzymol.*, 48:193–244.

212. Valentini, G., Chiarelli, L., Fortin, R., Speranza, M. L., Galizzi, A., and Mattevi, A. (2000). The allosteric regulation of pyruvate kinase. *J. Biol. Chem.*, 275(24):18145–18152.

213. van Dooren, G. G., Marti, M., Tonkin, C. J., Stimmler, L. M., Cowman, A. F., and McFadden, G. I. (2005). Development of the endoplasmic reticulum, mitochondrion and apicoplast during the asexual life cycle of *Plasmodium falciparum*. *Mol. Microbiol.*, 57(2):405–419.

214. van Dooren, G. G., Stimmler, L. M., and McFadden, G. I. (2006). Metabolic maps and functions of the *Plasmodium* mitochondrion. *FEMS Microbiol. Rev.*, 30(4):596–630.

215. van Eunen, K., Bouwman, J., Daran-Lapujade, P., Postmus, J., Canelas, A., Mensonides, F., Orij, R., Tuzun, I., van den Brink, J., Smits, G., van Gulik, W., Brul, S., Heijnen, J., de Winde, J., de Mattos, M., Kettner, C., Nielsen, J., Westerhoff, H., and Bakker, B. (2010). Measuring enzyme activities under standardized *in vivo*-like conditions for systems biology. *FEBS J.*, 277(3):749 – 760.

216. Velanker, S. S., Ray, S. S., Gokhale, R. S., Suma, S., Balaram, H., Balaram, P., and Murthy, M. R. (1997). Triosephosphate isomerase from *Plasmodium falciparum*: the crystal structure provides insights into antimalarial drug design. *Structure*, 5(6):751–761.

217. Walsh, M. C., Smits, H. P., Scholte, M., Smits, G., and van Dam, K. (1994a). Rapid kinetics of glucose uptake in *Saccharomyces cerevisiae*. *Folia Microbiol (Praha)*, 39(6):557–559.

218. Walsh, M. C., Smits, H. P., Scholte, M., and van Dam, K. (1994b). Affinity of glucose transport in *Saccharomyces cerevisiae* is modulated during growth on glucose. *J. Bacteriol.*, 176(4):953–958.

219. Wanidworanun, C., Nagel, R. L., and Shear, H. L. (1999). Antisense oligonucleotides targeting malarial aldolase inhibit the asexual erythrocytic stages of *Plasmodium falciparum*. *Mol. Biochem. Parasitol.*, 102(1):91–101.

220. Williamson, D. H., Lund, P., and Krebs, H. A. (1967). The redox state of free nicotinamide-adenine dinucleotide in the cytoplasm and mitochondria of rat liver. *Biochem. J.*, 103(2):514–527.

221. Winter, V. J., Cameron, A., Tranter, R., Sessions, R. B., and Brady, R. L. (2003). Crystal structure of *Plasmodium berghei* lactate dehydrogenase indicates the unique structural differences of these enzymes are shared across the plasmodium genus. *Mol. Biochem. Parasitol.*, 131(1):1–10.

222. Woodrow, C. J., Burchmore, R. J., and Krishna, S. (2000). Hexose permeation pathways in *Plasmodium falciparum*-infected erythrocytes. *Proc. Natl. Acad. Sci. U. S. A.*, 97(18):9931–9936.

223. Woodrow, C. J., Penny, J. I., and Krishna, S. (1999). Intraerythrocytic *Plasmodium falciparum* expresses a high affinity facilitative hexose transporter. *J. Biol. Chem.*, 274(11):7272–7277.

224. Wünsch, S., Sanchez, C., Gekle, M., Grosse-Wortmann, L., Wiesner, J., and Lanzer, M. (1998). Differential stimulation of the Na^+/H^+ exchanger determines chloroquine uptake in *Plasmodium falciparum*. *J. Cell. Biol.*, 140(2):335–345.

225. Wünsch, S., Sanchez, C., Gekle, M., Kersting, U., Fischer, K., Horrocks, P., and Lanzer, M. (1997). A method to measure the cytoplasmic pH of single, living *Plasmodium falciparum* parasites. *Behring Inst. Mitt.*, 99(99):44 –50.

226. Yoshida, A. and Roth, Jr, E. (1987). Glucose-6-phosphate dehydrogenase of malaria parasite *Plasmodium falciparum*. *Blood*, 69(5):1528–1530.

227. Young, H. and Pace, N. (1958). Some physical and chemical properties of crystalline alpha-glycerophosphate dehydrogenase. *Arch. Biochem. Biophys.*, 75(1):125 –141.